EVALUATION OF THE FORMABILITY PROPERTIES OF NITROGEN ALLOYED METASTABLE AUSTENITIC STAINLESS STEELS

by

Mandla Sibanda

A thesis submitted to the Faculty of Engineering, University of Cape Town in fulfilment of the degree of Master of Science (Engineering)

Department of Materials Engineering
University of Cape Town

February 1994

ACKNOWLEDGEMENTS

I would like to express my thanks to all who helped me during the course of this thesis. Special mention goes to the following:

Dr Robert Knutsen for supervising this project and for his guidance and support when I needed it.

Mr Otto Schmid for his help in the early stages of the project.

Mr Bernard Greeves and Mr James Petersen for preparing the photographs despite their tight schedules.

Mr Nick Dreze for his advice on operating the Zwick.

Mr Glen Newins for patiently machining the test specimens.

Mr Gavin Doyle for assistance with the XRD.

My office mate Vin-Ree Ming for his support.

The departmental staff and students for their advice and support.

Mr Bruce Muller of Columbus Stainless for his assistance and hospitality during the drawability testing.

To Columbus Stainless and the FRD for their financial support.

Ngiyabonga.

Dedicated to my father.

SYNOPSIS

This study examines the formability of an AISI 301 based metastable austenitic stainless steel, in which nitrogen partially substitutes nickel. In order to understand the formability of the experimental alloys, the tensile behaviour of the alloys is characterised.

The tensile properties of metastable austenitic stainless steels are governed by austenite stability which is related to alloy composition and test temperature. At certain alloy compositions, transformation induced plasticity (TRIP) occurs. TRIP depends on the manner in which deformation induced martensite forms in the steels. Incipient necking is resisted if the martensite forms gradually and selectively, preventing propagation of micronecks and microcracks. Tensile tests performed from -5 to 100°C were used to study the effect of TRIP on the ductility of these alloys and optimum tensile properties were obtained at room temperature. In addition, the effect of copper on TRIP and subsequently formability were ascertained using copper alloyed stainless steels. Important stretch formability parameters were obtained from the tensile test which is an intrinsic formability test.

TRIP results in improved formability of metastable austenitic stainless steels, and a simulative Engelhardt test was performed to ascertain the effect of TRIP on drawability of the test alloys. It was found that alloys with TRIP characteristics exhibited good drawability and in all cases the test alloys had better limiting drawing ratios than AISI 304 stainless steel. Delayed cracking occurred in alloys with more than 0.2 percent nitrogen content and a low austenite stability, probably as a result of embrittlement of the deformation induced martensite by nitrogen.

A study of the cavitation erosion of the test alloys was initiated because it is known that TRIP enhances cavitation erosion resistance in stainless steels. Results indicate that the metastable test alloys demonstrate superior erosion resistance when compared with the stable experimental alloys. Cavitation induced martensite was found in metastable alloys using x-ray diffraction.

GLOSSARY

TRIP - Transformation Induced Plasticity
ε_u - Maximum uniform elongation
UTS - Ultimate Tensile Strength
CT - Cold Transformation
Ms - Martensite start
ΔG - Chemical free energy
BCC - Body Centred Cubic
FCC - Face Centred Cubic
MPa - Mega Pascals
Md - Temperature at which Deformation Induced Martensite Forms
ASP - Austenite Stability Parameter
I - Instability factor
SFE - Stacking Fault Energy
WHR - Work Hardening Rate
σ - Stress
ϕ - Instantaneous strain
ε - Strain
VFM - Volume Fraction Martensite
MET - Maximum Elongation Temperature
σ_{ys} -Yield stress
m - Strain rate sensitivity
r - Plastic strain ratio
n - Strain hardening exponent
f - Formability factor
LDR - Limiting Drawing Ratio
ASTM - American Society for Testing and Materials
LDF - Limiting Drawing Force
BHF - Blank Holder Force
XRD - X-Ray Diffraction
GSN - Grain Size Number
CWL - Cavitation Weight Loss
CVL - Cavitation Volume Loss
$\dot{E}$ - Rate of volume loss in steady state zone

CONTENTS

			Page
CHAPTER 1		INTRODUCTION	1
	1.1	METASTABLE AUSTENITIC STAINLESS STEELS	1
	1.2	OBJECTIVES OF RESEARCH	2
CHAPTER 2		LITERATURE REVIEW	4
	2.1	STAINLESS STEELS	4
	2.1.1	Austenitic Stainless steels	5
	2.2	THE ALLOYING ELEMENTS	6
	2.2.1	Schaeffler Diagram	6
	2.2.2	Empirical Equations for Austenitic Stainless Steels	12
	2.3	TENSILE BEHAVIOUR	14
	2.3.1	Stable Austenitic Stainless Steels	14
	2.3.2	Metastable Austenitic Stainless Steels	15
	2.4	TRANSFORMATION INDUCED PLASTICITY	16
	2.4.1	Strain Hardening Exponent	18
	2.4.2	Martensitic Transformations	19
	2.5	EFFECT OF STRAIN RATE	21
	2.6	FORMABILITY	22
	2.6.1	Effects of Materials Properties on Formability	22
	2.6.2	Process Variables	25
	2.6.3	Effect of Temperature on Formability	26
	2.6.4	Types of Formability Tests	27
	2.6.5	Lubricants	27
	2.6.6	Delayed Cracking	28
	2.7	CAVITATION EROSION	29
	2.7.1	Background	29
	2.7.2	Prediction of Materials Performance	30
	2.7.3	Mechanics of Cavitation Damage	31
	2.7.4	Fracture Modes	31
	2.7.5	Cavitation Erosion of Stainless Steels	32
CHAPTER 3		MATERIALS AND METHODS	33
		3.1 EXPERIMENTAL MATERIALS	33
	3.1.1	Heat Treatment	34
	3.2	Tensile Testing	34
	3.2.1	Test Apparatus	35

3.2.3 Tensile Test Specimen 35
3.2.4 Data Analysis 36
3.4 DRAWABILITY TEST 37
3.4.1 The Engelhardt Test 38
3.4.2 Calculation of LDR 39
3.5 CAVITATION EROSION 40
3.5.1 Cavitation Testing Apparatus 40
3.6 X-RAY DIFFRACTOMETRY 41
3.6.1 Calculation of Phase Volume Fraction 41
3.6.2 Instrument Settings 43
3.6.3 Magnetic Detection Device 44
3.7 ELECTROPOLISHING AND ELECTROETCHING 44
3.7.1 Electropolishing 44
3.7.2 Electro-etching 45
3.7.3 Tint Etching 45
3.8 METALLOGRAPHY 46
3.8.1 Light Microscopy 46
3.8.2 Scanning Electron Microscopy 46
3.9 BULK HARDNESS TESTING 46
CHAPTER 4 RESULTS 48
4.1. MICROSTRUCTURES 48
4.1.1 Microstructures of the Solution Treated Alloys 48
4.1.2 Microstructure of the Fractured Tensile Samples 50
4.2 TENSILE DEFORMATION BEHAVIOUR 53
4.2.1 Tensile Curves 54
4.2.2 Work Hardening Rate Behaviour 55
4.2.3 Properties Related to Forming 62
4.3 DRAWABILITY TEST 64
4.3.1 Appearance of the Drawn Cups 67
4.4 BULK HARDNESS 69
4.5 X-RAY DIFFRACTION RESULTS 69
4.6 CAVITATION EROSION RESULTS 70
4.6.1 Volume Loss and Incubation Period 70
4.6.2 Micrographs of Cavitated Surfaces 72
4.6.3 Cavitation Induced Martensite 73
CHAPTER 5 DISCUSSION 75
5.1 OPTICAL MICROGRAPHS 75
5.1.1 Microstructure of Solution Treated Alloys 75

5.1.2 Microstructure of Tensile Samples 76
5.2 TENSILE BEHAVIOUR 77
5.2.1 Maximum Uniform Elongation 78
5.2.2 Tensile Strength 80
5.2.3 Work Hardening Rate Behaviour 81
5.2.4 Proof Stress 82
5.2.5 The Strain Hardening Exponent 83
5.3 DRAWABILITY 83
5.3.1 Delayed Cracking 85
5.3.2 Effect of Temperature on Drawability 86
5.4 CAVITATION EROSION 87
CHAPTER 6 SUMMARY AND CONCLUSIONS 89
6.1 SUMMARY 89
6.2 CONCLUSIONS 90
REFERENCES 92
PUBLICATIONS: Conference Paper
Presented at the 'Innovation Stainless Steel' Conference.
Florence, Italy. 11-14 October 1993. Associazione
Italiana di Metallurgia.

CHAPTER 1: INTRODUCTION

In 1913 Harry Brearley of Sheffield was experimenting with alloy steels for gun barrels, and among the samples which he threw aside as being unsuitable was one containing about 14 % chromium. Some months later he noticed that most of the steels had rusted but the chromium steel remained bright. This led to the development of stainless steels, which possess a very high resistance to corrosion[1]. These steels are widely employed in corrosive environments and in some cases where high temperatures are experienced by materials in service. The oxide film makes the steel passive by forming an impervious chromium oxide layer on the surface of the steel. Since chromium is a ferrite former, the stainless steels will normally have a ferritic microstructure that limits their application (due to poor mechanical properties of the ferritic steels) and this has led to the development of martensitic and austenitic stainless steels. The austenitic stainless steels are alloyed mainly with nickel which stabilises austenite down to room temperature. The austenitic stainless steels are now widely used and this can be attributed to their good formability, weldability and corrosion resistance.

1.1 METASTABLE AUSTENITIC STAINLESS STEELS

The most common austenitic stainless steels are the AISI 300 series. These are alloyed with at least 18% chromium and at least 6% nickel. The AISI 200 series is another group of these steels which was developed in order to produce a cheaper stainless steel by substituting for nickel with large amounts of manganese and nitrogen.

In all austenitic stainless steels both mechanical and corrosion properties are heavily influenced by the stability of the austenite. Transformation of austenite to martensite occurs in the leaner alloys. These steels are known as metastable austenitic stainless steels. The transformation of austenite to martensite is induced during any type of deformation on these steels. It depends on alloy chemistry and on temperature of the steel during deformation. This transformation can lead to enhanced mechanical properties such as increased maximum uniform elongation (ε_u) which is known as TRansformation Induced Plasticity (TRIP).This transformation also leads to a much higher ultimate tensile strength (UTS).

One of the most important alloying elements for controlling austenite stability is nickel. If the amount of nickel is reduced in the steel, then the austenite becomes highly

unstable. This poses a problem in stabilising austenite in stainless steel because to ensure good stability in the steel there should be more than 6% nickel. However nickel is very expensive so that the production costs of stainless steel are high. A solution to this problem is found in substituting nickel with either manganese or nitrogen.

Nitrogen is the more desirable alloying element since it is cheaper and it has been found that nitrogen enhances mechanical properties of the steel. Previous work has been done on the deformation behaviour of a series of nitrogen alloyed stainless steels[2]. It was found during this study that some of these alloys which had nickel partially substituted for by nitrogen displayed desirable tensile properties with good maximum uniform elongation (ε_u) and ultimate tensile strength (UTS). As as result certain alloys whose compositions indicate similar or superior mechanical properties to AISI 301 stainless steel were chosen for formability testing and cavitation erosion tests. Two copper alloyed austenitic stainless steels were also tested in order to study the effect of copper in these stainless steels.

1.2 OBJECTIVES OF RESEARCH

The objectives of this project are:

1. To characterise the tensile behaviour of a range of alloys whose chemical analysis shows that they could have good TRIP properties.
2. To determine the microstructures in the solution treated condition of alloys which exhibit good TRIP properties and of the alloys after deformation.
3. To undertake formability testing of the alloys in a simulative test and compare the results of this test with those of tensile tests and thus possibly link formability to transformation behaviour of these steels.
4. To investigate the cavitation erosion of the alloys and determine the effect of austenite stability on erosion resistance.
5. To determine if these steels will be able to supersede AISI 301 stainless steel in certain industrial applications thus providing a cheaper stainless steel.
6. To study the effect of copper on TRIP and cavitation in these alloys.

Approach to research

This study is based on an applied approach to formability testing of materials using the basic formability testing techniques to determine parameters that can be used to rank the formability of these materials with respect to each other and AISI 301. The

investigation into the cavitation erosion of these materials is of an academic interest because the widespread use of these materials in mining machines prone to cavitation will need more work than has been done to date. However, it is of interest to study the cavitation modes in these steels and discover the effect of transformation on erosion because the good formability of austenitic stainless steel could reduce the cost of manufacturing these machines.

CHAPTER 2: LITERATURE REVIEW

2.1 STAINLESS STEELS

There are three main groups of stainless steels:

1. ferritic
2. martensitic
3. austenitic.

They all have varying mechanical properties which are mostly better than those of mild steels. The mechanical properties of the various steels can be seen in table 2.1 below.

STEEL	YS (MPa)	UTS (MPa)	ELONG (%)
MILD	300	430	18-25
MARTENSITIC	400-900	900-2000	10-20
FERRITIC	280-450	450-580	20-35
AUSTENITIC	300-500	800-1300	45-65

Table 2.1: Table of mechanical properties of mild ,ferritic, martensitic and austenitic steels[3].

Stainless steels are considered to be high alloy steels because of the large amounts of alloying elements, whereas mild steel has less than 1% total alloying elements. Stainless steels are replacing mild steels in many applications due to their superior corrosion resistance[4]. The bulk of the stainless steels in use today are the austenitic stainless steels, which constitute about 70% of the stainless steel production in the world. Types AISI 301 and 304 constitute about 65% of the stainless steels in use in the world today[5]. Although these steels cost about twice as much as martensitic and ferritic stainless steels (see table 2.2), they are more widely employed than the other steels due to their superior resistance to localised corrosion, good weldability and formability, and excellent toughness at ambient temperatures. However, ferritic stainless steels have excellent resistance to chloride stress corrosion cracking (a common occurrence due to the abundance of chloride ions on the earth's surface).

Alloy	Description	Microstructure	US$/kg
Type 304	Utility austenitic	100 % austenite	2.59
Type 316	Quality austenitic	95% austenite	3.38
Type 409	Low cost ferritic	100% ferritic	1.55
Type 430	Utility ferritic	100% ferritic	1.58

Table 2.2: Prices of cold rolled stainless steel sheet in the USA in February 1993[5].

2.1.1 AUSTENITIC STAINLESS STEELS

Austenitic stainless steels comprise the AISI 300 series which are alloyed with nickel, and the AISI 200 in which the nickel has been substituted with manganese. The main role of nickel in austenitic stainless steels is that of austenite formation and stabilisation. The type AISI 300 stainless steels contain at least 17% chromium and 7% nickel. Type 301 which is mainly employed for fabrication of formed articles is the leanest of these alloys and is commonly referred to as the 17/7 stainless steel. It is the most metastable of these alloys, easily transforming to a martensitic microstructure when formed;, this transformation results in good formability in this steel. Type 301 is used mainly at ambient temperatures. Types 302 and 304 represent primarily the 'bread and butter' alloys, having greater stability and improved corrosion resistance when compared to type 301. Type 304 is the most widely produced stainless steel and it is used considerably at elevated temperatures. The addition of molybdenum to a type 304 base steel gives the type 316 and type 317. These alloys have enhanced corrosion resistance and improved elevated temperature strength. The high alloy content stainless steels (types 309, 310 and 314) are used primarily in elevated temperature environments.

Transformation of austenite to martensite has been used for decades to improve the mechanical properties of controlled transformation (CT) and steels possessing the so-called transformation induced plasticity (TRIP) behaviour. The metastable austenitic stainless steels (such as 301 and 304), were invented to supersede the CT steels which needed costly and unreliable methods to effect transformation. CT steels have carefully controlled chemistries (originally difficult to achieve) which give a fully austenitic microstructure after casting and are easily workable at room temperature[6]. After forming to the required shape, these steels are then cooled down to below the Ms (martensite start) temperature in order to form martensite, which gives the steel good final strength. Alternatively they are placed in an oven at 700°C to precipitate carbides and thus form martensite by raising the Ms temperature to above room temperature. Both these processes are time and energy consuming if compared to the one step

process needed to shape the steel and transform it to martensite in the case of TRIP steels.

Steels	C (max)	Si (max)	Mn (max)	Cr	Ni	Mo
301	0.15	1.00	2.00	16-18	6-8	
302	0.15	1.00	2.00	17-19	8-10	
304	0.08	1.00	2.00	18-20	8-12	
310	0.25	1.50	2.00	24-26	19-22	
316	0.08	1.00	2.00	16-18	10-14	2.00-3.00

Table 2.3: Specified analysis (wt percent) of the AISI 300 series austenitic stainless steels[7].

2.2 THE ALLOYING ELEMENTS

The formation of austenite at the solution heat treatment temperature is controlled by the alloying elements. These elements lower the chemical free energy (ΔG) of the face centred cubic (FCC) structure with respect to the body centred cubic (BCC) structure. This is characteristic of the austenite forming elements like nickel. The retention of this austenitic microstructure during cooling or deformation is also controlled by the alloying elements[2]. The stability of the austenite is very important due to its effects on the TRIP properties of these steels. The propensity to form martensite in these steels is greatly influenced by elements like nitrogen, nickel and manganese and, to a small extent, copper.

2.2.1 THE SCHAEFFLER DIAGRAM

Various equations have been derived to relate the effect of the alloying elements to the properties of stainless steels. The relative ferrite and austenite forming tendencies of the elements are calculated using the nickel and chromium equivalents. Schaeffler developed a microstructure diagram (fig. 2.1) from which the structure of austenitic stainless steels could be predicted and this led to the formulation of the nickel and chromium equivalent expressions which take into account the potency of various elements in forming austenite or ferrite (the nickel equivalent is a measure of austenite forming ability and stability). The volume fraction of deformation induced martensite is inversely proportional to the Ni equivalent. For AISI 301 stainless steel the maximum

elongation occurs at a Ni equivalent of between 22 and 23[8]. Recently an equation for nickel equivalent was derived by Stanko[9] which takes into account the variation in the effect of nitrogen due to its limited solubility in stainless steel. The multiplying factor for nitrogen is seen to decrease as the nitrogen content increases and this is probably due to the formation of nitrides.

Nickel equivalent= Ni + 30C + 0.87Mn + 0.33Cu + (N-0.045)xa 2.1
a= 30 when N= 0 to 0.20
a= 22 when N= 0.21 to 0.25
a= 20 when N= 0.26 to 0.35

The chromium equivalent equation is as follows:

Chromium equivalent= Cr + Mo + 1.5Si + 0.5Nb + 5V + 3Al 2.2

Mo, Cr etc represent weight percentages of the various elements. The above equations were used in the calculation of nickel and chromium equivalents in preference to other equations because they consider the effect of copper and that of nitrogen which are the alloying elements under scrutiny in this study.

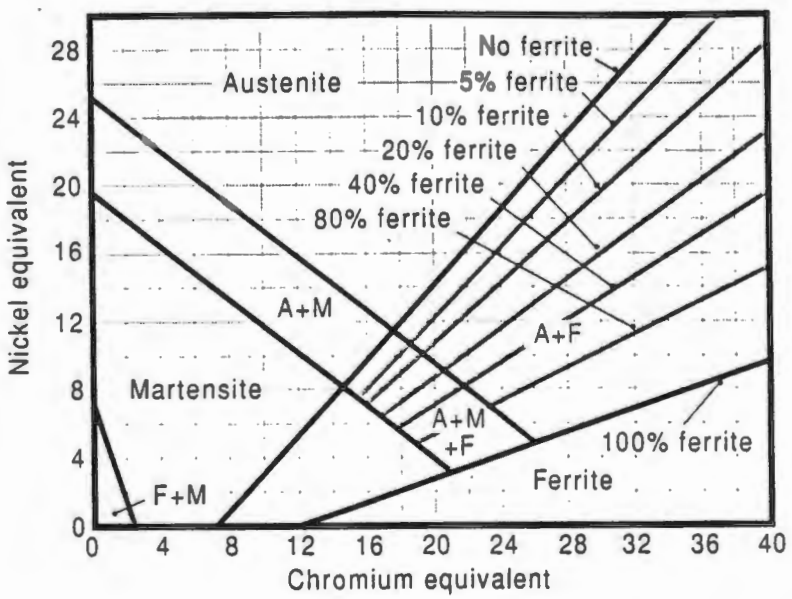

Fig 2.1: The Schaeffler diagram used for determination of microstructure in stainless steels[9].

By applying the Schaeffler diagram (see fig 2.1) the microstructure of stainless steels can be deduced from their chemical analysis. This is useful in steel plants because the

type of stainless steel which will be yielded from a certain heat can be deduced even before casting.

a) Effect of nickel

Nickel is the strongest austenite former and stabiliser among the substitutional alloying elements although it is about 30 times less potent than the interstitial alloy elements. Because of its austenite forming potency, nickel is a major alloying element in austenitic stainless steels. The drawback with nickel is its high cost, currently about R17 per kilogram and since nickel usually constitutes about 8% of the weight in an austenitic stainless steel, it has a marked effect on the production costs.

An increase in nickel content reduces the work hardening factor of nickel chromium steels in an exponential manner[10]. Similar behaviour is noted for the effect of nickel on drawability and tensile stress of stainless steels. The limiting drawing ratio which is a measure of drawability, decreases with increasing nickel. From all this information it can be deduced that increasing nickel above 10% reduces the energy needed to deform 18% Cr steels either in the stretching or drawing modes, but it also reduces the amount of deformation attainable in any given part. Therefore, the nickel level desired for any given part will depend on the capability of the forming equipment and the dimensions of the part being formed. Nickel is also known to reduce the transformation of austenite to martensite during mechanical working, thus an increase in nickel leads to lower UTS and ε_u of austenitic stainless steels[2,10,11,12].

b) Effect of nitrogen

Carbon and nitrogen are present as interstitials in stainless steels. Both are austenite forming elements and have a potency of at least 30 times that of the strongest substitutional alloying element which is nickel. The alloying of stainless steels with nitrogen has developed rapidly due to the argon-oxygen refining in stainless steel melting[13,14]. Nitrogen is substituted in part for argon during refining to control alloy constitution within the AISI ranges. The resulting increased austenite forming tendency can be used to substitute some of the nickel. There is a double incremental advantage since nitrogen is cheaper than either nickel or argon and it is a stronger austenite former. Previously nitrogen was a deliberate alloying element added only in larger amounts to types 304 and 316 stainless steels, where it is introduced during melting to impart increased strength. The best known application of nitrogen as an alloying element was the development of the AISI 201 and 202 stainless steels in the

1950s. In these alloys manganese and nitrogen were used to replace nickel. Manganese is used not only to substitute nickel but to increase nitrogen solubility.

Effect of nitrogen on yield strength

It has been demonstrated that nitrogen can be substituted for carbon with no adverse effects on ductility and corrosion resistance. Moreover, it can reduce the sensitisation in stainless steel when compared to carbon addition. Most austenitic stainless steels have very low strength. For example the yield strength of mild steel is about 300 MPa, which is significantly higher than that of type 304, which is 220 MPa under similar conditions[15]. Nitrogen increases yield strength of an austenitic stainless steel in two ways[16]:

(i) By solid solution hardening
(ii) By boundary strengthening

Irvine et al[17] and Norstrom[16] have established regression equations relating strength to nitrogen concentration in steel. Irvine et al's equation can be used for calculation of 0.2 percent proof strength of different types of stainless steels:

$$\sigma_{0.2} = 15.4\{4.4 + 23(C) + 1.3(Si) + 0.24(Cr) + 0.94(Mo) + 1.2(V) + 0.29(W) + 2.6(Nb) + 1.7(Ti) + 0.82(Al) + 32(N) + 0.16(\delta\text{-ferrite}) + 0.46(d^{-1/2})\} \quad \ldots.2.3$$

All the elements are expressed as percentages by weight, d is the mean linear intercept (grain diameter) in millimetres and the strength is in megapascals (MPa).

Norstrom's equation is specifically for AISI 316L. It is used to estimate the 0.2 percent proof strength as a function of nitrogen, grain size and temperature.

$$\sigma_{0.2} = 15 + 33000/T + 65\{(1690-T)/T\}\ N + \{7 + 78(N)\}d^{-1/2} \quad \ldots.2.4$$

where T is the temperature in Kelvin.

The effect of nitrogen on the yield strength of 5 austenitic stainless steels is shown in figure 2.2. Where it can be seen that at temperatures above 500 K , the yield strength does not change significantly with increasing temperature[15]. However below 500 K the yield strength changes considerably.

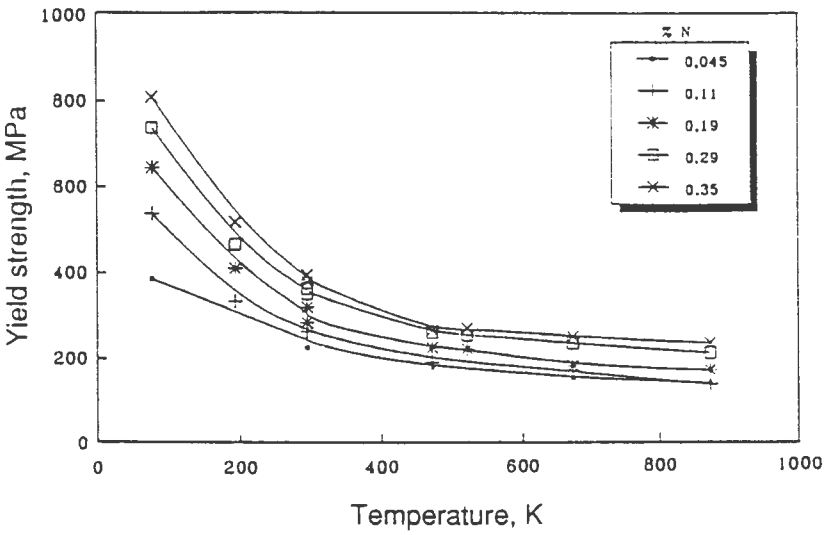

Fig 2.2 Variation of yield strength with temperature and concentration of nitrogen.

Effect of nitrogen on other properties

Several authors have reported that the ductility of nitrogen alloyed austenitic stainless steels is higher than that of nitrogen free steels[15]. These findings were based on tensile and Charpy impact test results. Figure 2.3 shows that the nitrogen alloyed stainless steels may constitute a group with the highest product of toughness and strength.

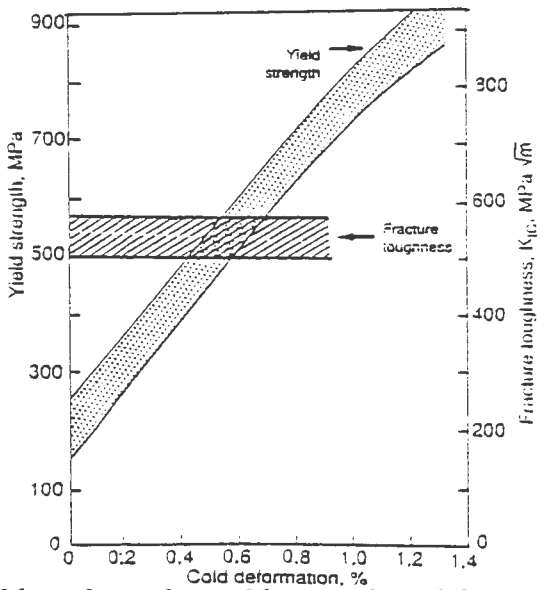

Fig 2.3: Effect of cold work on the yield strength and fracture toughness of a high nitrogen austenitic stainless steel[16].

One of the problems of alloying with nitrogen is its low solubility in stainless steels. Nitrogen should be in solution in order to avoid the deleterious effects of nitride precipitation. Nitride precipitation in solution treated stainless steel wire containing up to 0.7% N before drawing, greatly reduces ductility and only minor improvements in strength are realised[15]. The effect of nitrogen on the cracking of steels is notable and the precipitation of nitrides or carbo-nitrides reduces the resistance to stress-corrosion cracking[18]. Nitrogen is also associated with embrittlement in these steels. Meanwhile Du Toit[19] has found that nitrogen increases the resistance to delayed cracking in a 304 type stainless steel. It has been discovered that chromium increases the solubility of nitrogen while nickel decreases it. Nitrogen makes the steel more prone to porosity which can affect the mechanical properties of the steel[9].

c) Effect of Copper

The effect of copper on austenitic stainless steels has not been studied widely because copper is rarely used as an alloying element in these steels. Equation 2.5 takes into consideration the effect of copper[9,20] on the austenite stability. The above equations show that copper has about one third of the potency of nickel in stabilising austenite. Nohara and Ono[21] have tested the warm formability of a type 304 stainless steel and they have also published an equation for calculating the Md_{30} that includes the effect of copper (equation 2.7). Copper tends to decrease the work hardening rate and tensile strength of stable austenitic stainless steel. Brickner[22] demonstrated the effect of copper on the strain hardening exponent of a stable austenitic stainless steel and copper was seen to decrease the strain hardening exponent (fig. 2.4). Irvine et al[17] presented a graph showing that an increase in copper of up to 5% produced a decrease in the Ms temperature of a 17Cr-2Ni -2Mo austenitic stainless steel. It should be noted that more than 5% copper causes hot shortness.

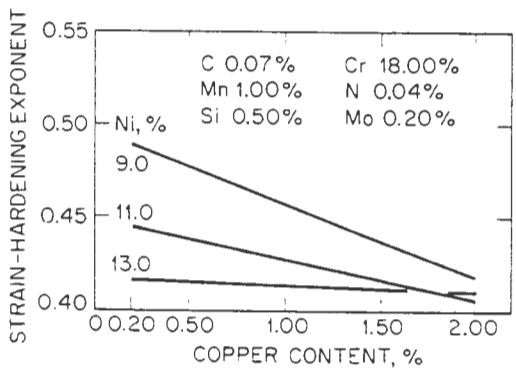

Fig 2.4: Effect of copper on the strain hardening exponent of a stable austenitic stainless steel at several nickel levels[22].

2.2.2 EMPIRICAL EQUATIONS FOR AUSTENITIC STAINLESS STEELS

Several expressions relating to stability and chemistry have been developed for austenitic stainless steels. The most widely used of these are the equations for the Ms temperature (temperature below which martensite will form in the steel due to quenching) and the nickel and chromium equivalent equations (2.1 and 2.2). Other equations include those of the austenite stability parameter (ASP) formulated by Griffith[23].

$$ASP = Ni - [(Cr + 15Mo - 20)^2/12 - 0.5Mn - 35C - Cu - 27N + 15] \quad ....2.5$$

The ASP was first developed by Post and Eberly[23] as a means of indicating the type of alloys that would resist transformation at cold reductions up to 80%. Griffiths and Wright[23] then modified the expression to include copper and nitrogen, they proceeded to show that the stability factor adequately described trends in composition versus work hardening behaviour. Fig 2.5 is a graph used by Griffith and Wright to predict the onset of α' martensite formation with respect to the ASP.

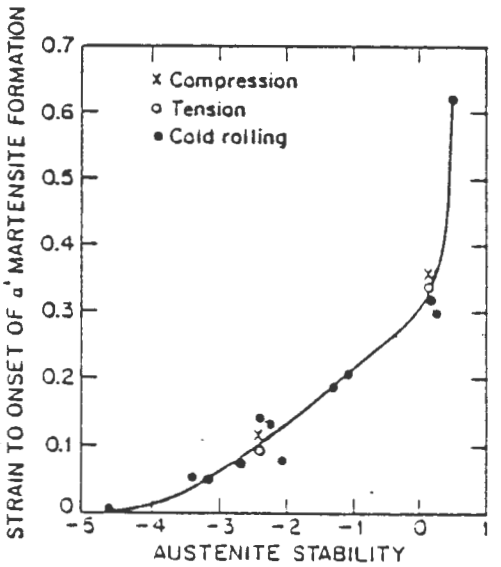

Fig 2.5: Effect of austenite stability on threshold strains for α' martensite formation[23].

Another useful equation is the instability factor (I), which was first used by Brickner[24] to relate elongation of a metastable austenitic stainless steel to I. He found that peak elongation occurred at I values between 0 and 2.9 for a 301 stainless steel, but concluded that for a 302 stainless steel there was little variation in ductility with composition if the I value is less than 0. Jackson[25] disputed Brickner's results for a 302

stainless steel claiming that for 302 steels with I values between -1.25 and 0 there was some martensite formation which had a positive effect on ductility. Jackson concluded that Brickner's results may have been inaccurate due to the small number of type 302 based alloys he tested. Jackson subsequently found that the maximum uniform elongation for the 302 stainless steels occurred at an I value of 1. The variation of elongation, with respect to austenite instability factor (I) according to Brickner (for AISI 301) and according to Jackson (for AISI 302) is shown in figure 2.6. The instability factor is determined from the following equation:

$$I = 37.19 - 51.2C - 1.02Mn - 2.59Ni - 0.467Cr - 34.4N \quad .....2.6$$

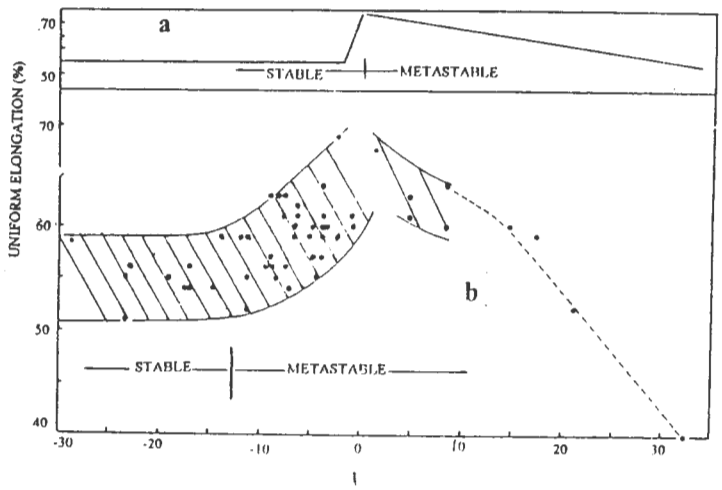

Fig 2.6: Variation of elongation in a uniaxial tensile test with the austenite instability factor (I) according to a)Brickner[24] b)Jackson[25].

The Md_{30} equations

The threshold temperature for the formation of deformation induced martensite is called the Md temperature. This temperature is difficult to determine, thus in 1954 Angel[26] suggested an Md_{30} temperature which represents the temperature at which 50% martensite forms at a strain of 0.3. He derived an empirical equation for the Md_{30} temperature which did not consider the effect of elements like copper on this temperature. Nohara and Ono[21] on the other hand developed a different equation for the Md_{30} temperature of austenitic stainless steels which relates the Md_{30} temperature to grain size and includes the effect of copper. A high Md_{30} temperature indicates low austenite stability. The equation is as follows:

$$Md_{30} = 551 - 462(C+N) - 9.2Si - 8.1Mn - 13.7Cr - 29.0(Ni+Cu) - 18.5Mo - 68Nb - 14(G.S.N. - 8.0) \quad .....2.7$$

where G.S.N. is the grain size number.

The temperature at which martensite starts to form during cooling is known as the Ms temperature. This temperature is also used to measure austenite stability, where a high Ms indicates low austenite stability. The Ms temperature is also used to predict the type of martensite that forms due to deformation since different types of martensite form at temperatures close to Md_{30} compared to those at temperatures close to Ms. A typical Ms temperature equation is one by Pickering[4].

$$Ms= 502 - 810C - 1230N - 13Mn - 30Ni - 12Cr - 54Cu - 46Mo \quad .....2.8$$

From these equations it can be deduced that the effect of alloy chemistry is important to the transformation behaviour of austenitic stainless steels and steel plants should be aware of this and control the level of C, N and Ni. In this study equations 2.7 and 2.8 were used because in these equations, effect of copper and nitrogen is taken into account.

2.3 TENSILE BEHAVIOUR

When austenitic stainless steels are subjected to deformation, the resulting microstructure is either austenitic or partly martensitic (the saturation level for transformation induced martensite is 90 %[26]), depending on the stability of the austenite phase. The transformation to martensite is governed by several factors such as the temperature of the material and the mode of deformation. Transformation to martensite influences the mechanical properties of the alloys and this is seen in the tensile curves. The most important effects of transformation are the enhanced ultimate tensile strength (UTS) and, in certain cases, increased ductility of the steel.

2.3.1 STABLE AUSTENITIC STAINLESS STEELS

Stable austenitic stainless steels do not transform during deformation; they retain their austenitic microstructure. They have a stacking fault energy (SFE) which is higher than those of metastable alloys, this is a result of the large amount of nickel used as an alloying element in these stainless steels. The work hardening rate of stable alloys drops continuously as the strain increases, this is related to the high SFE of these alloys and results in a low UTS and a reduced maximum uniform elongation[27]. The result of the low uniform elongation is poor stretch formability which can only be reversed by

grain size coarsening and addition of alloying elements which increase the SFE as well as having a solid solution strengthening effect.

2.3.2 METASTABLE AUSTENITIC STAINLESS STEELS (TRIP STEELS)

The SFE of the metastable alloys is lower than that of the stable alloys[2], so that their work hardening rates (WHR) are higher. This is a result of the low nickel concentration in these alloys and leads to transformation to martensite during deformation. The transformation to martensite in these steels leads to sigmoidal tensile curves, which has resulted in wide spread research into the mathematical modelling of the behaviour of these materials in an attempt to explain their tensile curves. The onset of the formation of martensite has been studied from first principles and a model created from the work of several authors[28,29,30]. The model is based on dislocation theory, thermodynamic and experimental observations. From dislocation theory Kocks[30] formulated an equation which describes the plastic deformation of metastable austenitic stainless steel provided that the deformation is homogeneous and not too big or too small. Schlipf[29] used a method of differentiating between mobile and stationary dislocations and defined the parameter H which characterises stability and homogeneity of deformations as a function of deformation.

$$H = \frac{\partial \ln \sigma}{\partial \phi} \quad .....2.9$$

where σ is the momentary stress and ϕ is the momentary strain. Typical H versus ϕ curves for a 304 stainless steel at different temperatures are given in fig. 2. 8.

The three types of tensile curves that can result from tensile testing of metals are given in figure 2.7. Curve 1 is a stable alloy with a normal parabolic curve. If ρ_{mo} is the initial density of mobile dislocations, ρ_{ms} is the steady state density of mobile dislocations and ρ_{mc} is the critical dislocation density, then for stable steels (curve 1) $\rho_{mo} \approx \rho_{ms}$. For a metastable steel (curve 2) $\rho_{mo} < \rho_{ms}$ and $\rho_{mo} > \rho_{mc}$ the resulting deformation is inhomogenous and stabilised at low strains, but at higher strains deformation becomes homogenous and destabilised. Curve 3 represents a material with Luders deformation which is not common in stainless steels.

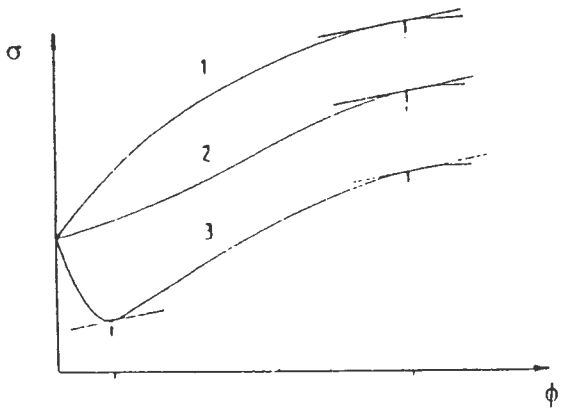

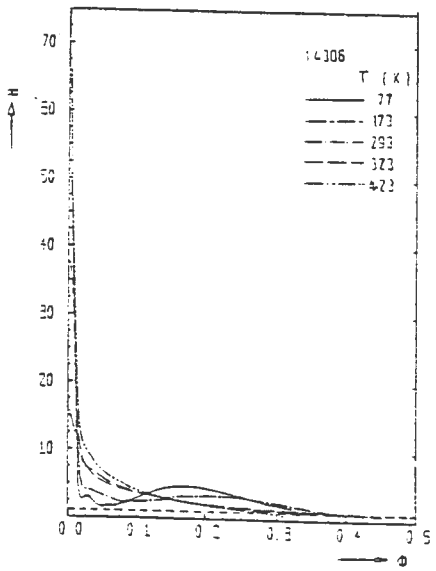

Fig 2.7: Schematic representation of stress strain curves.

Fig 2.8: curves of H versus ϕ for various stainless steels[28].

It is should be noted that the point of instability occurs when H=1 which has the same meaning as the instability condition given by Considere ($d\sigma/d\varepsilon = 0$).

It is well known that necking develops at the point where $d\sigma/d\varepsilon = \sigma$. Guimaraes et al[31] noted that this expression does not always describe the behaviuor of metastable austenitic stainless steels. They therefore developed an expression which they found fitted their experimental results for a Fe-Ni-C alloy. The reason for the difference in the necking was found to be due to the volume change caused by transformation which increases the actual elongation of the material. However for general experimental purposes the above expression is satisfactory since a difference of only 12% was observed between the experimental and calculated values of the point of instability in extreme cases for the author's alloys.

2.4 TRANSFORMATION INDUCED PLASTICITY

It is known that deformation of metastable austenitic stainless steels leads to deformation induced martensite in these steels. Under the proper temperature and strain rate conditions this martensite in turn leads to an enhancement of ductility in these steels. This enhanced ductility is a result of resistance to incipient necking and also of transformation strain. This increase in ductility is a result of a phenomenon known as transformation induced plasticity (TRIP). This acronym not only refers to

the behaviour of the steels but also to a group of Fe-Cr-Ni alloys developed by Zackay and co-workers[32,33,34,35]. The ductility is improved if the martensite forms gradually and selectively; this is due to the fact that it is not so much the total amount of martensite that is important, but the strain at which it forms[36]. An optimum amount of martensite should form at a point when necking would normally occur. If too much martensite forms too early then low strain to fracture is observed because the microstructure will be mainly composed of brittle martensite. If too little martensite forms too late during straining, low ductility results because there is not enough martensite to resist localised necking. Ludwigson and Berger[37] derived an equation which could better explain the flow curve of metastable austenitic stainless steels since the more common Ludwik or Hollomon equation (or power law) had failed to fit the sigmoidal shape of this curve. The Ludwik equation is only applicable to materials which produce parabolic flow curves. The Ludwik equation is as follows:

$$\sigma = k\varepsilon^{n} \quad .....2.10$$

σ is the true stress, ε is the true plastic strain, n is the strain hardening exponent and k is constant of proportionality.

The Ludwigson and Berger equation accounts for the contributions of austenite strain hardening, transformation and the strength of the resulting martensite.

$$\sigma = K[\ln(1+e)]^{n}(1-VFM) + C(VFM)^{Q} \quad .....2.11$$

K is the austenite strength factor, n is the strain hardening index and VFM is the volume fraction of martensite. C is the martensite stength factor and Q is the martensite strength index.

$$VFM = [1+(e^{-B/A})]^{-1} \quad .....2.12$$

A measures the propensity to transform and B describes the rate of transformation with increasing strain.

Equation 2.11 was compatible with the behaviour 99% of the Ludwigson and Berger's 301 stainless steel flow curves. From this equation, VFM can be used to explain the effect of martensite on the uniform elongation of austenitic stainless steels. Fig 2.9 a, b and c show the variation in uniform elongation for steels with three different values of A (the propensity to transform to martensite). If A=0 the steel does not transform,

therefore the flow curve is parabolic and the work hardening rate curve intercepts the flow curve at low strains. If A is increased to 30, the flow becomes sigmoidal (fig 2.9b), the ε_u is enhanced and good TRIP properties are realised. The hump in the WHR curve should also be noted. This is related to an increase in the work hardening rate as martensite forms in the material. In figure c the value of A is now increased to about 600 and the sigmoidal nature of the flow curve is exaggerated. It should also to be noted that the low ε_u is due to the formation of martensite too early during straining. From these curves one can see that there is an optimum rate of martensite formation where transformation induced plasticity occurs. The martensite must form gradually and selectively. In order to obtain optimum stretch formability (which results from optimum TRIP) martensite should not be present prior to forming, but a critical amount of martensite should form (2-6%)[8] during straining to a true strain of 20 percent.

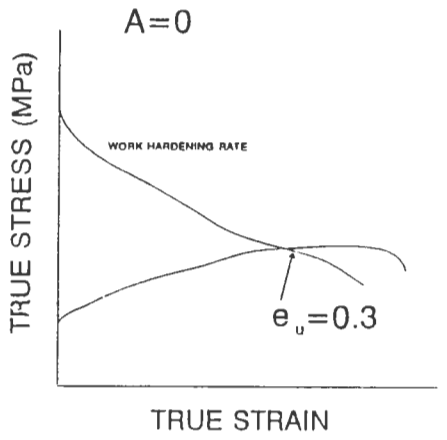

Fig 2.9 a

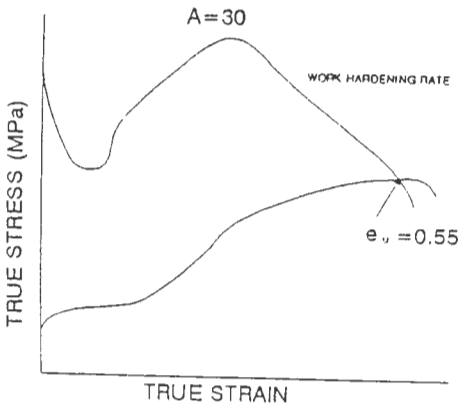

Fig 2.9 b

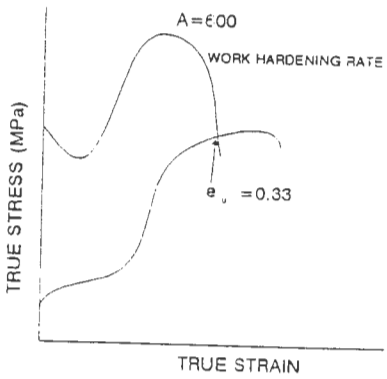

Fig 2.9 c

Fig 2.9 a) Flow and WHR curve for a stable steel (A=0)

Fig 2.9 b) Flow and WHR curves for a metastable steels with good TRIP properties (A=30)

Fig 2.9 c) Flow and WHR curve for a very metastable alloy with a low ε_u (A=650)

2.4.1 STRAIN HARDENING EXPONENT

Equation 2.11 can also be used to calculate a more accurate strain hardening exponent (n-value) for metastable austenitic stainless steels, the only drawback with this equation is that it is slightly complicated for everyday use. Jackson[25] suggested that in order to determine a simple unique strain hardening parameter which can be used to compare

the behaviour of the steels, the Ludwik equation will have to be used. A plot of $\log\sigma$ - $\log\varepsilon$ for a metastable stainless steel yields a curve which gives 'double n' behaviour for these steels. The first n value is for the region of the flow curve before transformation and the second n value, which is a better measure of strain hardening behaviour, accounts for the region where transformation has occurred. For most steels the n values are comparable to the ε_u, but this does not apply to metastable steels which have a final n value that is greater than the ε_u. This is due to a sharp decrease in the n value at strains close to the uniform strain, or to the lowering of uniform strain to a value below the instability strain on account of the formation of brittle martensite.

2.4.2 MARTENSITIC TRANSFORMATIONS

Angel stated that the martensitic transformation is associated with a shear strain during deformation[26], and observed that transformation occurs at a strain of 0.2. It should be noted that martensite formation is not only a function of strain but is also a function of stress as well. Martensite forms at a threshold stress which is activated through the work hardening action of strain[26]. Further evidence of this is given by Barclay[38] who observed the formation of martensite during straining (observations appear in table 2.4). The onset of the formation of martensite is important because it is associated with an increase in work hardening rate (seen as a sudden positive upturn in these graphs) and it determines whether or not optimum TRIP properties will be achieved.

True Strain	Observation
0.8-1.0	Dislocation tangles form into dense cells. Appearance of stacking faults. Increase in stacking fault density.
0.2	Heavy dislocation density in austenite. Deformation twins of lenticular shape form. Onset of formation of martensite.
0.3	Martensite forms.
0.6	Martensite volume fraction increases. Twinned austenite volume fraction increases. Austenite dislocation density is very heavy
>0.6	Twin Like martensite forms

Table 2.4: Course of martensite formation as a function of strain in AISI stainless steel

Schiel[39] noted that the amount of strain induced martensite in a TRIP steel increased with increasing degree of cold working and decreased with increasing deformation temperature until the Md temperature. This is illustrated by Angel[26] in his S curves (figure 2.10) where he plots volume percent of martensite as a function of true plastic strain for various test temperatures. It is seen that for this alloy (a type AISI 301) the observations of Schiel apply, suggesting that there is a temperature where the elongation is a maximum. Plots of martensite percentage versus temperature produce the well known reverse S curve which have been observed by many authors[12,25,26]. These curves are useful in calculating the Md_{30} which can be read as the temperature at which 50% martensite occurs at a strain of 0.3. The formation of martensite enhances the ε_u by hardening the necked region and thus further deformation takes place in the adjacent region, leading to the retardation of incipient necking.

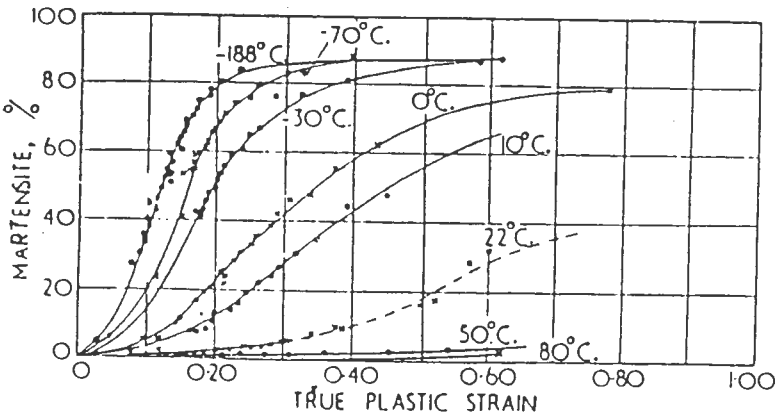

Fig 2.10: Formation of martensite in an 18-8 stainless steel[26].

Angel found that the martensite volume fraction in an 18-8 stainless steel increased in a sigmoidal fashion with decreasing temperature. He also stated that the saturation martensite volume fraction was 90%[26]. Previous researchers[2,12,40] have found that in metastable austenitic stainless steels the relationship between test temperature and ε_u exhibits a peak in the ε_u at a certain temperature. Huang et al[41] observed that the peak uniform elongation temperature is lower than the peak total elongation temperature. AISI 301 shows a sharp peak in ε_u at temperatures between 40° and 60° C, while the AISI 304 stainless steel has a less pronounced and broader peak as a result of its high stability (fig. 2.11). The maximum elongation temperature (MET) is found in these peaks. METs according to various authors are shown in table 2.5.

Author	MET
Bressanelli and Moskowitz[40]	50
Fukase et al[42]	52
Rosen et al[12]	55
Schmid[2]	60

Table 2.5: Maximum elongation temperatures of type 301 steels.

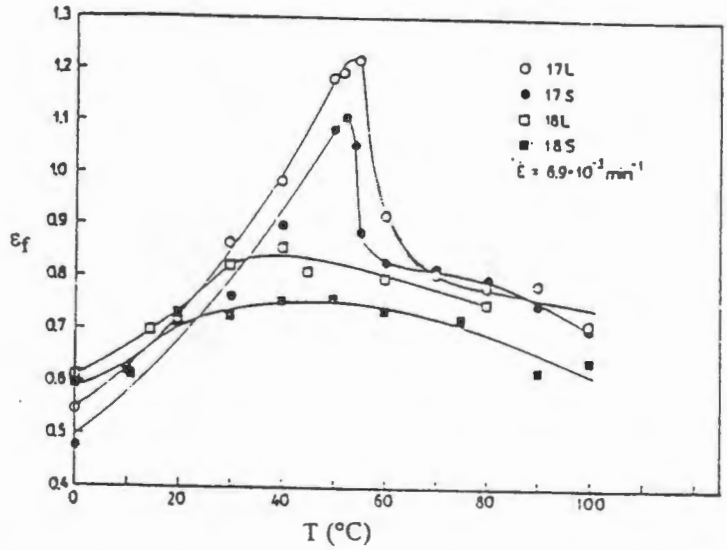

Fig 2.11: Elongation versus testing temperature[12]. 17S and 17L are type 301 stainless steels, 18S and 18L are type 304 stainless steels.

2.5 EFFECT OF STRAIN RATE

Bressanelli and Moskowitz[40] carried out thorough studies to determine the effect of strain rate on an AISI 301. They found that increasing the strain rate to beyond 8×10^{-3} s^{-1} had no effect on tensile properties and that variation in speed below that figure had little effect on tensile properties. Livitsanos et al[36] found that increasing the strain rate reduced the volume percent of martensite formed in the test specimens. This was attributed to adiabatic heating which increases the actual test temperature of the specimen. Jackson[25] found that there was a slight decrease in ε_u and n values for tests conducted in air when the strain rate was varied from 1.16×10^{-3} to 1.16×10^{-2} s^{-1}. In the case of tests conducted in oil baths to minimise adiabatic heating there was no variation in tensile properties. Both reports concluded that the materials properties obtained from low strain rate tests could be used to predict the behaviour of metastable austenitic stainless steels at high strain rates experienced in commercial forming operations. This is because the tensile properties of various steels do not change by much from low strain rates to high strain rates.

2.6 FORMABILITY

There are many ways of defining formability but an accurate general definition is "formability is the ability of a material to tolerate deformation"[43]. In terms of stresses imposed in various sheet-metal forming processes, formability breaks down into amenability to deep drawing, stretch forming and collar forming. Deep drawing is determined by the working range between folding and crack formation, while stretch formability is determined by the distribution of deformation. The limit in metal forming is not normally defined as crack formation but as localised thinning.

Sheet metal forming is undergoing a transition from an art to a science[44] as trial and error gives way to knowledge. The state of the art in metal forming is using finite element methods to predict the forming behaviour of various sheet-metals using different dies although the methods of using tensile formability parameters and forming limit diagrams are still widely used. Formability is however, an elusive quality to measure. There is no single index that will enable the formability of a specific material to be predicted for all production conditions or stampings. When an article is being formed, the undesirable condition is cracking or fracture, but other commercially undesirable conditions are poor surface finish, sheet wrinkling, or lack of die fill[45].

2.6.1 EFFECTS OF MATERIALS PROPERTIES ON FORMABILITY

The materials properties that are important in sheet metal forming are plastic flow and fracture modes[44,46]. These properties can be controlled through chemical composition and hot and cold rolling practices. Processing steps that increase the strength of a material also decrease its formability. These steps include

- alloying that produces solid solution hardening
- fine grain size and cold work
- hard phases in the material such as martensite

Material properties vary considerably depending on the base metal, alloying elements and processing. In selecting a material compromise must be made between functional properties required and formability of the material[47]. For optimum formability the material should have the following characteristics:

1. Distribute strain uniformly.
2. Reach high strain levels without necking or fracturing.
3. Be able to withstand in plane compressive stresses.

4. Retain part of the formed shape on removal of the die.
5. Retain good surface appearance.

Three material properties determine the strain distribution in a forming operation, namely the n-value, strain rate sensitivity (m-value) and the plastic anisotropy (r-value). The first two are particularly responsible for a material's ability to reach high strain values[47].

The strain hardening exponent (n-value)

The n value is possibly the most important property influencing cold formability[46,47,48], as it gives a measure of a sheet's ability to harden with deformation. A region undergoing thinning can resist further deformation by strain hardening and spreads deformation to its neighbouring regions. Materials with a high n-value also have a rapid increase in flow stress with strain which is evidenced by the sigmoidal flow curves for metastable austenitic stainless steels. Maintanence of a high n-value up to large strains is also important for good formability because it assists in resisting necking.

Strain hardening is caused by the storage of dislocations within a metal and the resistance they offer to the passage of other dislocations. Annihilation, rearrangement and cross slip of dislocations reduce the rate of hardening so that it can come into balance with the rate of thinning. These processes are responsible for plastic instability which eventually leads to fracture. Low SFE materials have good formability due to difficulty of cross slip which results in a high n-value.

For most steels $n=\varepsilon_u$ and the relationship between the n-value and yield strength is generally satisfied by the following equation:

$$n=70/\sigma_{ys} \quad .....2.13$$

where σ_{ys} is the yield stress.

Equation 2.13 may not apply to metastable austenitic stainless steels because of the double n behaviour of these steels which is a result of transformation to martensite. A high n value leads to a considerable difference between yield stress and UTS therefore the n value can be used as a formability parameter (giving the amount of elongation between the yield point and the point of instability).

Strain rate sensitivity (m-value)

Positive strain rate sensitivity is another important property that aids uniform strain distribution which results in increased formability. This property is described by an increase in flow stress with increasing strain rate. In forming operations, gradients in strain and strain rate develop owing to frictional and geometrical constraints[46]. Strain rate sensitivity acts to reduce the resultant non uniformity of thinning[47]. The positive m value has two consequences:

- Higher stresses are required to form articles at higher rates.
- At a given forming rate, the material resists further deformation in regions that are being strained more than adjacent regions by increasing flow stress in the strained regions.

The strain rate sensitivity is defined by:

$$m = \frac{d \ln \sigma_T}{d \ln \dot{\varepsilon}} \quad .....2.14$$

σ_T is the tensile stress and $\dot{\varepsilon}$ is the strain rate

As with the n-value, the m-value has no direct correlation to drawability, but high m-value leads to good stretch forming. The reasons for this are found in the mode of deformation in drawing. In drawing, the flange must be drawn in without causing fracture in the wall. In this instance high n and m values strengthen the wall, which is beneficial but they also strengthen the flange which makes drawing more difficult and is thus detrimental.

Plastic strain ratio (r-value)

The r-value relates to the drawability of a material. This value is influenced by the texture in a material. The r-value is defined as follows:

$$r = \varepsilon_w / \varepsilon_t \quad .....2.15$$

ε_w is the strain along the width of the specimen and ε_t is the strain along the thickness of the specimen.

In drawing the material is stretched in the radial direction and compressed in the perpendicular direction. The frequent changes with direction of the r value in a sheet leads to a defect known as earring, therefore it is common to measure the average normal anisotropy (r_m) and the planar anisotropy (Δr). The r_m determines the average depth of the deepest draw possible. The extent of earring is determined by Δr[46,47]. For isotropic sheets (such as metastable austenitic stainless steel) r=1 indicates that the metal is equally strong in all directions. Commercially produced flat rolled stainless steels have a weak texture[49] because the sequences known to generate significant texture in these materials (very extensive deformation, intermediate to elevated temperature deformation and very specific heat treatments) are not used in the production of stainless steel sheets.

A formability parameter that is calculated from tensile data is the Boeing formability factor (f)[8].

$$f = \frac{\ln[Rm(1-\gamma_g)]}{A\gamma_g} \quad .....2.16$$

Rm is the UTS, A is the area under the flow curve and γ_g is the ε_u. A low f value indicates improved formability, so that a steel which has high UTS, high ε_u and a large A will have good formability.

2.6.2 PROCESS VARIABLES

The most important process variables are the forming equipment geometries, blank holder pressure, clearance and lubrication. Punch and die radii are the most critical parameters for metal forming. Small punch radii are desired for sharp feature lines on components, but sharp lines give rise to strain concentrations which may cause an early fracture. This is circumvented to some extent by increased blank holder force and a larger punch radius[46]. The blank hold down force has to be carefully controlled because too large a force causes tearing, while too small a force leads to wrinkling. Press speed is neither well understood nor well documented. Conflicting reports are obtained depending on the forming process and the material to be formed[46]. Increasing the speed can reduce the die/sheet friction considerably, leading to more uniform thinning. Furthermore, local heating can cause additional changes in the material behaviour[50]. As a result, different material responses can be obtained for different press speeds. In a metastable austenitic stainless steel the adiabatic heating can suppress the formation of martensite which leads to inferior formability on account of the lack of TRIP in the steel due to low ε_u and UTS.

2.6.3 EFFECT OF TEMPERATURE ON FORMABILITY

A change in temperature causes changes in properties of a material, also local temperature differences within the deforming blank lead to local differences in the properties that affect formability[47]. At a high temperature (above one half the melting temperature) fine grained Al, Cu, Mg, stainless steel and other alloys become super plastic. Super plasticity is characterised by extremely high elongation which can be as much as 1000%, but only at low strain rates. This has limited the applications of super plasticity to low volume production operations. Local increases in temperature occur during deformation due to surface friction and adiabatic heating produced by deformation. Generally this is detrimental to formability because it lowers flow stress in the area of greatest strain and leads to localised necking.

Heating the die to lower flow stress in the deformation zone on top of the draw wall has also been found to be beneficial. This process increases the drawability of an austenitic stainless steel by more than 20%[47]. Nohara and Ono[21] noted that the deformation behaviour of stainless steels is temperature dependent when they performed tests on 304, 301 and 430 stainless steels. They concluded that raising the die temperature to 100°C and maintaining a low punch temperature improved drawability. Warm drawing improves drawability because the maximum drawing forces decrease with rising temperature.

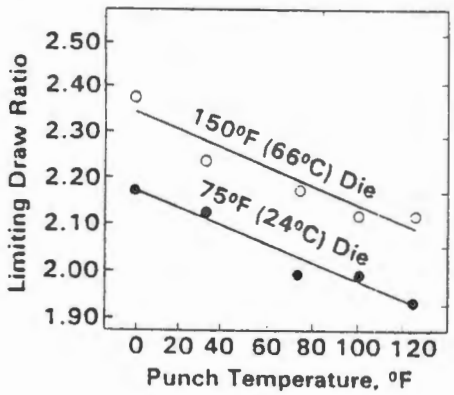

Fig 2.12: Effect of Punch and Die Temperature on the LDR of 304 stainless steel[51]

Fig 2.12 illustrates that increasing the punch temperature reduces the LDR, while increasing the die temperature increases drawability. This occurs as a result of the amount of martensite induced during drawing, large amounts of martensite in the punch area are advantageous to drawability while the converse is true for the die area.

2.6.4 TYPES OF FORMABILITY TESTS

There are two basic types of formability tests, the intrinsic test and the simulative test[46,47].

Intrinsic tests these tests measure the basic characteristic properties of materials that can be related to their formability. The comprehensive information provided by intrinsic tests cannot be related to the material thickness and surface condition. The most important and extensively used intrinsic test is the uniaxial tensile test which provides values for most materials properties which are useful in a wide range of forming operations. Other commercially important intrinsic tests are the Marciniak stretching and sheet torsion tests and the hydraulic bulge test.

Simulative tests subject the material to deformation as it appears in a particular forming operation. The information provided by this test is limited and specific, and information is usually sensitive to thickness, surface condition, lubrication and tooling. It usually relates to one type of forming operation only. Typical simulative tests are the Olsen cupping test and the limiting dome height test for measuring stretch formability, while the Swift cup test measures drawability. Many simulative tests have been used extensively with good correlation to specific forming operations.

2.6.5 LUBRICANTS

Lubricants are essential in formability operations. Effective lubricants provide the following advantages[46,47].

1. Reduction or elimination of direct sheet to die contact, which can cause galling or die wear.
2. Control of friction.
3. Reduction of heating.
4. More uniform strain distribution and thus an increase in the overall level of deformation.

Friction is detrimental to drawing because it increases drawing force. Drawing of a cup into a high pressure medium such as oil or water allows much deeper cups to formed because lateral pressure forces the sheet to transfer load to the punch. This helps avoid instability and fracture near the cup bottom.

2.6.6 DELAYED CRACKING

The subject of delayed cracking (delayed fracture) has not not been widely investigated because it is not a common anomaly in stainless steel. Manufacturers of various stainless steel products have observed that articles drawn out of alloys with high carbon or nitrogen contents experience delayed fracture and the problem occurs more frequently in winter. Divers[52] investigated delayed cracking in deep drawn chromium plated stainless steel hub caps. He attributed the cracking to stress corrosion cracking which is accelerated by catalytic action of hydrogen evolved during plating. It is suspected that the hydrogen evolved during pickling also contributes to delayed fracture. Divers found that delayed cracking is linked to the n-value of the 301 stainless steel. An n-value greater than 0.52 results in hydrogen embrittlement, while an n-value less than 0.48 shows no embrittlement. This behaviour could be linked to the amount of martensite formed during transformation and to the strength of this martensite.

Nohara and Ono[21] discovered that delayed cracking in a copper alloyed 304 stainless steel was influenced by the Md_{30} temperature of the material calculated, according to equation 2.7. A graph showing the drawability of a copper alloyed 304 stainless steel was presented in their report and is shown in fig 2.13. This figure shows that there is a range of Md_{30} temperature where optimum formability is achieved without defects. The peak in drawing cup height over a particular temperature range is a result of formability testing being carried out where optimum TRIP characteristics are experienced.

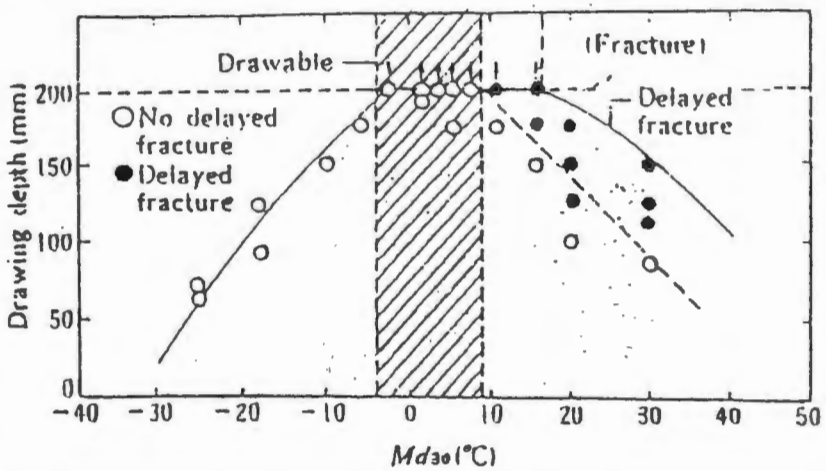

Fig 2.13: The relationship between cup height and Md_{30} temperature.

A reduction in the amount of martensite formed by the material can be ensured by warm press forming. When the authors[21] investigated the effects of warm press

forming on delayed cracking, they found the reduction of the martensite formed to be beneficial to drawability and in reducing delayed cracking. Moreover they advise that the martensite content in drawn articles should not exceed 10% if delayed fracture is to be avoided. Ward et al[50] has investigated the modelling of TRIP in the deep drawing of stainless steel and has found that martensite is formed in localised areas. This leads to stress concentrations during cooling due to the lower density of martensite compared to austenite. It has been suggested by Ward et al that these stress levels might be sufficient to induce delayed fracture while a formed article cools after drawing. Du Toit[19] has found that an increase in nitrogen content is beneficial in reducing delayed cracking in a high nitrogen 304 stainless steel. In this case delayed cracking was measured using the embrittlement index after slow strain rate tensile testing at room temperature. The embrittlement index for the high nitrogen stainless steel was lower than that of the low nitrogen stainless steel.

Hoshino[53] concluded that the cause of delayed cracking is due to the the volume fraction of the α' and the effects of the chemical composition on this phase. Hoshino found N to be a less harmful element in delayed cracking than C, and Al and Si prevent delayed cracking.

2.7 CAVITATION EROSION

2.7.1 BACKGROUND

Cavitation is a liquid phenomenon which embraces any process involving the appearance and disappearance of cavities in a liquid[54]. Most studies of cavitation examine the unstable growth and collapse of gas bubbles. Cavitation transforms the low energy density of a pressure field into a high energy density field characteristic of the neighbourhood and the interior of a collapsing cavity. The concentration of energy into a small volume enables cavitation to produce effects such as erosion of solids. When the liquid is subjected to a tensile stress, which is theoretically equal to the tensile stress of the liquid, localised rupturing of the cavities occurs. In practice, cavities form at stresses well below the theoretical strength corresponding to a pressure equal to vapour pressure of the liquid. This anomaly results in the presence of nucleating sites in the liquid, which act as nucleating sites for rupture. A free gas bubble is a form of cavitation nucleus, but it is unstable. However stable sites do exist in the form gas pockets in a crevice and in hydrophobic impurities. Cavity collapse occurs when ambient pressure increases to more than the pressure within cavities. A

clear indication of stresses caused by cavitation is when high strength alloys with a yield strength of more than 1000 MPa are damaged by cavitation[54].

2.7.2 PREDICTION OF MATERIALS PERFORMANCE

Due to the need for a parameter which can be used to specify material components of systems prone to cavitation, efforts have been made to correlate materials properties to cavitation. Good correlation has been found for hardness, yield stress and UTS for materials with a common base metal (i.e. mild steel and stainless steel)[54]. Various energy based parameters have been proposed as erosion resistance controlling properties and these include Hobb's ultimate resilience and strain energy to fracture (fig. 2.14). Ultimate resilience approximately represents elastic energy absorbed up to fracture in tension if the failure mode is brittle.

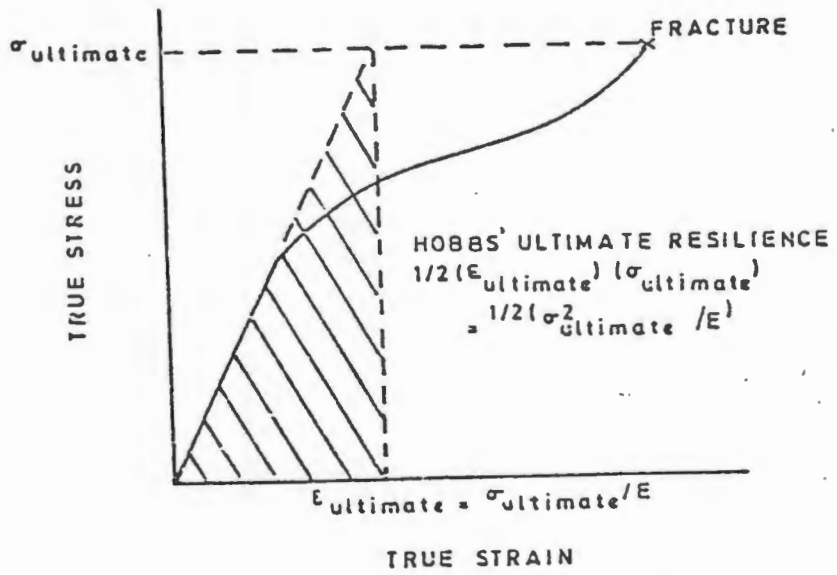

Fig 2.14: Illustration of ultimate resilience.

The method compared elastic resilience, ultimate resilience and strain energy to fracture for a large number of alloys. Best fit was found to occur with ultimate resilience. The limitation of this method is the assumption that all materials fail in a brittle manner. It was also discovered that for a small group of alloys that good agreement exists between erosion resistance and the product of either strain energy and ultimate resilience and hardness[54].

2.7.3 MECHANICS OF CAVITATION DAMAGE

Mechanical stressing has been found to be the main mechanism of cavitation damage. This mechanism involves accumulation of fatigue damage followed by work hardening and finally fracture. Corrosion plays a negligible part in vibratory cavitation since intensity of erosion is high, although inflow cavitation intensities are lower. Corrosion therefore is only useful in material removal.

Mechanical stressing was proven by x-ray analysis of Ni, brass, AISI 4340 steel and 301 stainless steel[54,55]. The x-ray patterns were broadened after cavitation, indicating the occurence of plastic deformation. Presence of plastic deformation led investigators to conclude that firstly fatigue, then work hardening and finally fracture was the process followed in cavitation damage.

2.7.4 FRACTURE MODES

The two modes of erosion are ductile and brittle, normally erosion is due to variations of these modes. Diffusion in crystal structure, microstructure and mechanics of plastic deformation influence the fracture mode. Brittle fracture leads to high rates of erosion in materials due to their susceptibility to sudden fracture[57]. Examples of the two fracture modes are show below

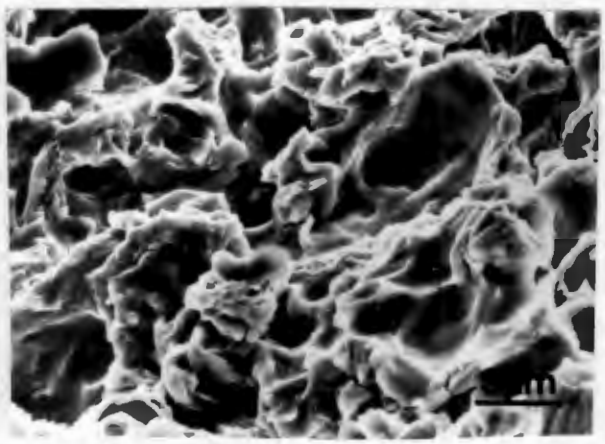

Fig 2.15a: Ductile fracture in cavitation

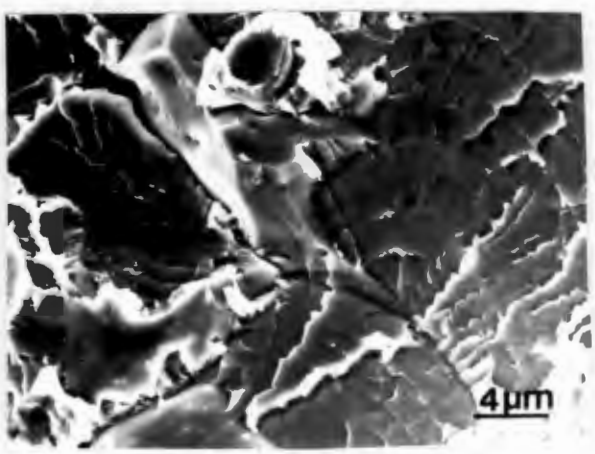

Fig 2.15b: Brittle fracture in cavitation erosion

2.7.5 CAVITATION EROSION OF STAINLESS STEELS

Austenitic stainless steels which have low SFE and FCC crystal structures, erode in a manner similar to other low SFE materials such as copper zinc-alloys[54]. Material piled at the grain and twin boundaries is lost by ductile fracture. Austenitic stainless steels and austenitic manganese steel have a higher resistance to erosion than is expected due to transformation[54,55,56]. Although these steels exhibit a higher erosion resistance than most steels their resistance to cavitation is much lower than materials such as stellite and martensitic stainless steels. The reasons for this are that stellite has much higher work hardening rates than these steels and martensitic stainless steel is a much harder material. Metastable austenitic stainless steels transform to α' and ε martensite while TRIP steels (Fe-Cr-Ni-C alloys) transform only to the α' phase. Most TRIP steels are more resistant to erosion than AISI 301 stainless steel, because they have better mechanical properties (higher UTS and ε_u). In the same way AISI 304 stainless steel was found to have better erosion resistance than AISI 316. From the above facts it can be ascertained that a high work hardening rate ensures good cavitation erosion resistance because transformation to martensite increases the work hardening rate of steels. The increase in fatigue life of metastable steels also helps increase their erosion resistance by increasing their incubation periods.

An increase in interstitial alloy element concentration in stainless steels to leads an increment in erosion resistance, especially on materials that transform or those that are martensitic. The formation of precipitates such as carbides or nitrides is detrimental to the cavitation erosion resistance in these materials because precipitates provide sites for initiation of erosion.

From the information given above it can be concluded that for materials to have good erosion resistance they should possess the following characteristics[54]:

1. High UTS
2. High WHR which is a result of high n-values.
3. High ε_u
4. Low SFE which is a property of austenitic stainless steels.
5. Ductile erosion
6. No secondary phase particles should be present
7. Good fatigue resistance.

CHAPTER 3: MATERIALS AND EXPERIMENTAL PROCEDURE

In this chapter, the materials used, the heat treatments they were subjected to, the various mechanical tests and microstructural characterisations are discussed. Tests were carried out to determine the various tensile properties of the materials which can be used to determine formability. The Swift test was used as a simulative test to determine drawability as it would be impossible to determine this from the tensile tests. Resistance to cavitation wear was determined by means of ultrasonic cavitation on flat samples.

3.1 EXPERIMENTAL MATERIALS

Six experimental alloys prepared by Columbus Stainless (Middleburg) were selected from a range of alloys based on the AISI 301 stainless steel, but with varying nickel to nitrogen ratios. Copper was added to two of these alloys in order to ascertain the effect of Cu on their tensile properties, formability and erosion resistance. The alloys were chosen because their deformation behaviour was expected to closely simulate that of AISI 301 stainless steel, as determined in an earlier study[6]. The composition of these alloys is shown in table 3.1 together with the composition of 301 stainless steel for comparison. For easy reference the nomenclature used for the alloys is designated according to their nickel, nitrogen and copper levels. For example, the alloy 6016Cu0 has 6 weight percent nickel, 0.16% weight percent nitrogen and no copper (or a negligible amount), while the alloy 5422Cu33 has 5.4 weight % nickel, 0.22 weight % nitrogen and 3.3 weight % copper.

Alloy	C	Cr	Ni	N	Cu	Mn	Si
6016Cu0	0.03	17.4	6.0	0.16	-	1.52	0.3
5623Cu0	0.03	17.0	5.6	0.23	-	1.55	0.3
5428Cu0	0.03	17.7	5.4	0.28	-	1.40	0.4
8630Cu0	0.03	17.1	8.6	0.30	-	1.29	0.4
5422Cu13	0.03	17.6	5.4	0.22	1.3	1.69	0.3
5422Cu33	0.03	17.2	5.4	0.22	3.3	1.54	0.6
AISI 301	0.03	17.7	7.5	0.07	-	1.52	0.4

Table 3.1: Composition of experimental alloys (in weight percentages).

Each experimental alloy was prepared in an experimental furnace and cast into 5 kilogram ingots (50 millimetres thick) which were subsequently rolled down to a thickness of 2-3 millimetres. The sheets which were used for biaxial formability testing were rolled down further to a thickness of about 1mm.

3.1.1 HEAT TREATMENT

Solution treatment was carried out on all the as received plates so as to ensure a fully austenitic microstructure in the alloys, before testing. The tensile test specimen and x-ray diffraction samples were solution treated in a vacuum furnace using an argon atmosphere after machining and cutting in order to destroy the martensite which may have been induced during these processes. The treatment procedure was as follows:

1. Furnace temperature= 1050°C
2. Heat treatment time= 30 minutes
3. Oil quench

The plates used for biaxial formability testing were heat treated in a Naber oven because they were too large to fit into the vacuum furnace. They were subjected to the same heat treatment conditions as the tensile specimens except for the argon atmosphere which cannot be attained in the Naber furnace. After solution treatment of these plates, they were pickled in a solution of 15 ml nitric acid, 15 ml hydrofluoric acid and 80 ml water. The solution was heated to a temperature of 60°C and the plates were submerged in the solution until their surfaces were shiny. They were then washed thoroughly in water.

3.2 TENSILE TESTING

Tensile test results provide basic materials properties which are often related to the formability of a material. These tests were performed on the steels at varying temperatures up to fracture in order to determine various formability parameters. Each test was duplicated to ensure reproducibility of results; in certain cases where the tensile properties had a huge difference in the two results, a third test was performed and the result which differed notably from the others was rejected.

3.2.1 TEST APPARATUS

The uniaxial tensile tests were performed on a computer interfaced Zwick 1484 materials tester with facilities for data capture. The captured data produced results of the force (in Newtons) and the elongation (in millimetres) for each test. The strain was measured using a crosshead. These data were presented in a format that could be processed in a spreadsheet. The bath used for isothermal test conditions utilised oil at high temperatures (above room temperature) and was regulated by a Eurotherm temperature controller to within 2°C of the desired temperature. The bath was heated by means of a helical coil around the narrowed section of the test specimen. Low temperature tests were performed in ice water and in a dry ice and alcohol environment for extremely low temperatures. In all cases a chromel-alumel thermocouple (type K) situated near the middle of the specimen was used to measure temperature. The initial strain rate was maintained at 10^{-3} s^{-1} for all tests.

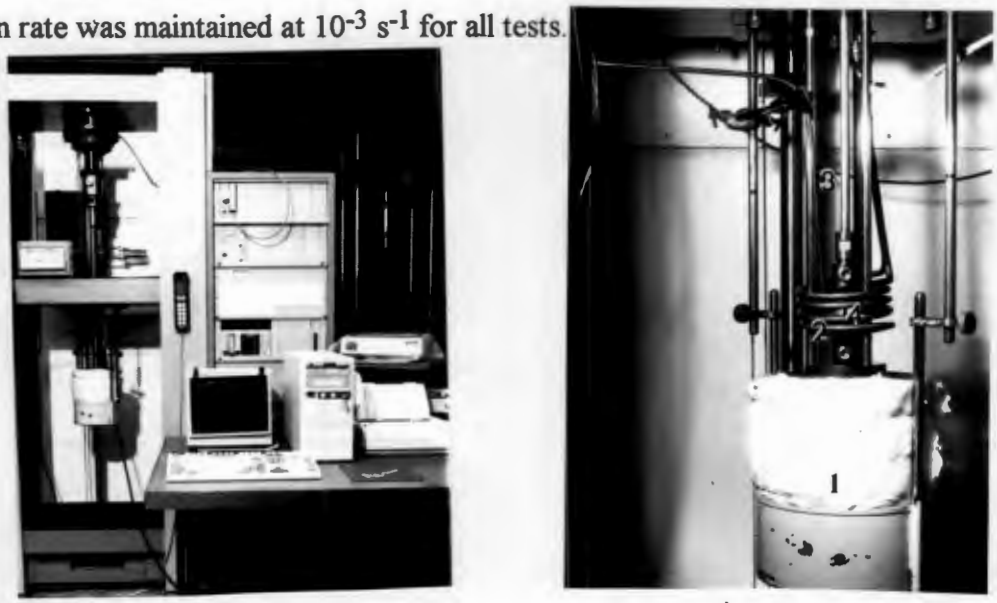

Fig 3.1 (a): The computer interfaced Zwick 1484 materials tester, with isothermal bath beneath the cross head.

(b): Close up view of the isothermal bath system. 1) temperature bath, 2)heating coil, 3) thermocouple, 4) specimen.

3.2.3 TENSILE TEST SPECIMEN

The tensile test specimens were machined according to ASTM standard E8M[45], and the specimen geometry is given figure 3.2.

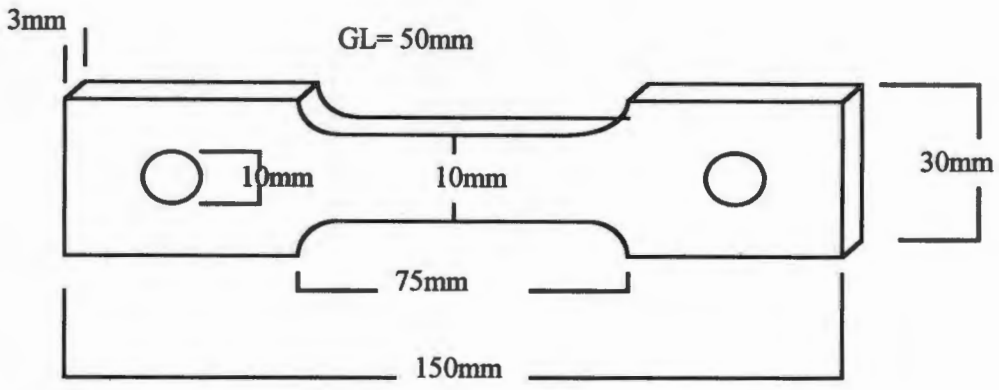

Fig 3.2: Tensile Test Specimen.

3.2.4 DATA ANALYSIS

The true stress-true strain was derived using the well known tensile curve equations in a spreadsheet from the captured load-extension data.

$$\varepsilon_t = \ln(1+\varepsilon_n) \quad .....3.1 \qquad\qquad \sigma_t = \sigma_n(1+\varepsilon_n) \quad .....3.2$$

where ε_t and σ_t are the true strain and true stress respectively and ε_n and σ_n are the engineering strain and engineering stress respectively.

The work hardening rate curve was obtained using linear regression . The equation 3.3 shows the equation used.

$$\frac{\sum \varepsilon\sigma - n\sum \bar{\varepsilon}\bar{\sigma}}{\sum \varepsilon^2 - \sum \bar{\varepsilon}^2} \quad .....3.3$$

One hundred points were regressed to obtain the instantaneous gradient which when plotted for all the points against strain gives the $\frac{d\sigma}{d\varepsilon}$ which represents the work hardening rate of the tensile curve.

The maximum uniform elongation (ε_u) was determined from the yield strain up to the point of instability which represents the case where the work hardening rate is equal to the true stress (i.e $\frac{d\sigma}{d\varepsilon} = \sigma_t$). Another method of determining uniform elongation is by using Fang et al's method[28], where the point of instability is determined by plotting H (which is $\frac{d\ln\sigma}{d\varepsilon}$) versus true strain. The ε_u is determined at the point where H=1. The strain hardening exponent (n-value) is determined from a log σ - log ε graph.

Normally this graph yields a straight line whose gradient is equal to the n-value, but metastable austenitic stainless steels yield a curve. This is due to the nature of the work hardening which produces the double n behaviour described by Jackson[25]. Two gradients can be extrapolated from these graphs, but the second is the one that is truly representative of the work hardening behaviour of these metastable austenitic stainless steels because it measures the strain hardening after commencement of transformation.

3.4 DRAWABILITY TESTS

As drawability could not be determined from the uniaxial tensile test results (no r-value tests were performed) and also due to the need for a simulative test to enable us to study the formability under conditions simulating production lines, a biaxial drawing test was performed. The Swift cup test is the most widely employed drawability test. For this report, a derivative of the Swift test, known as the Engelhardt test, was utilised.

In order to determine the blank diameter at which failure occurs, a trial and error method is employed where blanks of increasing diameter are drawn until one fails. This process is time consuming, but it can be shortened if a good estimate of the LDR is available (for most materials it is usually 2 ± 0.2). Typically 4 to 10 blanks of varying diameter give an acceptable LDR. Attempts have been made to short cut the trial and error method with 2 and 3 blank test. The oldest method was by Scmidt[46] where two subcritical size cups are drawn and loads are plotted versus D/d (where D is the blank diameter and d is the punch diameter). An oversize blank is then drawn to failure and the failure load read from the machine. The intersection of the failure load line with the straight line regression graph of maximum drawing force versus blank diameter for the subcritical cups, is taken to be the LDR. This technique does not yield sufficiently accurate results because the failure load is not constant. Engelhardt devised a single cup test which suffers from similar difficulties, hence the trial and error method remains the only reliable method for calculating the LDR. A single blank LDR test method has been attempted, its advantages are that it is quick and uses less material but it is not very accurate[58]. The Engelhardt test which was used in this investigation is described below.

3.4.1 THE ENGELHARDT TEST

The standard test for drawability is the Swift cup test, but the punch used in this test is 50 mm in diameter and thus it would be wasteful on material. The Engelhardt test was chosen because its smaller (32 mm diameter) punch would allow less material to be used while giving a good prediction of drawability. Figure 3.4 shows a schematic setup of the Engelhardt test.

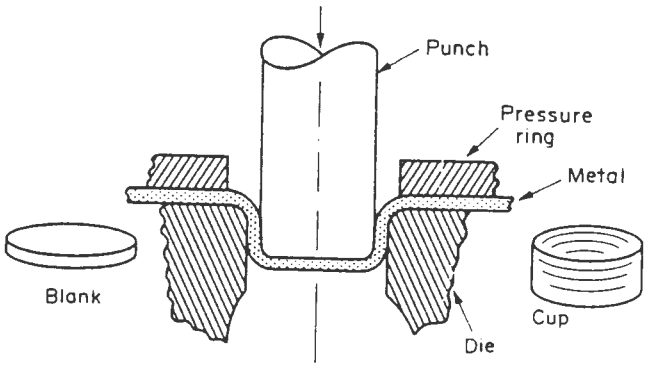

Fig 3.3: Schematic setup of the Engelhardt test.

An Erikssen machine at Columbus Stainless was used for drawability tests. Before testing, each of the 1 mm thick sheets was wrapped in a special polythene lubricant (which was one of the reasons for pickling). The blank holder force (BHF) was then calculated and set on the machine. The BHF is calculated using equation 3.4

$$BHF = \frac{\pi}{4}\left(D^2 - d^2\right)\frac{\sigma_y + \sigma_u}{200} \quad ...3.4$$

where D is the blank diameter, d is the punch diameter σ_u is the ultimate tensile strength and σ_y is the yield stress.

A BHF of 20 kN was calculated to be sufficient for these steels. The BHF is important because too low a BHF causes wrinkling, while too high a BHF leads to early fracture near the cup bottom. A test was performed to determine the blank diameter at which fracture occurs, and this was found to be at a blank diameter of 75 mm. Subsequently four blanks of 50, 60, 65 and 75 mm were chosen for the test. The test speed was kept constant throughout the test. A 304 stainless steel which was from the production line was used as a control sample.

3.4.2 CALCULATION OF LDR

The test data gathered from the Erikssen machine gave the force at which the cup was either drawn through or failed (in the case of the 75 mm blanks). A regression graph was drawn using spreadsheet data of load versus blank diameter for the sub-critical cups. A perpendicular dropped from the point of intersection of this line with the failure load gives the value D along the horizontal axis. The LDR is calculated as

$$LDR = \frac{D}{d_o} \quad ...3.5$$

A typical LDR graph is given in fig 3.4 below.

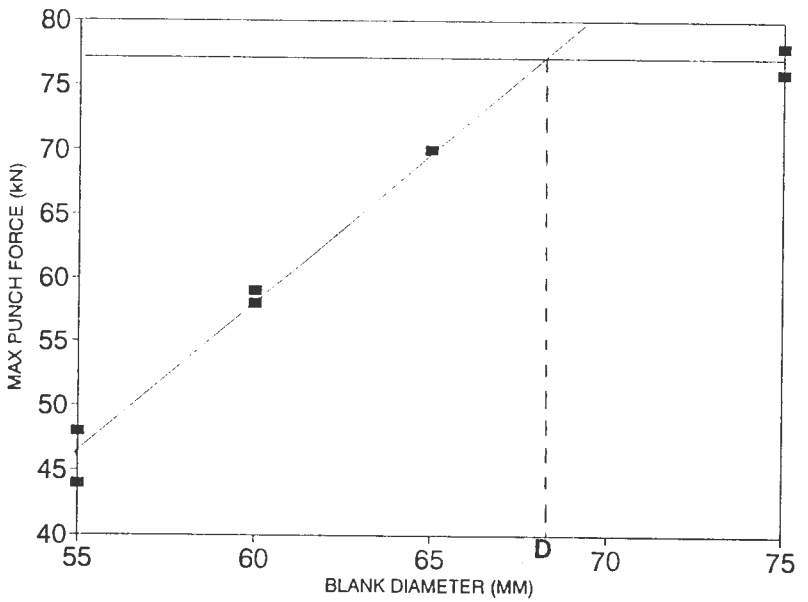

Fig 3.4: A graph for calculation of the LDR of AISI 304 stainless steel

The amount of martensite induced in the cups during drawability tests was determined with aid of a magnetic response machine[60]. Although this machine has not been calibrated, it is known that voltage response increases with the amount of deformation induced martensite. Since absolute values of martensite could not be determined by this method, it was used only for qualitative comparison.

3.5 CAVITATION EROSION

Cavitation erosion testing was performed in order to ascertain the role of TRIP in the wear resistance of these alloys. It has been found in earlier work that most TRIP steels exhibit low rates of erosion due to transformation.

3.5.1 CAVITATION TESTING APPARATUS

There are various apparatus for simulating cavitation wear systems; for example, the rotating disc simulates conditions in turbomachinery and pumps, while the vibratory cavitation rig simulates wear in vibrating machines such as water-cooled internal combustion engines. The advantage of the vibratory rig is that it is compact, easy to use and produces rapid results. The intensity of erosion can be easily controlled in this equipment. The disadvantage is that it can only simulate cavitation wear in vibratory systems.

Figure 3.5 shows the equipment used for cavitation. Before testing, each of the specimens was solution treated and pickled. The usual surface treatment such as fine diamond-paste polishing normally done on cavitation specimens was avoided because it is known that polishing induces martensite on the surface of metastable austenitic stainless steels. The 12 mm square specimens were cut from the 1 mm thick sheets and clamped on to the rig with aid of a perspex spacer.

The distance between the titanium horn tip and the specimen was set at 0.35 mm with a modified micrometer. This distance is necessary in order to ensure optimum cavitation of the specimen.

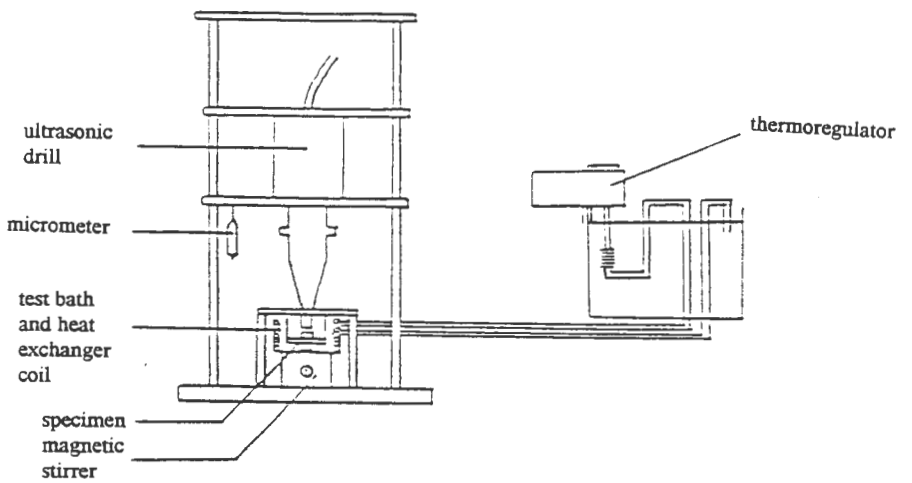

Fig 3.5: The cavitation erosion test rig.

The Ultrasonic horns were warmed up for one and a half hours with a new or refaced tip (tips are replaced after every eight hours) after adding fresh cooling water. The temperature of the equipment was kept below 30°C by a glass heat exchanger. A pre-weighed specimen (weighed on a chemical balance to an accuracy of 0.1 mg) was mounted on the rig before testing. After a suitable time, the specimen was changed (every 30 minutes for the first hour, then after 1 hour for the next 5 hours and finally every 2 hours for the final 8 hours). A 14-hour test run was deemed suitable for characterising the cavitation wear of these stainless steels.

3.6 X-RAY DIFFRACTOMETRY

The complex morphology of the deformation induced martensite militates against easy measurement of the volume fraction of martensite and austenite in a transformed TRIP alloy. It is difficult to distinguish individual martensite grains under the light microscope because martensite plates occurring as sheaves or elongated clusters are too small to be resolved individually. It has been found that optical microscopy of martensite indicates greater amounts of martensite than actually exists. There are various other ways of determining the volume fraction of martensite, and these include the magnetic balance and electrical response devices. However, the most accurate method of determining volume fraction martensite is x-ray diffractometry (XRD). The advantage of XRD is that no set calibration of samples is required. Its disadvantages are the cost of the equipment and the time it takes to obtain accurate values of the volume fraction martensite.

3.6.1 CALCULATION OF PHASE VOLUME FRACTIONS

The diffraction pattern of an irradiated sample is predicted using Bragg's law

$$n\lambda = 2d \sin\theta \quad .....3.6$$

Where n is an integer, λ is the wavelength, d is the interplanar spacing and θ is the angle between the atomic plane and the x-ray beam.

X-ray intensity (measured from the peak heights on the x-ray plot) of each phase is not proportional to the peak area. The volume fraction of each phase is therefore calculated using the area under the peak rather than the peak height. Dickson[59] determined a texture parameter (P) calculated from values of I_{hkl} and R_{hkl} to calculate

the type and intensity of preferred orientation. Using the P values shows that large errors can occur by considering too few peaks for each phase, especially in heavily cold rolled material. As many peaks as possible should be included to minimise errors, but practical limitations such as peak overlap limit the number of peaks that can be resolved. Dickson advocates that three peaks for each phase can produce a result within the limits of experimental error. In this experiment, some of the α' (martensite) peaks had overlap and therefore only two peaks could be used. The phase overlap occurred mostly on the $310\alpha'$ peaks with the MoKα tube. Schmid[2] observed that if only the 220γ and the 311γ were used for the austenite phase volume fraction, there would be discrepancy in the results because the martensite formed during tensile testing does not have the same preferred orientation with that of a cold rolled steel. The peaks used in this reaseach are given below.

Peak	Bragg Angle ($^\circ\theta$)	R_{hkl}
$200\alpha'$	32.5	32
$211\alpha'$	41.2	61
$310\alpha'$	58.0	19
$200\gamma'$	25.4	82
$220\gamma'$	37.3	44
$311\gamma'$	45.5	51

Table 3.2: Bragg angles and R-factors of the three austenite and three martensite peaks, which were used for the MoKα radiation.

Once the peaks were resolved, the volume percent martensite was calculated using equation 3.7[59].

$$V\alpha' = \frac{\frac{1}{n}\sum \frac{I_{\alpha'}}{R_{\alpha'}}}{\frac{1}{n}\sum \frac{I_{\alpha'}}{R_{\alpha'}} + \frac{1}{n}\sum \frac{I_{\gamma'}}{R_{\gamma'}}} \quad \text{.....3.7}$$

Where n is the number of peaks included in the calculation. The error margin in these calculations is within $\pm$ 3 percent.

In order to resolve the peaks, x-ray data was captured on computer and plotted using a spreadsheet package to produce an XRD plot. Peak and background angles were determined as illustrated in figure 3.6. The background was calculated using two methods:

- A straight line was fitted through the left and right backgrounds.
- A polynomial was fitted on the background.

Two integrated peak areas were obtained: one corresponding to the total area, minus the background fitted with the straight line; the other to the total area minus the background fitted with the polynomial. An average of the two areas then gave the integrated intensity corrected for background.

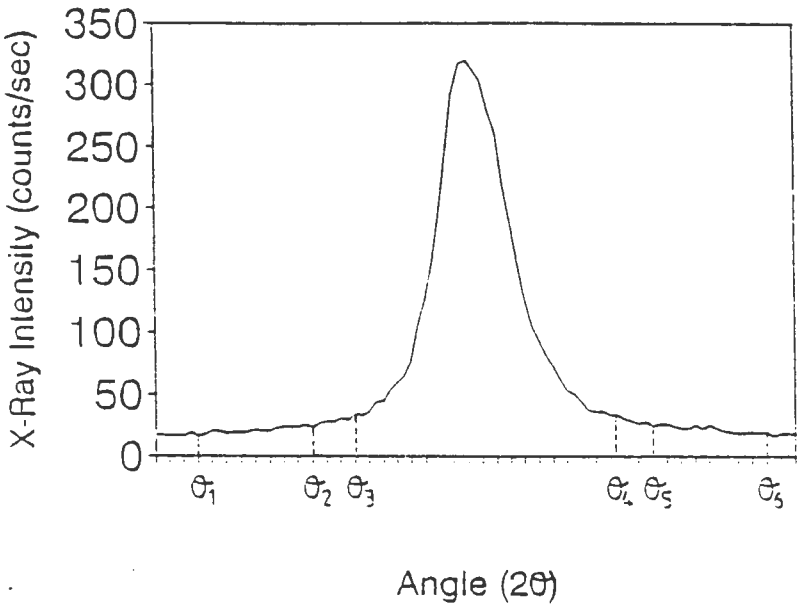

Fig 3.6: Determination of the left and right backgrounds (θ_1, θ_2, θ_5 and θ_6) as well as the left and right peak angles(θ_3 and θ_4).

3.6.2 INSTRUMENT SETTINGS

A Phillips x-ray generator with a parafocussing goniometer/detector system was used for the x-ray diffractometry. The x-ray machine's sample holder has automatic settings for the filter and slits. It was established in earlier work[2] that MoKα radiation was the best means of determining the crystal structure of the austenitic stainless steels. Voltage and current settings were optimised to protect the system from high loading of the x-ray tube which can lead to filament heating and subsequent spectrum contamination. The instrument settings are given below.

Current	30 mA
Voltage	40 kV
Start Angle	18°
End Angle	48°
Step Interval	0.1
Count Time	10 seconds
Radiation	Mo Kα

Samples used for XRD had to be polished down to 1 micron. This polishing was found to induce martensite on the surface of the samples so that electropolishing was necessary before carrying out XRD tests. X-ray diffractometry samples were taken from each end of the fractured tensile specimens. Cavitation specimens were not subjected to any form of surface treatment after cavitation and prior to XRD for fear of removing the cavitation induced martensite (this surface is not very deep).

3.6.3 MAGNETIC DETECTION DEVICE

It is known that austenite is a non magnetic phase while martensite responds to magnetic fields. This property was exploited by many researchers in the development of magnetic balances and magnetic detection devices in order to determine the relative amounts of martensite in the alloys. After deep drawing it was decided to use a magnetic detection device developed at the University of Cape Town. This device measures voltage response as a function of the amount of martensite induced. This method was effective in the case of the drawn cups because the peculiarity of their shapes would make it difficult to produce XRD specimens. The voltage response in millivolts was measured for the side walls and the bottom of the cups. The double coil magnetic device used in this study is described elsewhere[60].

3.7 ELECTROPOLISHING AND ELECTRO-ETCHING

3.7.1 ELECTROPOLISHING

Mechanical polishing of metastable austenitic stainless steel surfaces can induce martensite under suitable conditions. Therefore the resultant surface is not a true representation of the bulk microstructure. Electrochemical polishing can remove the martensite, but optimum electropolishing conditions of different alloys have to be determined independently.

A specimen which is mounted in thermosetting resin and mechanically polished using 1 micron diamond paste is normally used for electropolishing. The electropolishing solution normally consists of 133 ml glacial acetic acid, 25 grams of chromic acid (CrO_3) and 7 ml water. The electrolyte is continuously stirred to prevent bubble formation (which leads to uneven polishing) and avoid localised heating. The temperature was retained at between 15 and 20°C by immersing the solution in an ice and water bath. The specimen is made anodic by clamping the edge with crocodile clips, taking care not to damage the surface of the specimen. The voltage which was found to produce the best results for electropolishing these steels was 20 volts and a polishing time of four minutes gave the minimum amount of surface martensite without causing an electropolishing induced martensite[2]. The electrolyte was replaced after every hour of use because old electrolyte leads to an increase in current density and less efficient polishing.

3.7.2 ELECTRO-ETCHING

Ten percent oxalic acid solution is a suitable electroetching electrolyte for most austenitic stainless steels and it gave good results in the test alloys. No heating of the solution was necessary because a satisfactory etch was achieved after 75 to 90 seconds of electroetching. The specimen was made the anode and a voltage of 11 volts gave optimum polishing conditions.

3.7.3 TINT ETCHING

The presence of δ-ferrite was investigated using the Lictenegger-Bloech colour etch 1. The solution was prepared as follows:

- 20g ammonium bifluoride
- 0.5g potassium bisulphate
- 100 ml hot distilled water

An etching time of 1 to 5 minutes was employed. This tint etch detects even the smallest δ-ferrite precipitates in the matrix because austenite and martensite phases are coloured blue or brown while the delta ferrite remains white. A Nikon microscope was used for the examination of these microstructures.

3.8 METALLOGRAPHY

The Reichert MeF3a was used for light microscopy to examine microstructures, while cavitation eroded surfaces were examined on the Cambridge Stereoscan 200 scanning electron microscope.

3.8.1 LIGHT MICROSCOPY

The light micrographs of polished heat treated and tensile tested materials were obtained to qualitatively assess the extent of martensitic transformation which occurred during the straining of the steels. The ASTM grain size number of the heat treated austenitic steels was calculated using the ASTM standard E112-85, which is the Heyn linear intercept technique[61]. The equation for the grain size number is as follows:

$$GSN = -6.64 \log L_3 - 3.298 \quad ....3.8$$

Where GSN is the grain size number and L_3 is the linear intercept= L/(PM).
L= length of the line (in mm), P is the number of grains intersected by the line and M is the magnification.

3.8.2 SCANNING ELECTRON MICROSCOPY

Scanning electron microscopy was used to examine eroded surfaces. The secondary electron images were obtained with an acceleration voltage of 30 kV .

3.9 BULK HARDNESS TESTING

Bulk hardness values are widely used as a quick means of determining the formability of a material. Generally speaking the harder the material, the more difficult it is to form. Despite its speed, the hardness test is the least reliable method of testing the formability of a material, because surface conditions, the flatness of the specimen, test procedure and in the case of metastable alloys, the phase transformation all influence formability to a greater or lesser extent. Despite these drawbacks, the Rockwell hardness test remains a popular fundamental formability test in most production lines due to its simplicity.

Hardness tests were performed on the solution treated samples as a fundamental test of determining their formability. A Vickers hardness test was chosen in order to avoid deformation of the indentor if martensite formed during the test. A load of 50 kgf was selected and the Vickers hardness number was determined by converting the average of the two diagonals of the square formed by the indentor using tables.

CHAPTER 4: RESULTS

This chapter presents systematically the microstructures of the materials in both solution-treated and fractured conditions and the results of the tensile testing, formability testing, hardness and cavitation erosion tests. The results of the amount of martensite formed during testing, using methods such as XRD and the magnetic detection device, are also presented.

4.1 MICROSTRUCTURES

4.1.1 MICROSTRUCTURES OF SOLUTION TREATED ALLOYS

Microstructures of the solution treated alloys are shown in the micrographs (fig 4.1 to 4.6). Most of the alloys show surfaces that are fully austenitic and contain very little or no quenching or polishing induced martensite. The alloy 6016Cu0, on the other hand, displays an appreciable amount of surface martensite. This may not be a true reflection of the bulk microstructure because the martensite could be due to the mechanical polishing of the surface of the alloy. Electropolishing was used to reduce the amount of polishing induced martensite.

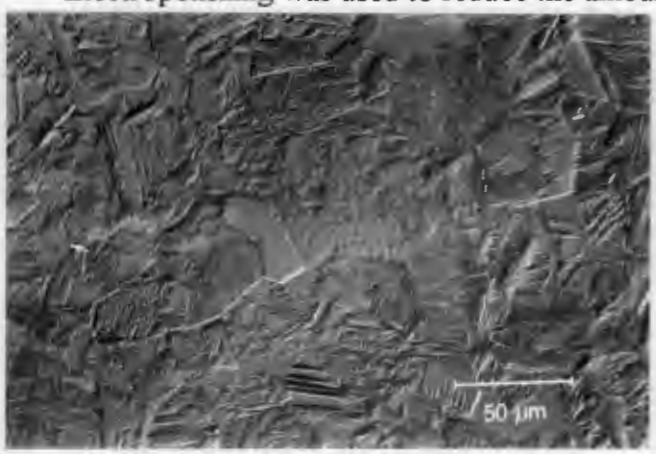

Plate 4.1: A micrograph of alloy 6016Cu0 (89±3% retained austenite)

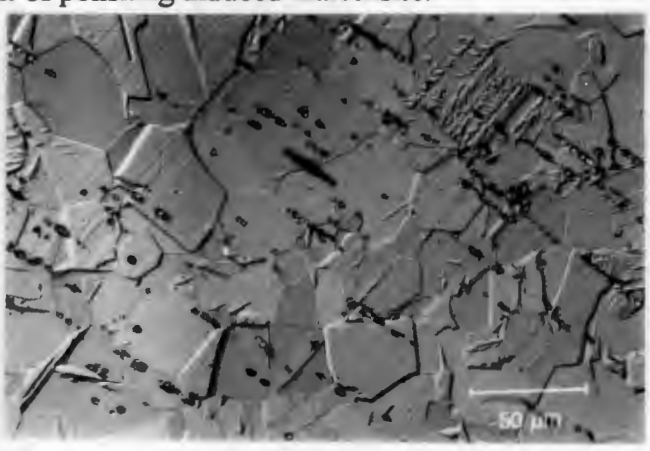

Plate 4.2: A micrograph of alloy 5623Cu0 (95±3% retained austenite)

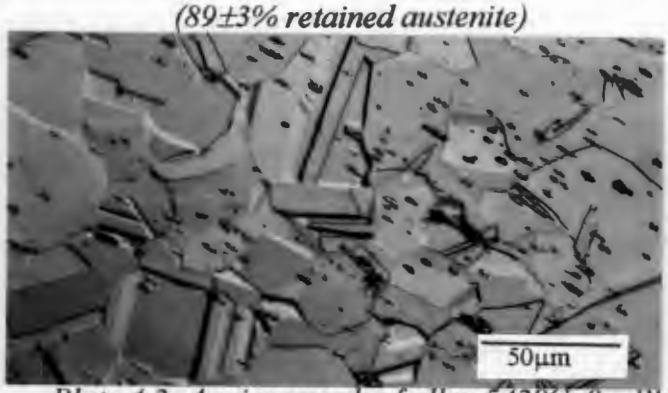

Plate 4.3: A micrograph of alloy 5428Cu0 (96±3% retained austenite)

Plate 4.4: A micrograph of alloy 8630Cu0 (97±3% retained austenite)

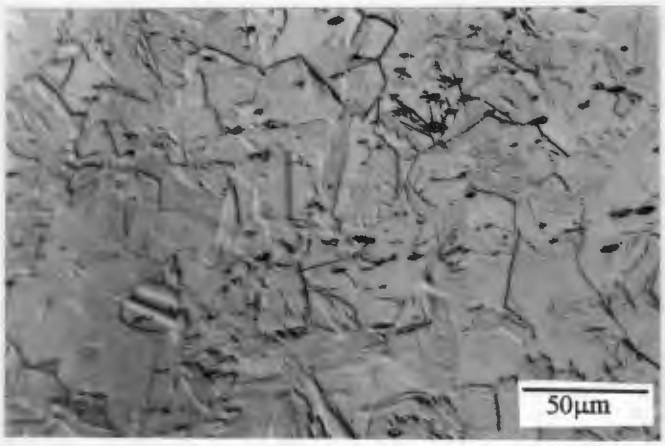

Plate 4.5: A micrograph of alloy 5422Cu13 (93±3% retained austenite)

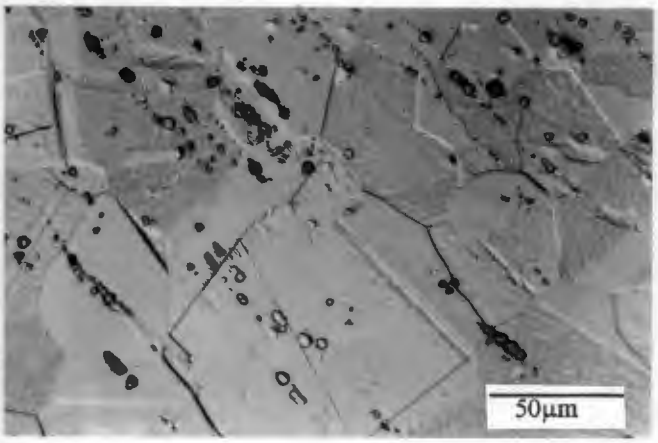

Plate 4.6:A micrograph of alloy 5422Cu33 (97±3% retained austenite)

The percentage retained austenite was measured using x-ray diffractometry.

From these micrographs the grain size of the stainless steels is shown to be different, with the stable steels indicating larger grain sizes than those of metastable alloys. This is supported by the ASTM grain size measurements, which are given in table 4.1. These measurements show that the stable copper alloy 5422Cu33 has the largest grain size. The grain size number affects the Md_{30} temperature as well as mechanical properties such as yield strength.

No delta ferrite was observed in these alloys after using the Litchnegger tint etch which reveals even the smallest amounts of δ-ferrite. Some of the micrographs (plates 4.2, 4.3 and 4.6) show what is believed to be holes in the microstructures which could represent areas where delta ferrite was present but has subsequently been removed during polishing or etching. If this is correct then it may be concluded that very little delta ferrite was present in these alloys and that this amount of delta ferrite will have little influence on tensile properties. It is also possible that some of these particles could be oxides.

The Schaeffler diagram can be used to calculate the amount of ferrite present in the alloy by using chemical composition. The values of Ni and Cr equivalent in table 4.1 indicate that a fully austenitic microstructure should occur in all the alloys after solution treatment. Formation of martensite during quenching should not occur because the Ms temperatures for all the alloys are low therefore the theory that quenching martensite is responsible for the surface appearance of alloy 6016Cu0 is not supported.

Alloy	Ms (°C)	Md_{30} (°C)	Ni eqv	Cr eqv	G.S.N.
6016Cu0	-137	55	11.81	183.47	6.28
5623Cu0	-207	35	12.12	17.92	6.62
5428Cu0	-270	22	12.49	18.80	6.618
8630Cu0	-382	-80	15.76	18.20	5.89
5422Cu13	-265	14	12.23	18.62	7.62
5422Cu33	-206	-30	12.56	18.62	4.92

Table 4.1: Values for the measurement of the propensity to form martensite

From the above figures alloy 8630Cu0 and 5422Cu33 are expected to exhibit stable tensile behaviour due to the low Ms temperature and Md_{30} temperature. Relating the GSN to the Hall-Petch equation, it can be concluded that alloys with high GSN should have a high 0.2% proof stress; this can be an erroneous conclusion because other factors such as chemical composition play an important part in the proof stress of these alloys.

4.1.2 MICROSTRUCTURES OF THE FRACTURED TENSILE SAMPLES

The microstructures of the fractured tensile samples are affected by test temperature and alloy stability. The stability of austenite can be assessed by examining the microstructures of the various samples at low to moderate temperatures (e.g. plates 4.7, 4.9, 4.11, 4.15 etc). At elevated temperatures the martensite rarely forms in these alloys because the Md temperature will have been exceeded (e.g. plates 4.10 and 4.14). There is a difference in the morphology of the deformed austenite and deformation induced martensite. Martensite formation is initiated at the slip-slip interactions, twin boundaries and other defects within the grains. The appearance of the martensitic microstructures shows no distinct grain boundaries because grain boundaries are sites for formation of martensite (e.g. plate 4.7 and 4.15), and thus it is difficult to discern the grain boundaries after transformation.

The deformation mode in the stable alloys is seen to occur mainly by slip and there is little if any transformation to martensite during deformation. The light micrographs of these alloys show distinct slip lines with less surface relief than the martensitic microstructures. This is due to the well-known phenomenon that martensite forms with surface relief. In some alloys, where transformation is not high, small clusters of martensite are observed, which are part of the gradual microstructural evolution during the deformation of metastable alloys. These clusters prove that deformation induced martensite forms gradually in bursts and not in the military manner of the quenching induced martensite.

Plate 4.7: The microstructure of alloy 6016Cu0 tested at 0°C

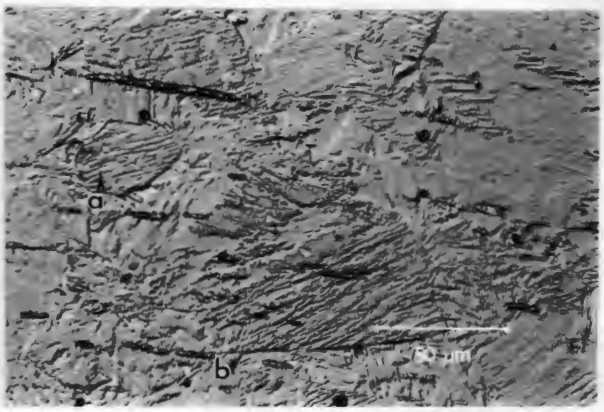

Plate 4.8: Microstucture of alloy 6016Cu0 tested at 40°C

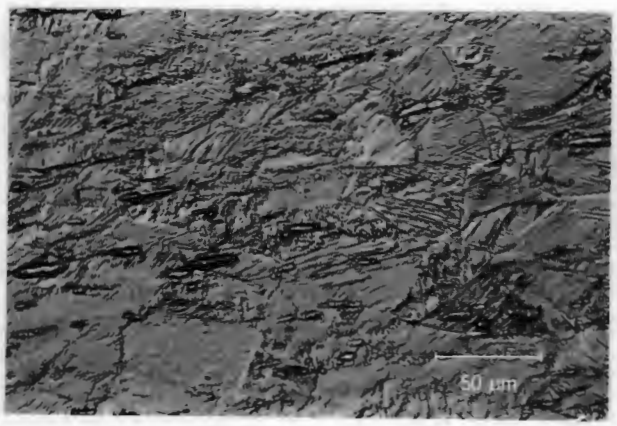

Plate 4.9: Microstructure of alloy 5428Cu0 at 0°C

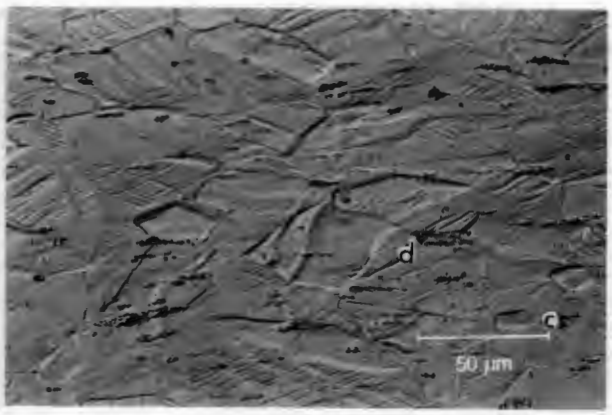

Plate 4.10: Microstructure of alloy 5428Cu0 at 100°C.

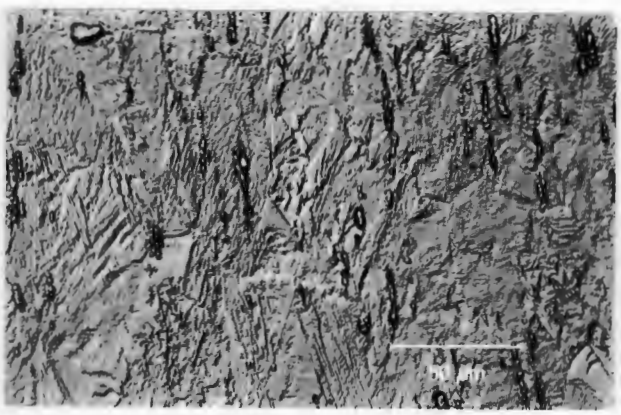

Plate 4.11: Microstructure of alloy 5623Cu0 at room temperature.

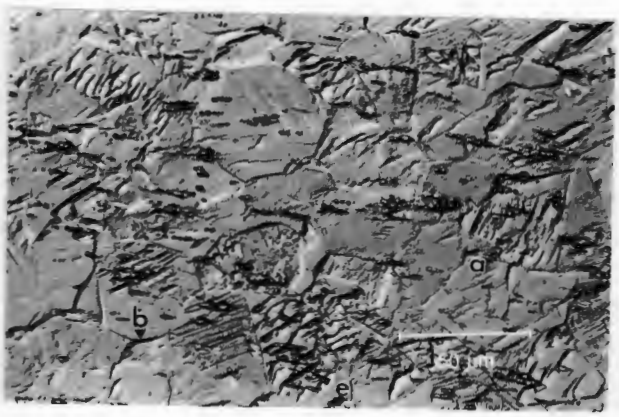

Plate 4.12:Microstructure of alloy 5623Cu0 at 60°C

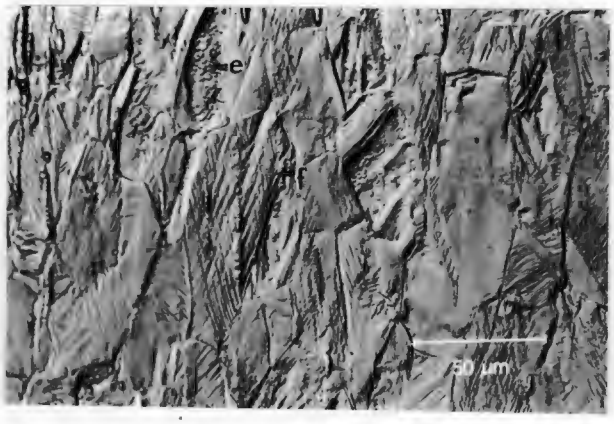

Plate 4.13: Microsturcture of alloy 8630Cu0 Dry ice (-5°C)

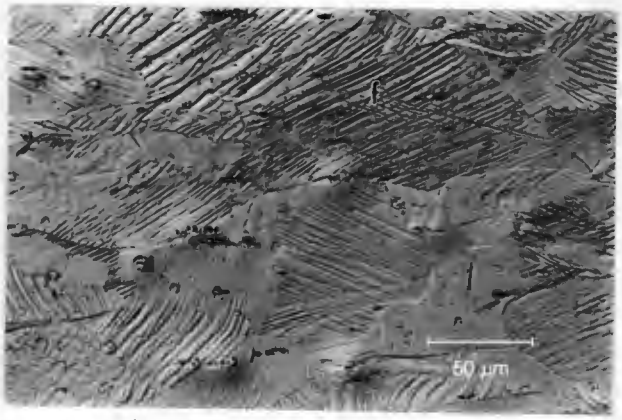

Plate 4.14: Microstructure of alloy 8630Cu0 at 60°C

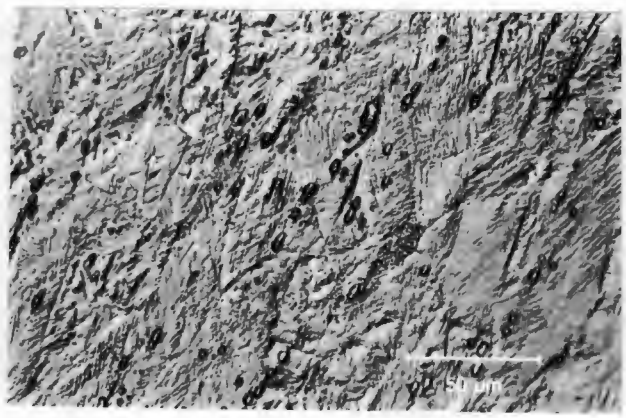

Plate 4.15: Microstructure of alloy 5422Cu13 at 0°C.

Plate 4.16: Microstructure of alloy 5422Cu13 at 40°C

Plate 4.17: Microstructure of alloy 5422Cu33 in dry ice (-5°C)

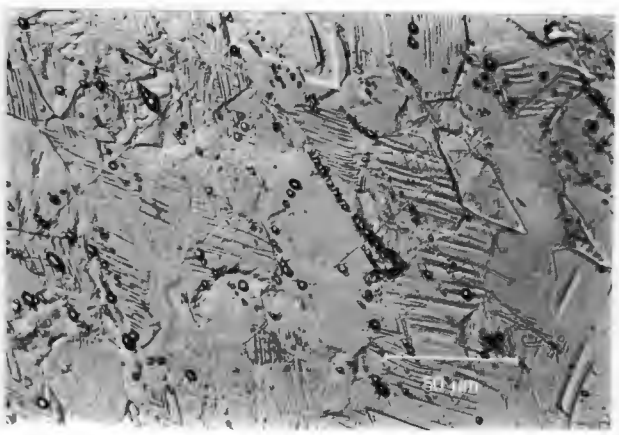

Plate 4.18: Microstructure of alloy 5422Cu33 at room temperature

From the above microstructures we observe that metastable alloys which are deformed at low temperatures form large amounts of martensite due to the morphology of their microstructures. This transformation destroys grain and twin boundaries which are the prime areas for the formation of martensite. This phenomenon is illustrated in plates 4.7, 4.9, 4.11 and 4.15. The metastable alloys which transformed to a lesser extent than the above examples such as those in plates 4.8 and 4.17 exhibit some slip lines (d) along with martensite laths. Their grain boundaries are still visible (b) although deformed. Metastable alloys subjected to high temperature testing (plates 4.10, 4.12 and 4.16) have very little martensite (a), distinct grain boundaries (b) and in some cases even twin boundaries (c). Slip lines dominate in these alloys (d). Plate 4.12 shows some martensite clusters forming (e) and very little grain deformation. There is no difference between stable alloys tested at low or high temperatures, the microstructures show that no martensite is formed and failure is due to slip (f) as seen in plates 4.13 and 4.14 although a few clusters of what might be the initiation of martensite seem to be present (e).

4.2 TENSILE DEFORMATION BEHAVIOUR

Deformation behaviour of the test alloys was studied with the aid of the tensile curves generated from test data. The true stress-true strain curves of the various alloys are useful tools for determining if transformation takes place during a test. A sigmoidal curve indicates the formation of martensite which is usually accompanied by a higher UTS compared to that of stable parabolic curves. The yield strength varies according to temperature, with high yield strengths observed at low temperatures for all the test alloys. An important application of tensile flow curves is that the various parameters obtained from them can be used for predicting formability. Work hardening behaviour is determined by using work hardening rate curves. An important parameter obtained from these curves is the ε_u. The strain at the onset of martensite formation can be roughly predicted from these graphs. The ε_u can also be determined from the H versus ε curves where H=1. These curves also aid in analysing work hardening behaviour of metastable austenitic stainless steels according to the information given on pages 15 and 16.

4.2.1 TENSILE CURVES

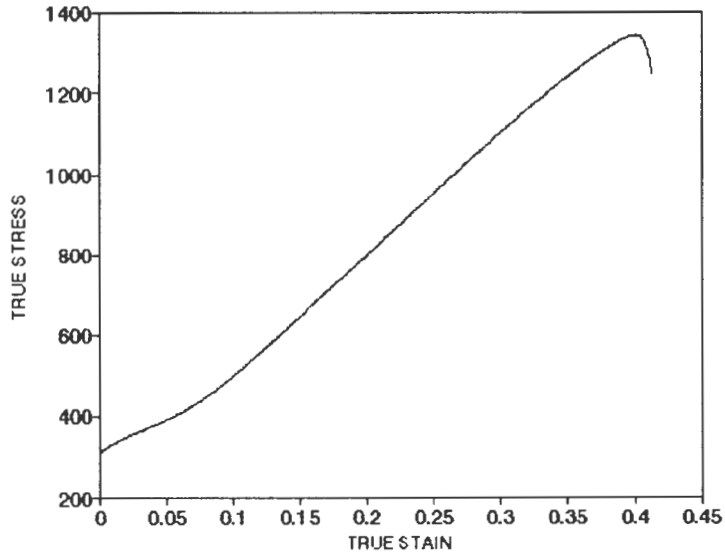

Fig 4.1: Tensile curve for a metastable alloy (alloy 6016Cu0 at 0°C)

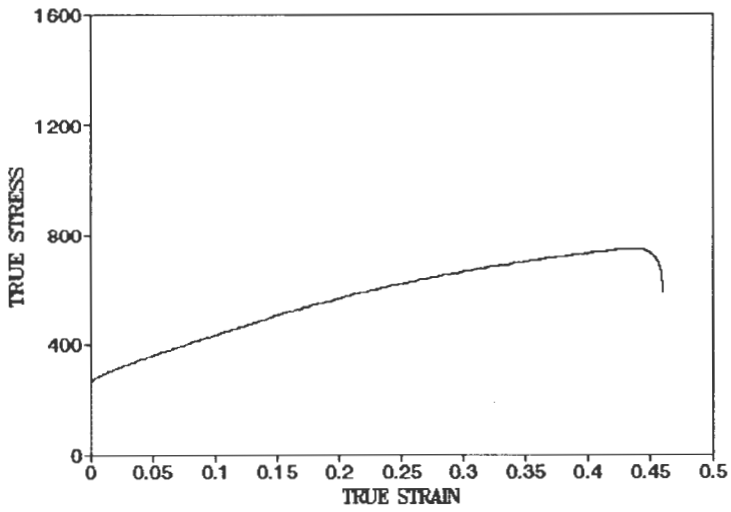

Fig 4.2: Tensile curve for a stable alloy (alloy 8630Cu0 at Room Temperature)

The two types of tensile curves obtained in this study are shown in fig 4.1 and 4.2. Fig 4.1 represents the tensile behaviour of a metastable alloy, in this case a sigmoidal curve, which is a result of transformation to the much stronger martensite phase. This leads to a higher UTS concomitant with an increase in the area under the tensile curve. Meanwhile, the tensile curve of the stable steel gives a hyperbolic curve which obeys the Hollomon equation. The UTS is lower in this case and the area under the curve is reduced. Besides stable steels, this curve also applies to metastable alloys which lose their transformation characteristics at higher temperatures.

4.2.2 WORK-HARDENING RATE BEHAVIOUR

Work hardening rate behaviour is examined using two methods:

- Tensile and $\frac{d\sigma}{d\varepsilon}$ curves
- H versus ε curves from Fang et al[28]

The work hardening rate behaviour is closely related to martensite formation during deformation and it has been ascertained that the onset of positive work hardening occurs as a consequence of martensite formation. In addition to indicating the formation of martensite, the work hardening rate also indicates the rate and strain interval at which the martensite occurs. Fig 4.3 to 4.5 show the work hardening rate and true stress as a function of strain at various temperatures for alloy 6016Cu0. At low temperatures a substantial amount of martensite forms early in these alloys, which is indicated by the low strains at which positive work hardening occurs. The result of this is seen in the low ε_u resulting from too much martensite forming too early during straining. This increases the brittleness of the alloy which leads to early fracture. On the other hand, at high temperatures metastable alloys fracture early due to too little martensite forming too late during straining (see fig 4.5, 4.7 and 4.9). The martensite volume fraction in this case is not large enough to resist incipient necking. Stable steels are not temperature sensitive; a good example of this is illustrated by alloy 8630Cu0 (see fig 4.10 and 4.11). This alloy is not susceptible to phase transformations during deformation due to the high stability of the austenite phase so that the work hardening rate decreases continuously with increasing strain, while the ε_u shows little variation with temperature. On the other hand the UTS of the alloy is very low.

The copper alloyed steels, show greater stability than their non-copper alloyed counterparts (a similar alloy would be 5428Cu0), this is demonstrated in figures 4.8, 4.12 and 4.15. Martensite forms at a retarded rate in these alloys and the high copper alloyed steel (5422Cu33) transforms only at extremely low temperatures (fig 4.14). However it should be noted that where transformation occurs in copper alloyed steels, the ε_u is very high, while the UTS remains below 1000 MPa. In the copper alloyed steels the work hardening rate remains constant over a large variation in strain (see fig 4.12 and 4.15).

Fang and Dahl[28] use another method of ascertaining whether martensite forms in metastable austenitic stainless steels. If a plot of H versus ε yields a continuous decrease in H with increasing ε, then the alloy will experience homogeneous deformation (i.e. no formation of martensite) leading to a low ε_u, (where H is equal to 1). Fang and Dahl use the H parameter because this parameter has been derived from first principles to model deformation behaviour in austenitic stainless steels using dislocation motion. Metastable alloys such as 6016Cu0 at 0°C

(see fig 4.17) show an initial decrease in H with increasing ε equivalent to homogeneous deformation of austenite, then a positive H with increasing ε which is a result of inhomogeneous deformation (due to the formation of martensite while there is still some austenite). In the final stages after the maximum H has been reached, deformation becomes homogeneous again (the microstructure is largely martensitic) and will finally end in rupture after necking. The stable alloys 5422Cu33 and the alloys tested at high temperature (both stable and metastable) show a continuous decrease in H. This behaviour is synonymous with homogeneous deformation (deformation of a mainly austenitic microstructure).

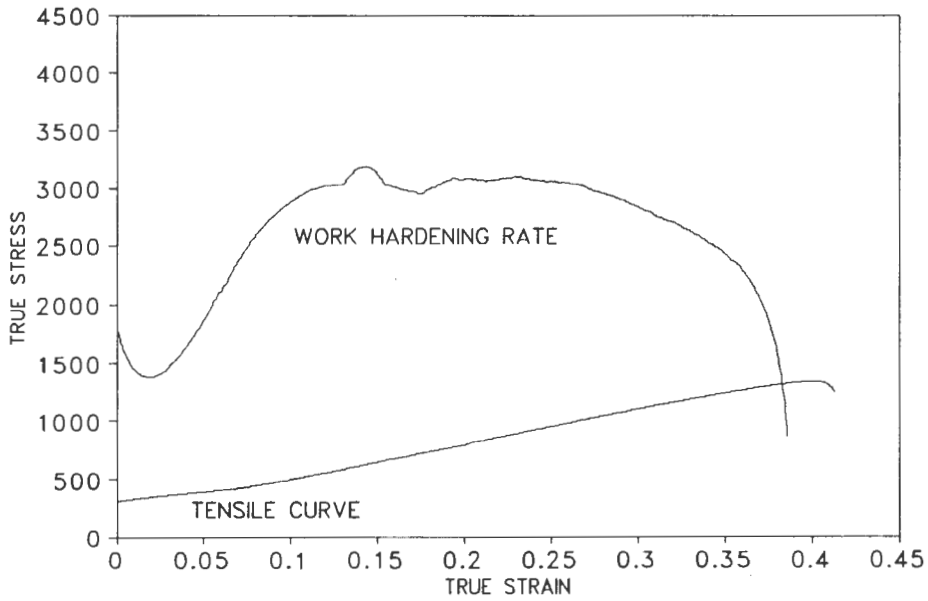

Fig 4.3: Tensile and work hardening rate graph of alloy 6016Cu0 at 0°C

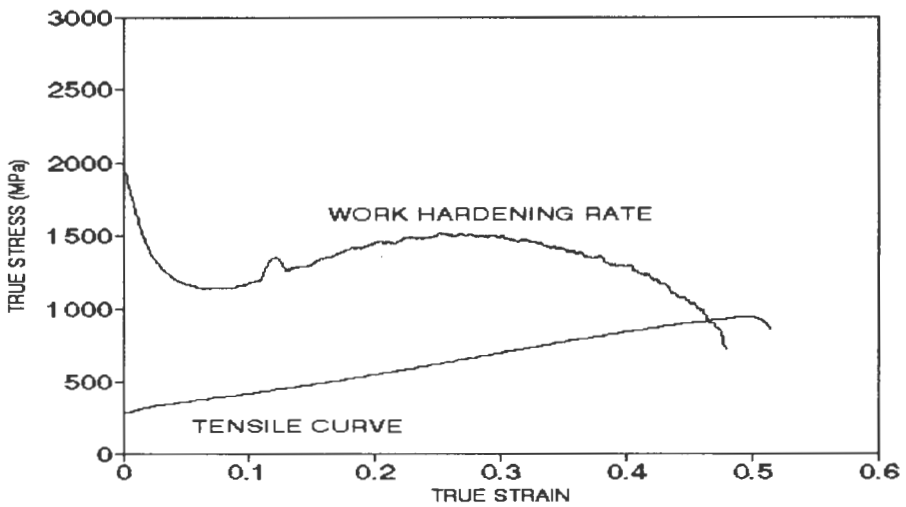

Fig 4.4: Tensile and work hardening rate curves for alloy 6016Cu0 at room temperature

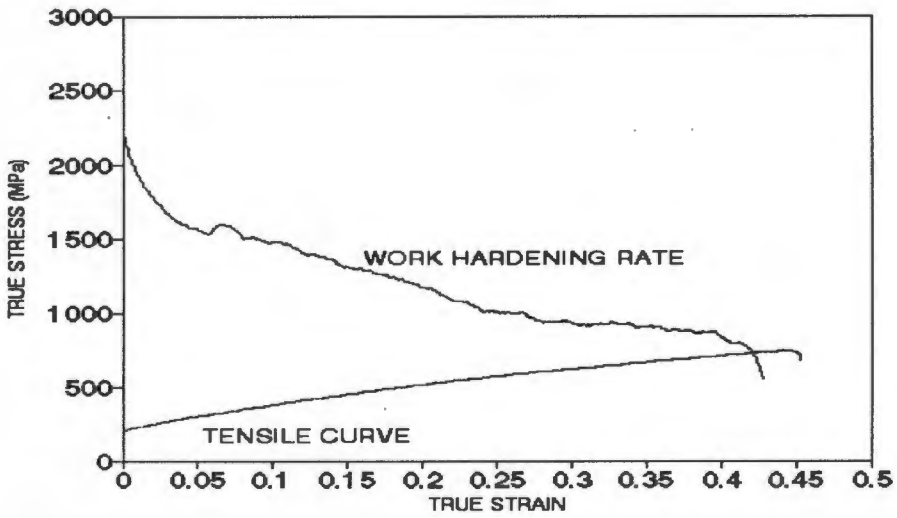

Fig 4.5: Tensile and work hardening rate curves for alloy 6016Cu0 at 100°C

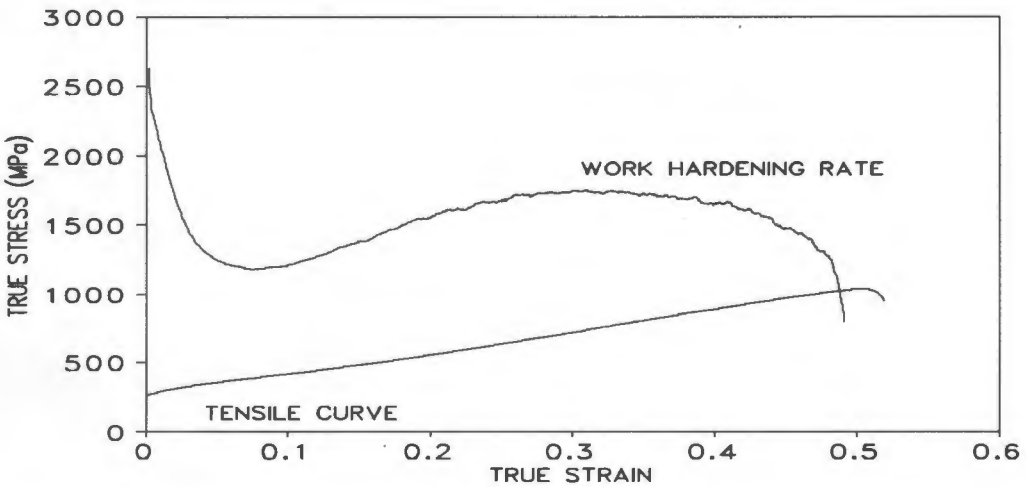

Fig4.6: Tensile and work hardening rate curves for alloy 5623Cu0 at room temperature

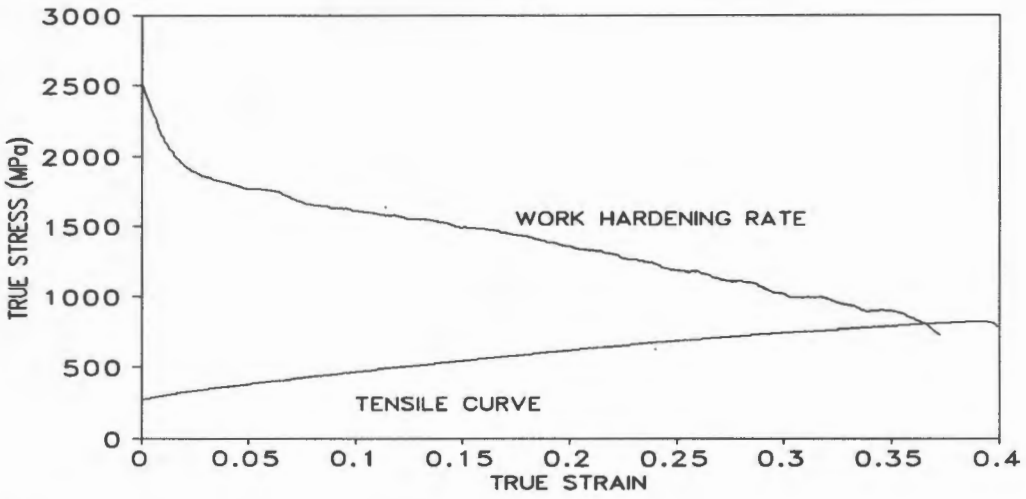

Fig 4.7: Tensile and work hardening rate curves for alloy 5623Cu0 at 100°C

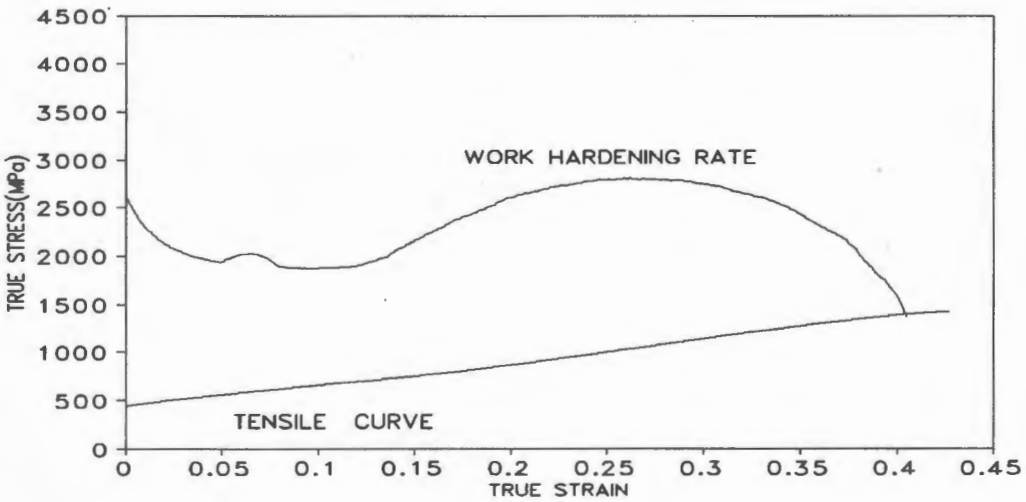

Fig 4.8: Tensile and work hardening rate curves for alloy 5428Cu0 at 0°C

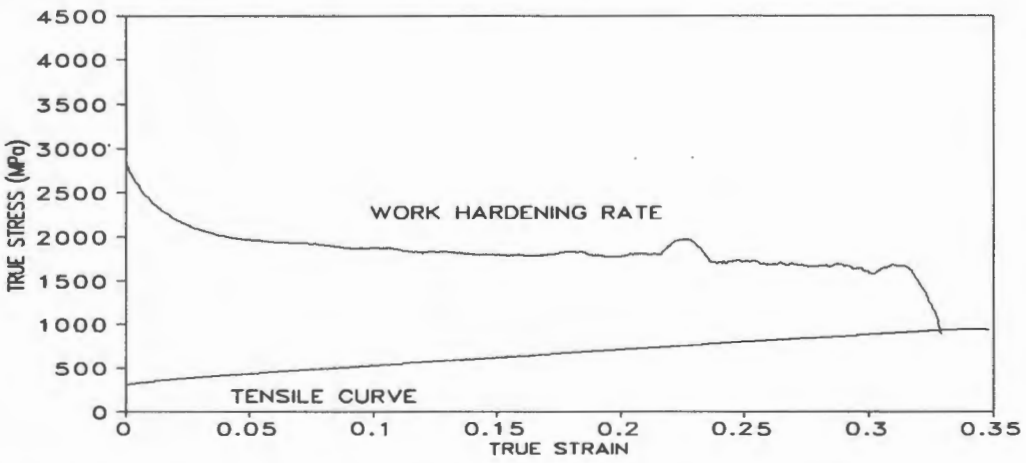

Fig 4.9: Tensile and work hardening rate curves for alloy 5428Cu0 at 60°C

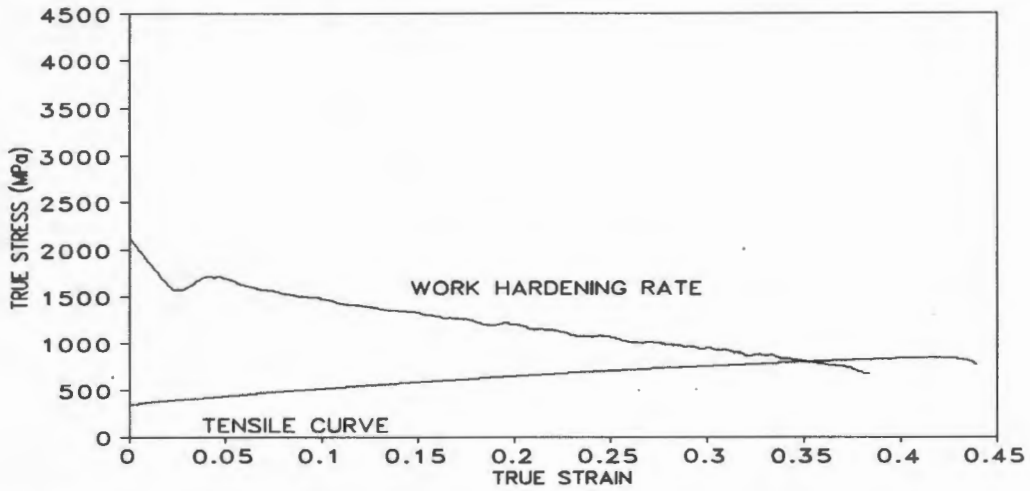

Fig 4.10: Tensile and work hardening rate curves for alloy 8630Cu0 at 0°C

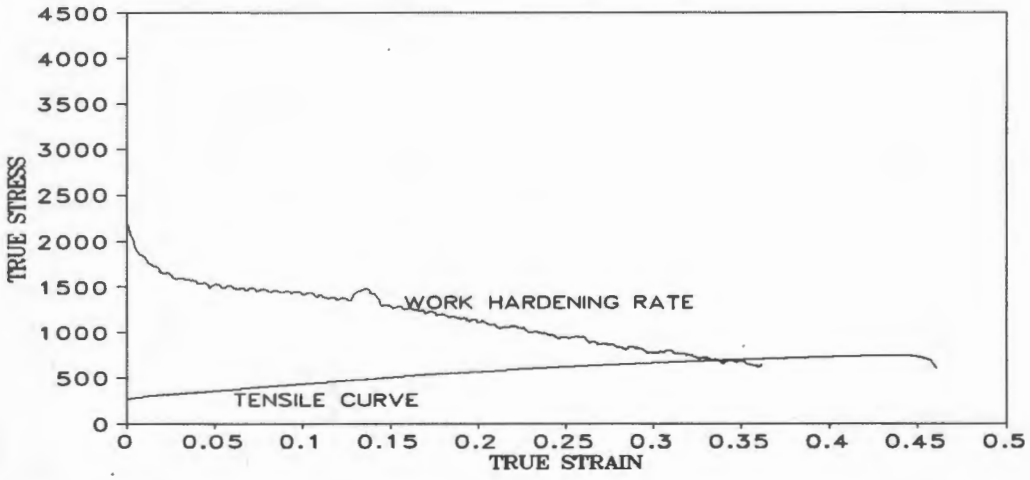

Fig 4.11: Tensile and work hardening rate curves for alloy 8630Cu0 at room temperature

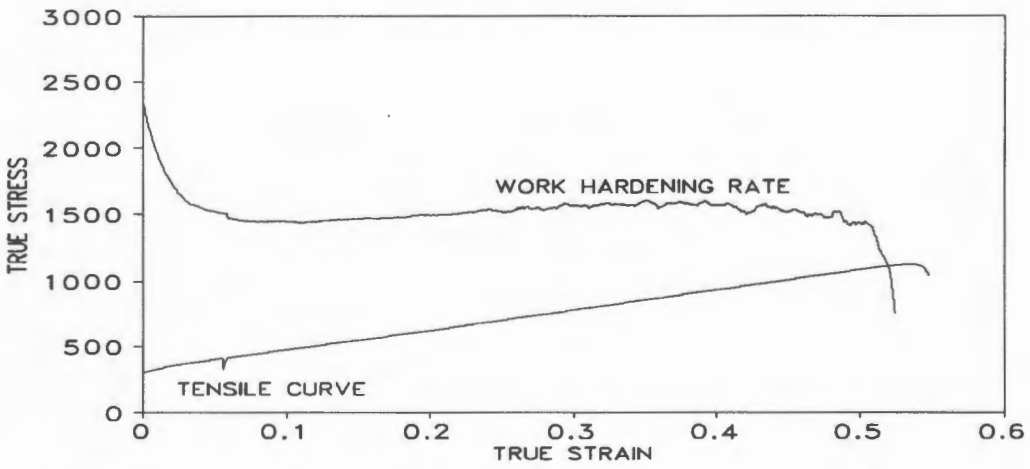

Fig 4.12: Tensile and work hardening rate curves for alloy 5422Cu13 at room temperature

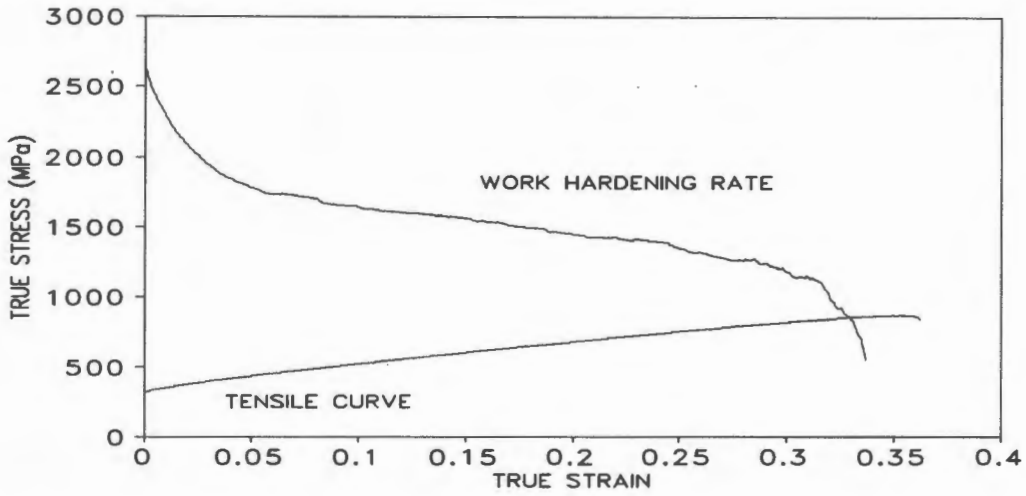

Fig 4.13: Tensile and work hardening rate curves for alloy 5422Cu13 at 40 °C

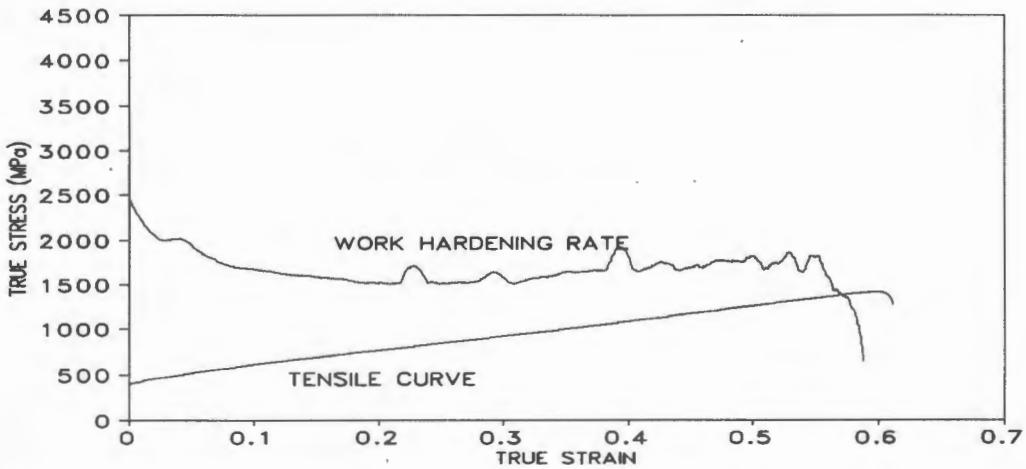

Fig 4.14: Tensile and work hardening rate curves for alloy 5422Cu33 at -5°C

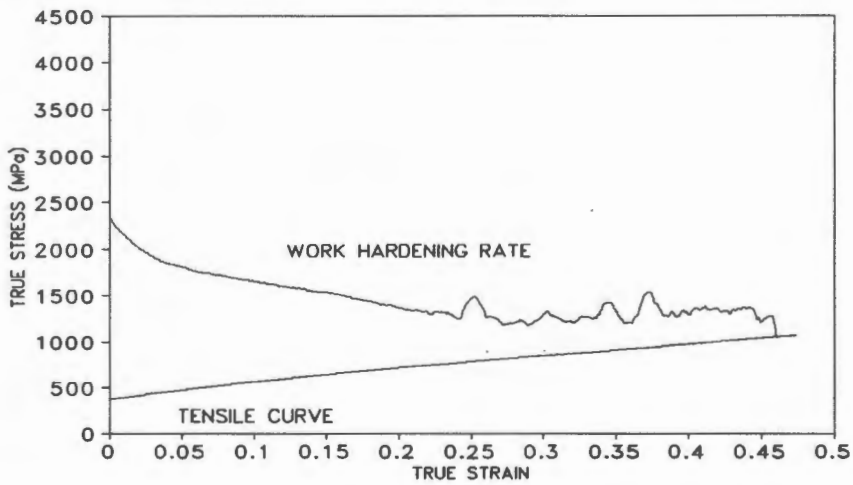

Fig 4.15: Tensile and work hardening rate graphs for alloy 5422Cu33 at 0°C

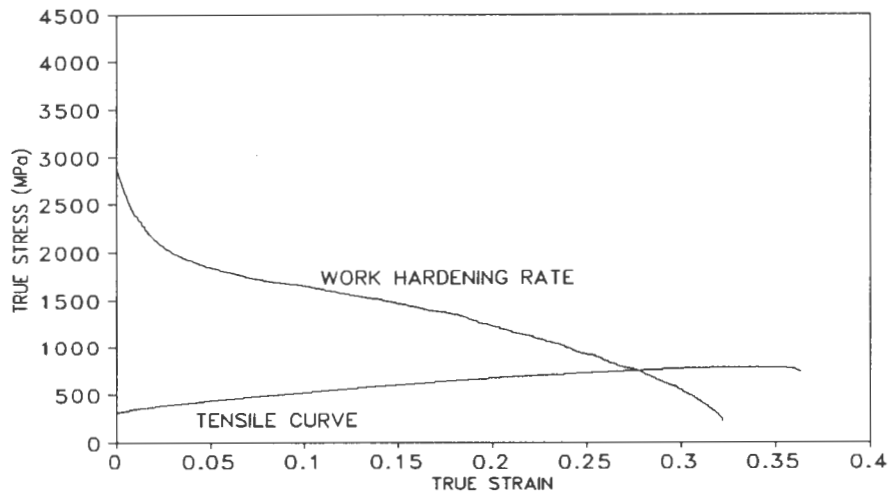

Fig 4.16: Tensile and work hardening rate curves for alloy 5422Cu33 at 60°C

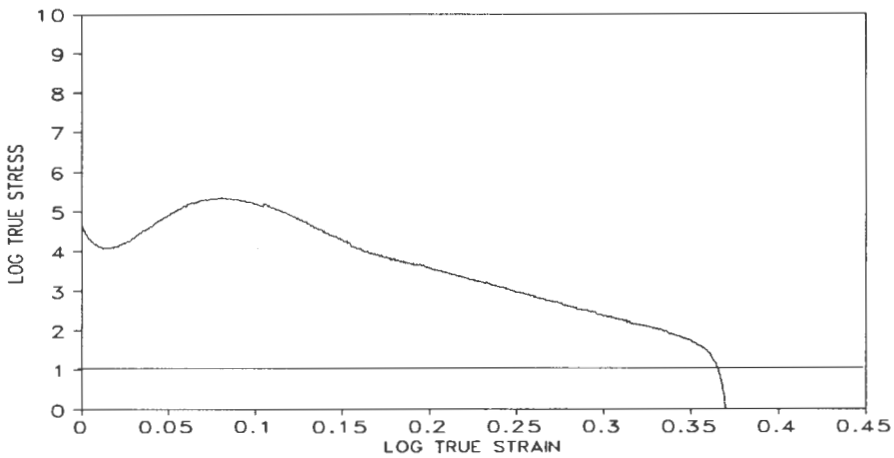

Fig 4.17: An H versus true strain graph for alloy 6016Cu0 at 0°C (highly metastable)

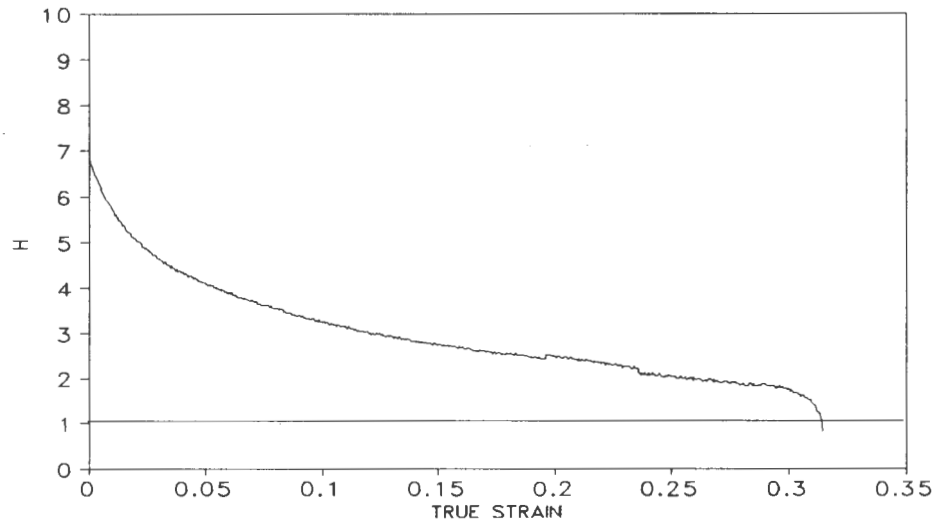

Fig 4.18: A graph of H versus true strain for alloy 6016Cu0 at 60°C (metastable steel at high temperature behaviour similar to that of a stable steel)

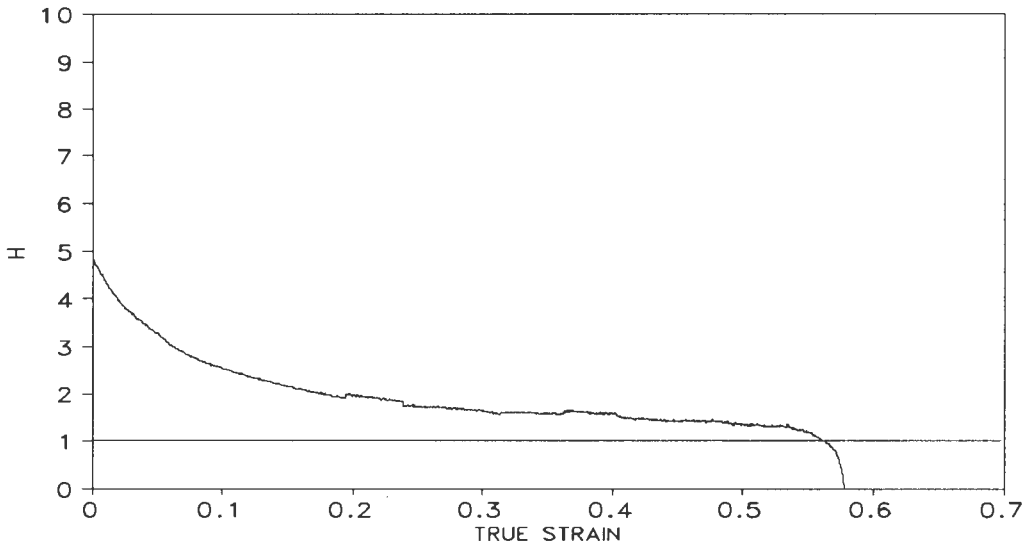

Fig 4.19: A graph of H versus true strain for alloy 5422Cu33 at room temperature

Fluctuations occur in the WHR curves even though tensile curves do not suggest such behaviour. This is explained by the fact that the WHR curves are a calculation of the the derivative of corresponding tensile curves, therefore any minor noise in the tensile curves results in large fluctuations in the WHR curves.

4.2.3 PROPERTIES RELATED TO FORMING

The formability of sheet metals is generally determined with the aid of certain tensile properties which are related to forming, and they are known as formability parameters.

- **The n-value,** as has been stated is calculated from the gradient of the log true stress-log true strain graphs. This property is a measure of a sheet metal's ability to harden with deformation thereby resisting early fracture. For this reason a high n-value is preferred for metal forming. Metastable austenitic stainless steels exhibit double n behaviour (figure 4.20) while stable steels yield a straight line in a plot of log σ-log ε. In the case of metastable steels, the second n value (n_2), which results after transformation, is used as a formability parameter.

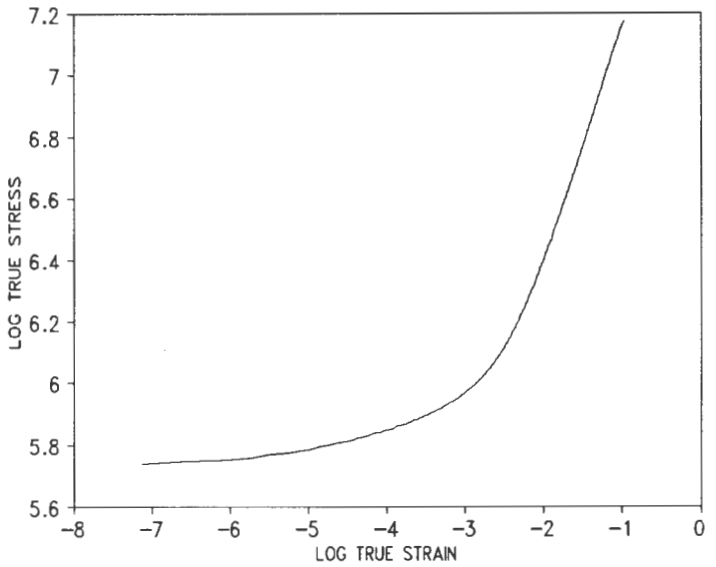

Fig 4.20: A plot of log true stress versus log true strain for a metastable austenitic stainless steel (6016Cu0) showing a curve reminiscent of double n behaviour.

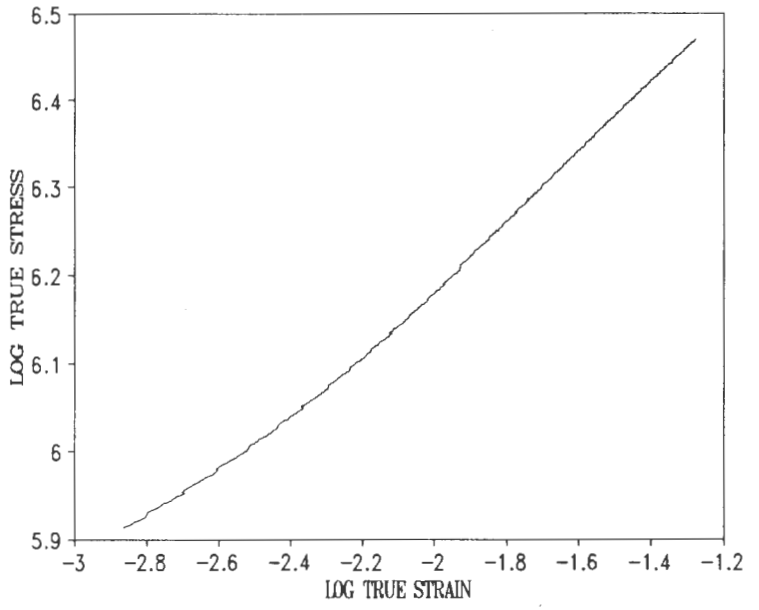

Fig 4.21: A plot of log true stress versus log true strain for a stable steel (8630Cu0).

- **The 0.2% proof stress** is an approximation of the yield point in alloys which do not exhibit a distinct yield point. This stress must be exceeded in all regions of the article being formed in order to develop a permanent set. A low proof stress therefore suggests better formability in a material.

- **The ultimate tensile strength** (UTS) determines the load that can be usefully applied during forming. The UTS can be related to fracture load during deep drawing.

- **The maximum uniform elongation** (ε_u) is a measure of the maximum strain a material can withstand before diffuse necking. A high uniform elongation is desirable for good formability. The four formability parameters discussed above are given in table 4.2 .

Alloy	n-value	ε_u	UTS (MPa)	0.2% Proof Stress (MPa)
6016Cu0	0.753	0.42	950	229
5623Cu0	0.763	0.50	1080	243
5428Cu0	0.647	0.50	1000	279
8630Cu0	0.549	0.40	800	283
5422Cu13	0.674	0.52	950	261
5422Cu33	0.419	0.36	750	233

Table 4.2: Formability parameters from room temperature uniaxial tensile tests.

4.3 DRAWABILITY TESTS

Tests for drawability are a good way of simulating a real metal forming process. In this research, a Swift cupping test was used to determine the LDR of each test alloy which was then compared with that of a standard production 304 stainless steel. The amount of martensite expressed in terms of relative voltage was determined using the magnetic detection device, in which case a high voltage indicates that a large amount of martensite is formed during deep drawing (table 4.3). The appearance of the drawn cups is also mentioned in this section. Delayed fracture occurred in some of the cups about 24 hours after deep drawing (plate 4.20). The variation in the amount of martensite formed on the side walls of the cups and cup bottom was plotted against blank diameter (proportional to fracture force); transformation occurs at a faster rate on the cup bottom than on the side walls (fig 4.23). This result is further confirmed by Ward[62] who modelled the deep drawing of the test alloys using an AISI 304 stainless steel based finite elememt method (see fig 4.22). He found that the concentration of martensite was higher at the cup bottom than on the side walls and the highest concentration of martensite occured at the edge of the cup bottom where failure of the cups occurs. This model can also be used to explain delayed cracking because it shows an uneven distribution of martenisite in areas prone to delayed cracking. This uneven distribution of martensite leads to stress build up and subsequently delayed fracture. Areas which have high martensite contents have darker shading.

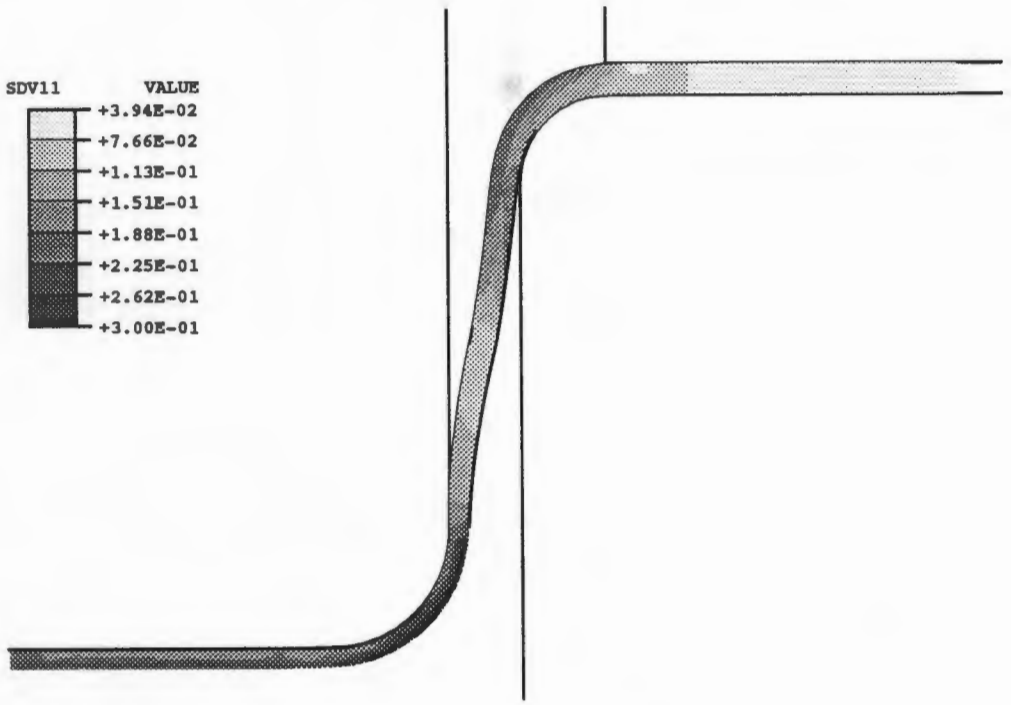

Fig 4.22: Volume fraction martensite in a formed cup. The insert gives the percentage martensite corresponding to the colours in the figure.

Alloy	Limiting Drawing Force (kN)	LDR	Voltage Response (mV)	Comments	UTS
6016Cu0	94	2.21	0.397	No Cracking	950
5623Cu0	95	2.27	0.328	Severe Cracking	1080
5428Cu0	93	2.22	0.282	Severe Cracking	1000
8630Cu0	93	2.14	0.011	No cracking	800
5422Cu13	88	2.15	0.217	No Cracking	950
5422Cu33	67	2.19	0.038	No Cracking	750
Type 304	77	2.12	0.099	Severe Earring	

Table 4.3: Results of the limiting drawing ratio tests for the test alloys and AISI 304.

The relative amount of martensite formed during drawing of the alloys can be compared using the voltage response given in the above table .

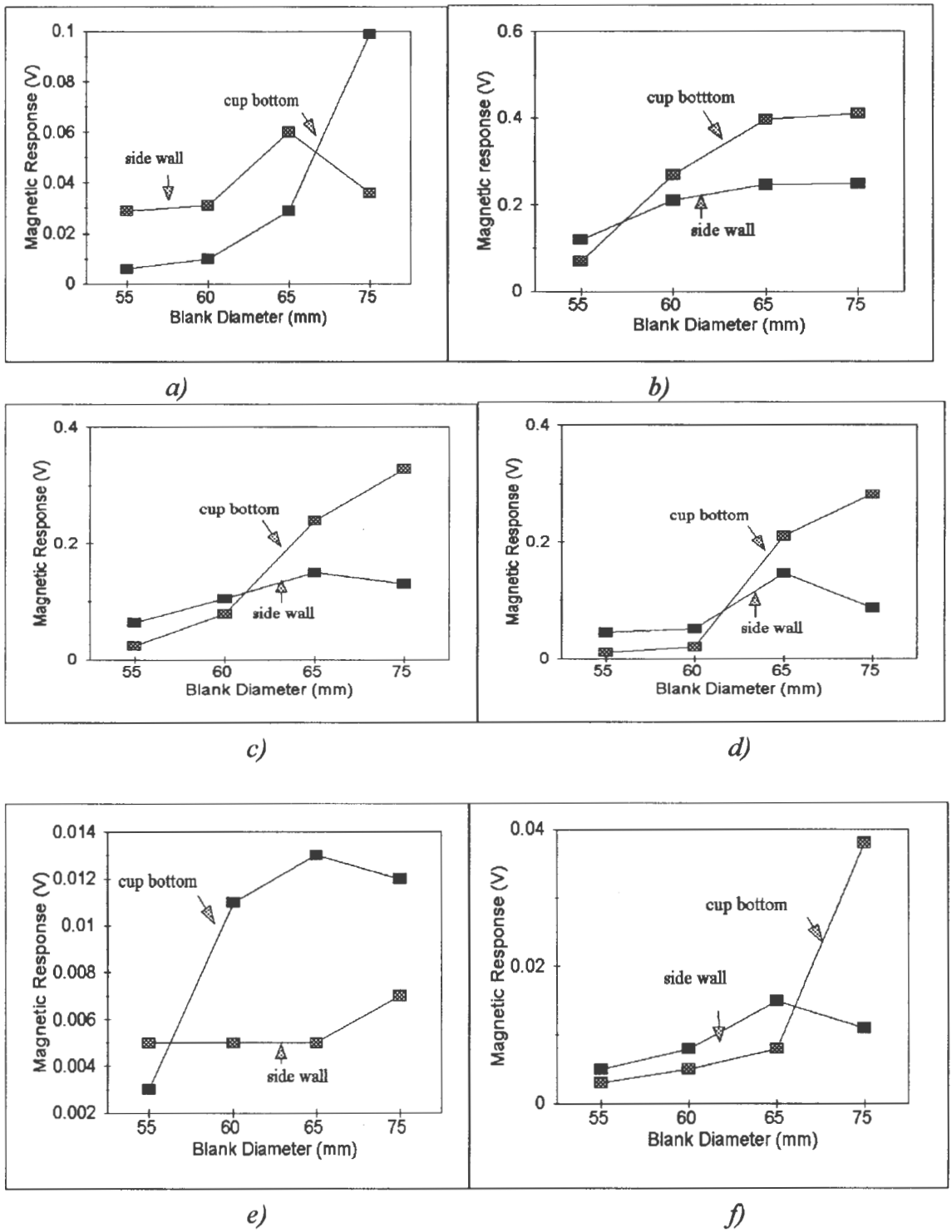

Fig 4.23: Graph of voltage response on the side walls and cup bottom versus blank diameter for the test alloys.

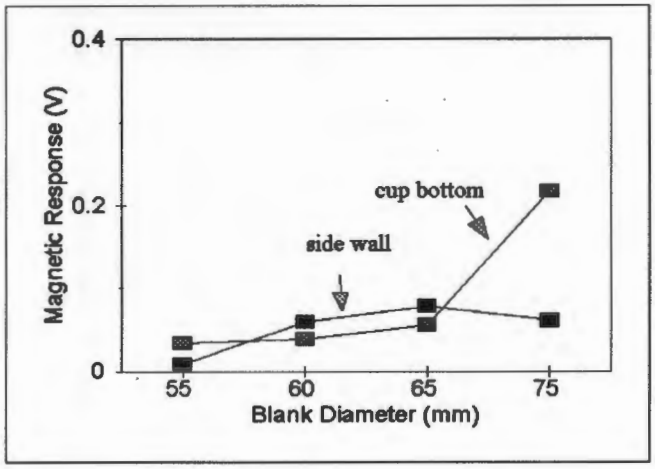

g)

Fig 4.23: Graph of voltage response on the side walls and cup bottom versus blank diameter for the test alloys. a)AISI 304, b)6016Cu0 c)5623Cu0 d)5428Cu0 e)8630Cu0 f)5422Cu33 g)5422Cu13

4.3.1 APPEARANCE OF THE DRAWN CUPS

Plate 4.19: A perfectly drawn through cup (alloy 8630Cu0)

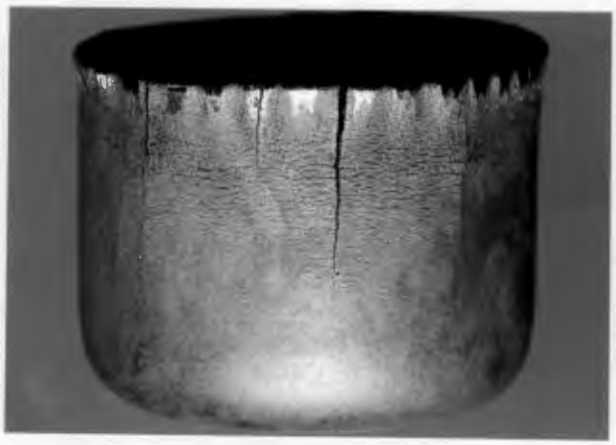

Plate 4.20: A cup showing severe delayed cracking (alloy 5623Cu0)

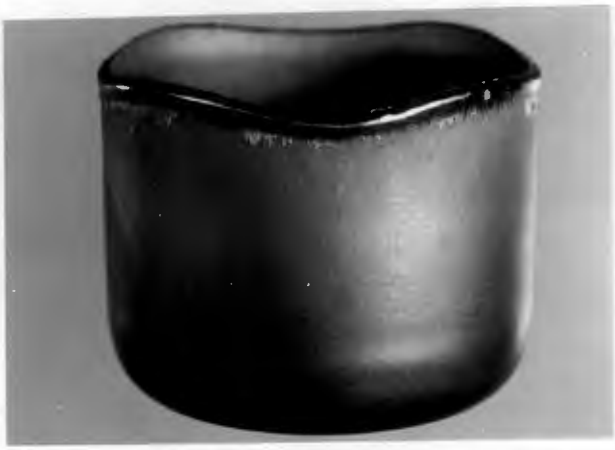

Plate 4.21: A cup showing earring in 304 stainless steels.

Plate 4.22: A cup that failed during drawing due to exceeding the critical drawing force (AISI 304).

Plate 4.23: Slight wrinkling which occurred in some cups after drawing at large blank diameters (alloy 6016Cu0)

AISI 304 (plate 4.21) exhibited earring especially in cups which were drawn at large blank diameters. This is due to the anisotropy of 304 stainless which is not experienced by AISI 301 stainless steel. Slight earring was observed on alloy 5623Cu0 at a blank diameter of 60 mm and on alloy 5428Cu0 at a blank diameter of 65 mm. This is not a common defect in metastable

austenitic stainless steels (type 301) and was probably caused by a material defect such as variation in sheet thickness. Plate 4.22 represents the appearence which was common to all cups that failed due to exceeding the critical drawing force. The failure resulted in rupture at the edge of the bottom of the cup. Plate 4.23 shows wrinkling which is common in plates which are drawn when the blank holder force is not large enough.

4.4 BULK HARDNESS RESULTS

The bulk hardness values of the experimental alloys in the heat treated condition are given in table 4.4. Alloy 5428Cu0 shows the highest hardness value, and this conflicts with the UTS values which are highest for alloy 5623Cu0. Generally a high hardness value indicates poor formability, but it should be noted that although hardness testing is the most popular fundamental test for formability, it is a very inaccurate method for determining this property. The accuracy occurs as a result of its unreliability and the fact that in metastastable stainless steels TRIP affects formability. The effects of TRIP may not occur during hardness testing.

Alloy	Hv_{50}
6016Cu0	229
5623Cu0	225
5428Cu0	271
8630Cu0	210
5422Cu13	224
5422Cu33	179

Table 4.4: Hardness values of solution treated alloys.

4.5 X-RAY DIFFRACTOMETRY RESULTS

The percentage martensite induced during tensile testing at various temperatures is given in figure 4.26, which shows that the resulting reverse S curves are similar to those that have been obtained by various researchers[26,40]. Note the similarity in the curves of alloy 5623Cu0 and 5422Cu13. These two alloys also possess the best tensile properties. Alloy 8630Cu0 experiences no transformation across the whole temperature range, while alloy 6016Cu0 transforms even at high temperatures and reaches saturation levels for martensite at lower temperatures. It has been noted before[26] that 100 percent martensite is not attainable even in the most transformable steels.

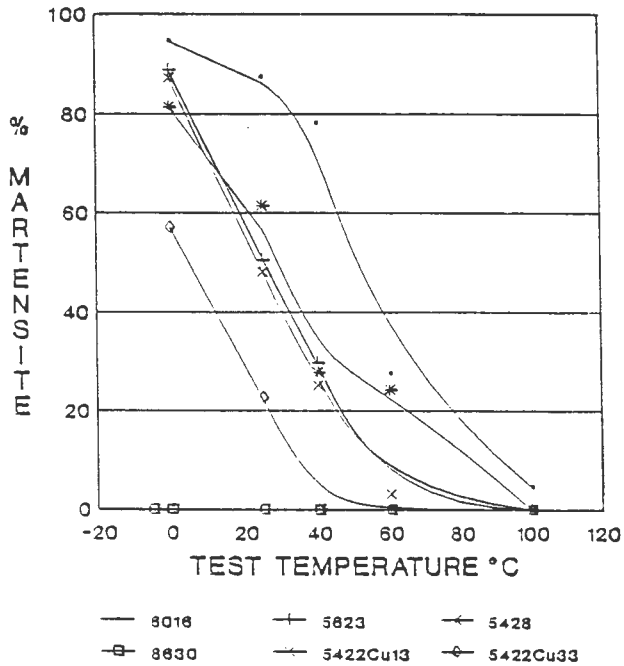

Fig 4.24: Martensite content in fractured specimens as a function of test temperature.

4.6 CAVITATION EROSION RESULTS

There are numerous parameters upon which erosion resistance may be based. These include incubation period (t_o), cumulative weight or volume loss (CWL, CVL), the rate of weight or volume loss in the steady state zone ($\dot{E}$) and time to reach maximum erosion rate (t_{max}). To obtain a true assessment of the material performance it is necessary to use more than one of these parameters, since an evaluation based on one parameter may be misleading. In this study three parameters are used to assess material performance: cumulative volume loss, the incubation period and the rate of volume loss in the steady state period. The wear modes in the alloys are examined by means of scanning electron micrographs.

4.6.1 VOLUME LOSS AND INCUBATION PERIOD

The results of the cavitation erosion tests, presented in graphical form in fig 4.25, show that volume loss is greatest in alloys which are stable (alloys 8630Cu0 and 5422Cu33), while the metastable alloys show increased resistance to cavitation wear. The cavitation wear rate ($\dot{E}$) correlates well with the hardness values of the solution treated alloys, and the alloy 5623Cu0 which has the best TRIP properties, also exhibits the best wear resistance.

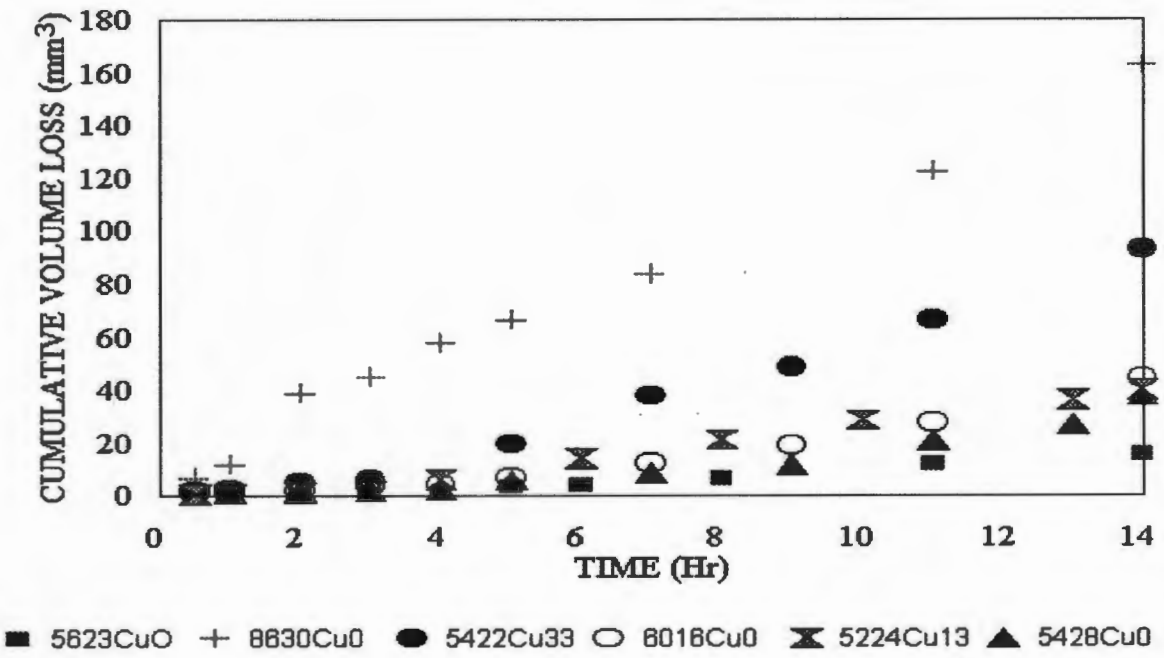

Fig 4.25: Cumulative volume loss versus cavitation time for the test alloys.

The incubation period is defined as the time it takes for the slope of the cumulative volume loss versus time curve to deviate from the average slope of the initial low erosion rate period. The two types of initial erosion behaviour obtained in this work are depicted in fig 4.26. Also depicted in this figure is the method of calculating the rate of volume loss in the steady state ($\dot{E}$). Table 4.5 lists the values of CVL at 14 hours, t_o and $\dot{E}$ for all the alloys.

Alloy	CVL (at 14hrs) (mm^3)	t_o (Hr)	$\dot{E}$ (mm^3/Hr)	Vol % α' after 14 Hrs
6016Cu0	44	3.5	3.85	28
5623Cu0	16	5.5	1.40	65
5428Cu0	38	4	2.55	56
8630Cu0	163	-	9.69	0
5422Cu13	40	3	2.99	30
5422Cu33	93	3.5	7.15	12

Table 4.5: Cumulative volume loss, incubation period and rate of volume loss for the experimental alloys.

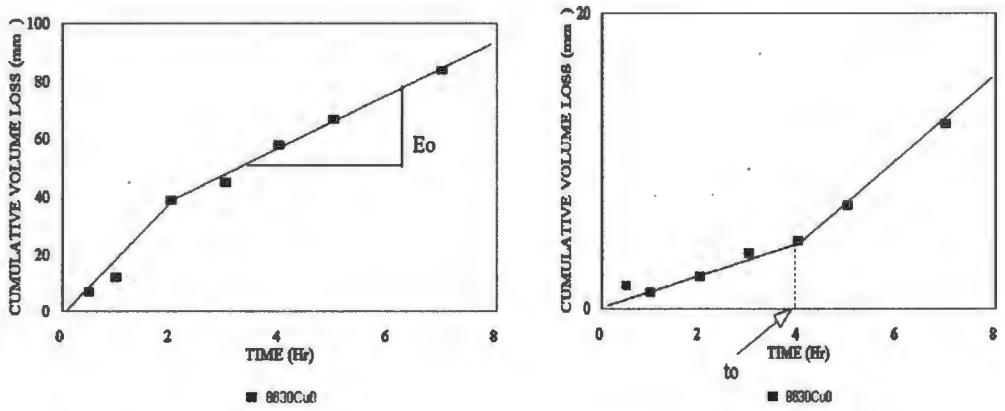

a *b*

Fig 4.26: The various forms of erosion curves obtained in this study
a) For an alloy with no incubation period b) for an alloy with an incubation period. $\dot{E}$ is the rate of volume loss in the steady state.

4.6.2 MICROGRAPHS OF CAVITATED SURFACES

A scanning electron microscope was used to examine the surface of the cavitated specimens at various magnifications. The micrographs are presented in plates 4.24 and 4.25. The wear mode observed in all the alloys was ductile as would be expected for austenitic stainless steels.

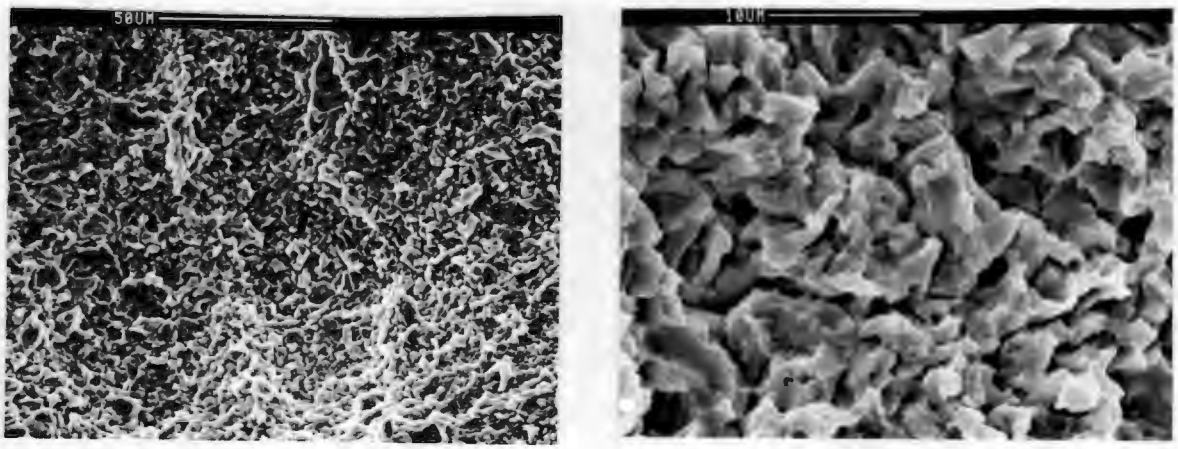

a) b)

Plate 4.24: Ductile erosion wear and advanced damage on the cavitated surface :a) at low magnification; b) at high magnification

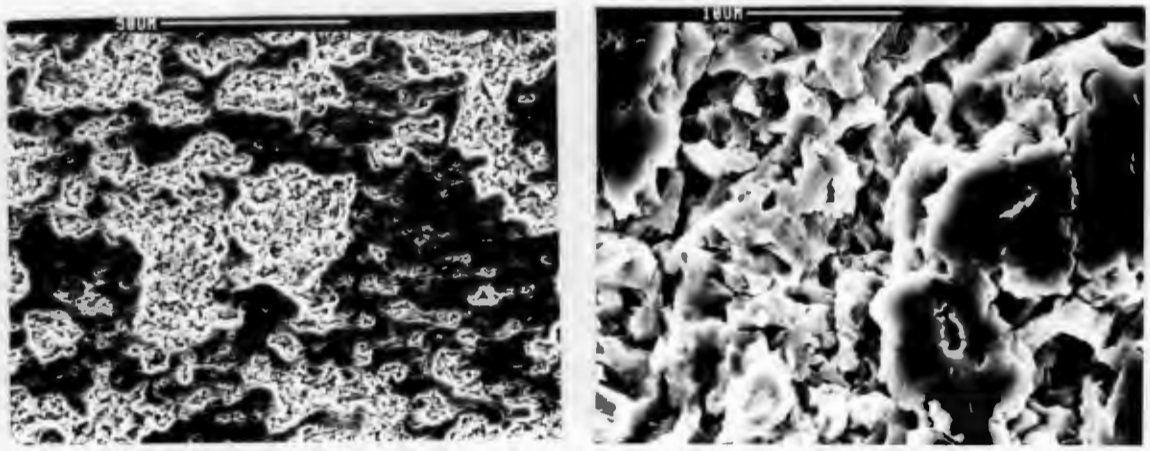

a) *b)*

Plate 4.25: Damage near the edge of a cavitated surface a) at low magnification b) at high magnification

4.6.3 CAVITATION INDUCED MARTENSITE

It is known that erosion resistance in metastable austenitic stainless steels is enhanced by transformation of the austenite to martensite during erosion wear[54,63,64]. In order to study the transformation phenomenon in these steels, XRD was used to determine the amount of cavitation induced martensite in the alloys and table 4.5 shows that metastable alloys have substantial amounts of martensite induced by cavitation erosion. This means that the stresses during cavitation are large enough to cause transformation. Fig 4.27 shows the XRD plots for alloy 5428Cu0 and alloy 8630Cu0 after 14 hours of wear. There is a difference in the peaks of the two alloys due to the appearance of α' peaks and the reduction of intensity of γ peaks.

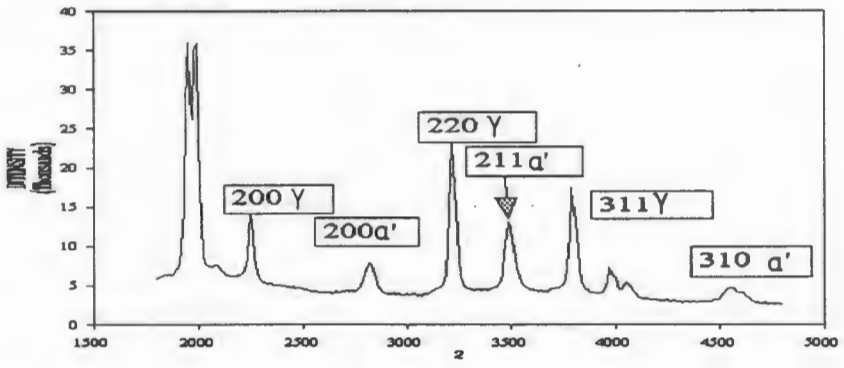

Fig 4.27 a: An XRD plot of alloy 5428Cu0 in the solution treated condition

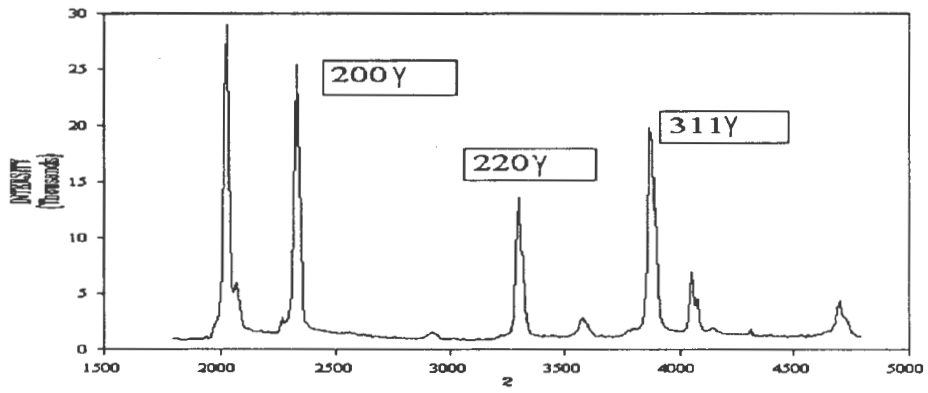

Fig 4.27 b: An XRD plot of alloy 8630Cu0 in the cavitated condition

CHAPTER 5: DISCUSSION

This chapter provides a synthesis of the preceding chapters by discussing the techniques applied in this study and associated results. The information is presented according to the type of test performed and the results yielded by this test or exercise. A comparison of the properties of each material (either tensile, drawability or cavitation erosion resistance) is made to determine which materials have the best properties for a particular application.

5.1 OPTICAL MICROGRAPHS

The main emphasis of the microstructural studies has been to characterise the microstructures of the alloys in the solution-treated condition, determine the level of austenite stability, grain size and whether secondary phases such as δ-ferrite exist. The extent of transformation and type of transformation product after fracture is observed on microstructures of offcuts from the fractured ends of tensile specimens.

5.1.1 MICROSTRUCTURE OF SOLUTION-TREATED ALLOYS

Austenite stability has an important effect on the mechanical properties and on formability and erosion resistance of these alloys. The stability can be determined by applying many methods, the easiest of which is the use of empirical equations (Ms, Md_{30} etc.) and by microstructural examination. The Schaeffler diagram (fig 2.1) is a useful method for the estimation of the microstructure of solution-treated alloys in that only the composition of the alloys needs to be established in order to calculate the Ni equivalent and Cr equivalent. The application of these equations for the test alloys shows that they are mainly austenitic although alloys 6016Cu0 and 5422Cu13 have slight variations. The Schaeffler diagram indicates that small amount of δ-ferrite is present in alloy 5422Cu13, whereas alloy 6016Cu0 is shown to have the same amount of δ-ferrite and some martensite because the composition of this alloy infringes on both the δ-ferrite and martensite lines (see fig 2.1 and table 4.1).

It should be noted that in all cases, except in alloy 6016Cu0, the XRD results for solution-treated alloys indicate over 90 % austenite. This method allows for an error of ±3 %. Alloy 6016Cu0 understandably has less than 90 % austenite, and this may be a result of the synergistic effect of the δ-ferrite and martensite which will be discussed

later. The rather low amount of retained austenite in alloy 5422Cu13 (93% ± 3%) may be due to δ-ferrite in the alloy, as indicated by the Schaeffler diagram.

Examination of the light micrographs shows mainly austenitic microstructures (such as the usual austenite twins) with varying grain sizes (see the GSN in table 4.1) and some voids which may be the result of the removal of δ-ferrite or oxides. The only radically different microstructure is that of alloy 6016Cu0 (plate 4.1). This has a large amount of surface martensite which may have been induced during polishing. Schmid[2] observed similar microstructures for some of his solution treated and electropolished alloys, and concluded that this martensite was induced during electropolishing. The reason for the ease with which such a process occurs in this alloy is obviously linked to its low stability. Evidence of δ-ferrite on the surface of the alloy is probably obscured by the surface martensite.

It can be concluded that solution-treated alloys are mainly austenitic although some have small amounts of delta ferrite. Alloy 6016Cu0 has an appreciable amount of martensite after solution treatment and very little δ-ferrite. Therefore the effect of delta ferrite on mechanical properties of these alloys is not noticeable (delta ferrite increases the 0.2% proof stress and is detrimental to TRIP). Good microstructural predictions can be made by using the Schaeffler diagram for these test alloys, and this may be an easy method of controlling alloy chemistry to achieve desired mechanical properties during production in the steel plant.

5.1.2 MICROSTRUCTURES OF TENSILE SAMPLES

The microstructures of the tensile tested alloys are taken from the fractured ends of the alloys and are examined using a light microscope with Normaski interference, as outlined in the preceding section. These microstructures demonstrate elongation parallel to the tensile direction and the microstructures can generally be classified into three groups:

i) **Highly transformed microstructures** are seen mainly on metastable alloys tested at low temperatures. Examples of these microstructures are alloys 6016Cu0 at 0°C (plate 4.7), room temperature and 40°C (plate 4.8); alloy 5623Cu0 at 0°C, room temperature and 40°C (plate 4.11) and alloy 5422Cu13 (plate 4.15) at 0 and room temperature. All these alloys have large amounts of lath martensite characteristic of deformation induced martensite. LeCroisy and Pineau[65] discovered that nucleation of martensite occurs mainly along twin and

grain boundaries and that preferential growth of martensite occurs parallel to the active slip planes. This explains the lack of clearly defined grain and twin boundaries in these alloys as opposed to the micrographs of alloys where no transformation occurred. Plate-like martensite is a product of quenching to below Ms and/or deformation at low temperatures (Ms±70°C) and low strains[32], while lath martensite occurs after straining to large strains and at higher temperatures. We can therefore conclude that due to the relatively 'high' test temperatures lath martensite forms.

ii) **Martensite clusters** are formed in metastable alloys tested at higher temperatures (40-60°C) and in some of the more stable steels at low temperatures. Occurrence of cluster martensite has been noted by many authors[2,32] although it is referred to by many different labels. Maxwell et al[32] identified clusters of martensite as 'a few small irregular plates of stress assisted martensite'. These clusters are induced where there are low rates of transformation which occur in the test alloys under the situations mentioned above. From the XRD results it may be concluded that this type of martensite will occur in alloys which have less than 50% deformation induced martensite after straining. The polishing induced martensite seen in plate 4.1 is mainly clusters of martensite due to its morphology. Martensite clusters can be seen in alloy 8630Cu0 in dry ice (-5°C) and 5623Cu0 at 60°C (plate 4.12) and alloy 5422Cu33 at 0°C because of the low rates of transformation in these alloys.

iii) **Slip lines** are observed in stable alloys where no transformation occurs and are the result of austenite slip during deformation. The micrographs for these alloys have distinct grain and twin boundaries, although the grains are elongated. Slip lines can be distinguished from martensite laths by their lack of surface relief and by the fact that the grain and twin boundaries of these alloys are easily defined. Alloys 8630Cu0 at room temperature and 5623Cu13 at 40°C (plate 4.16) have well defined slip lines.

5.2 TENSILE BEHAVIOUR

The tensile behaviour of the alloys is elucidated by the flow and WHR curves, which assist in identifying alloys in which TRIP occurs and provide basic mechanical properties for the alloys. Whereas micrographs only show the presence of deformation induced martensite and XRD results give the amount of this martensite, tensile and

WHR curves clarify whether this transformation enhances the mechanical properties. Improved strength in austenitic stainless steels is mainly achieved by transformation to martensite (though work hardening of stainless steels can also increase strength without transformation to martensite) which under appropriate circumstances also leads to an increased ε_u. In this section the various formability parameters obtained from the intrinsic test are discussed.

5.2.1 MAXIMUM UNIFORM ELONGATION

TRIP is temperature dependent and therefore deformation temperature is an important factor in enhancing mechanical properties of these alloys. Fig 5.1 is a graph of maximum uniform elongation versus test temperature for the experimental alloys. The peak in the uniform uniform elongation which was noted by other authors[2,12,66,67] for various TRIP alloys and austenitic stainless steels, also occurs in these alloys, although at a much lower temperature. It should be noted that enhanced ε_u indicates improved formability. Alloys 5623Cu0, 5428Cu0 and 5422Cu13 show good peak uniform elongation of about 50 % at a temperature of 25 °C. This maximum elongation temperature (MET) is lower than that observed by Rosen[12] for AISI 301 and AISI 304. Alloy 6016Cu0 also has a MET at 25°C, although in this case the ε_u is reduced; this behaviour is due to the rapid transformation in this alloy which leads to early fracture of the mainly martensitic specimen, while at 60°C and above no martensite forms to resist incipient necking (see fig 4.5). The behaviour of alloy 5422Cu33 is interesting because the MET seems to be at sub-zero temperatures. The ε_u at -5°C is shown to be high and continues to drop steadily with increasing temperature. The cause of this behaviour may be the large amount of copper alloyed with this steel. Copper has been found to retard the rate of transformation[22] and, as such, TRIP characteristics of high copper stainless steels should only be noticeable at low temperatures.

Alloy 8630Cu0 displays consistent uniform elongation across the test temperature range. This is because the alloy is very stable (as shown by its low Ms and Md_{30} values). With reference to figure 4.10, no martensite forms across the entire test temperature range, except at -5°C, and even then the martensite is still less than 10%.

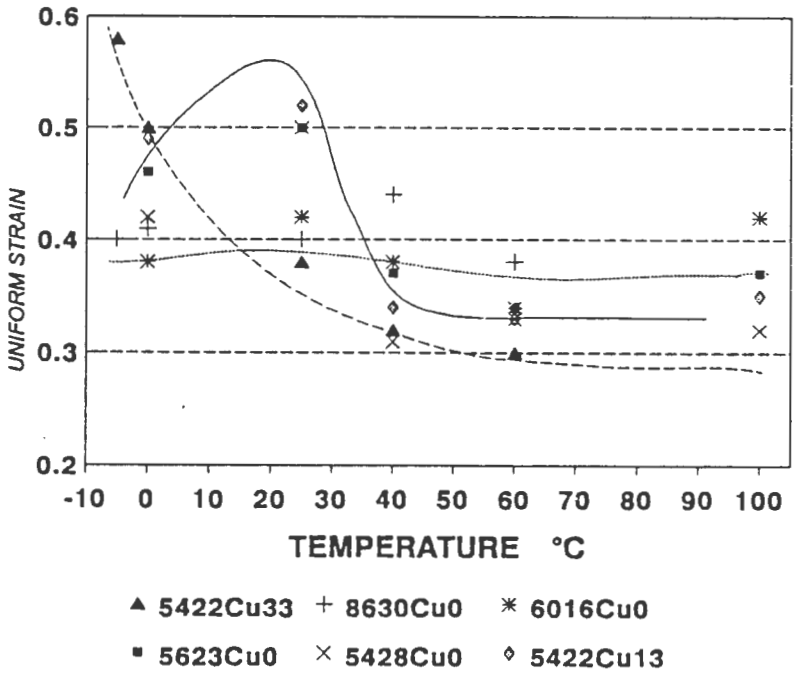

Fig 5.1: Graph of maximum uniform elongation versus test temperature

The composition of the alloys influences the ε_u and this is illustrated by plotting maximum uniform elongation against Brickner's instability factor (I) (fig 5.2). In accordance with other authors' results[24,25], a peak in the ε_u (for room temperature tests) occurs at a certain interval of I and is between 1.5 and 3.5 which compares well with that of AISI 301[24]. The advantage of using the I value is its ability to assist the steelmaker in predicting the ε_u of the alloy during the melting process from the sample analysis. Its drawback is that this equation is not applicable for copper alloyed steels because the coefficient of copper is not included. Therefore, the plot in fig 5.2 is for the non-copper alloyed experimental alloys at room temperature. The significance of using the room temperature values is that the formability testing focuses on room temperature tests and the maximum elongation for these alloys occurs at room temperature.

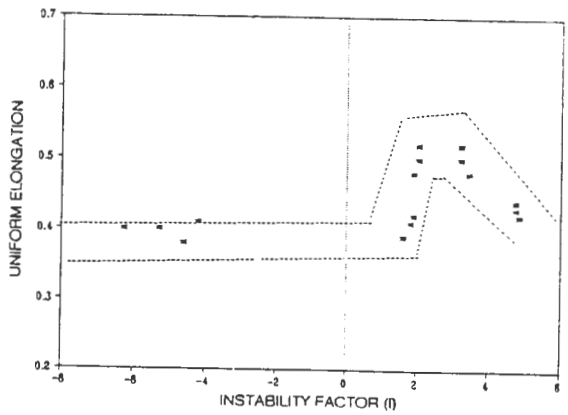

Fig 5.2: A plot of I versus maximum uniform elongation

5.2.2 TENSILE STRENGTH

In order to have strength in the formed article, high transformation is desirable because of the strengthening effect of martensite. Generally alloys with good TRIP properties have good UTS, but like TRIP behaviour, UTS is strongly temperature dependent as can be seen in figure 5.3 below. There is a decrease in UTS with increasing temperature, for all the alloys although to varying extents. The reason for this is the effect of temperature on transformation (less martensite forms at high temperatures). Low temperatures result in high transformations leading to high strength because of the deformation induced martensite, whereas high temperatures result only in the deformation of austenite which has a low strength. The curve of alloy 5422Cu33 in fig 5.3 is explained by the fact that, at temperatures above 0°C there is no strain induced martensite in the alloy so that UTS is constant across the whole temperature range, while at low temperatures (-5°C) there is a large amount of deformation induced martensite (about 60%) which greatly increases the tensile strength of the alloy at this temperature. Alloy 8630Cu0 has negligible variation in UTS as temperature increases. This is acceptable for a stable alloy where there is no deformation induced martensite even at low temperatures. All the other alloys have a steady decrease in UTS with increasing temperature and is similar to behaviour that has been noted for metastable austenitic stainless steels[2,26,40].

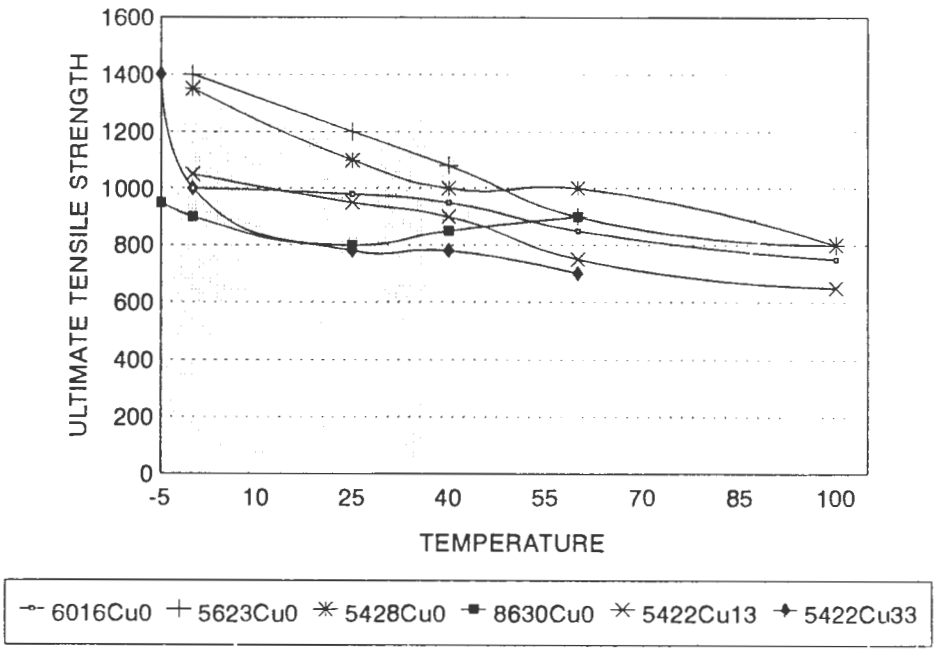

Fig 5.3: Ultimate Tensile Strength versus test temperature

5.2.3 WORK HARDENING RATE (WHR) BEHAVIOUR

Strain hardening of metastable alloys can be described with the aid of WHR curves or H versus ε curves according to Fang and Dahl[28]. Strain hardenability of austenitic stainless steels is controlled by their propensity to transform to martensite which is identified in Ludwigson and Berger's equation by the parameter A (see page 18). This parameter is dependent on the stability of the austenite which is governed by alloy chemistry and temperature.

Very unstable alloys

If the value of A (propensity to form martensite) is high, too much martensite forms too early which results in positive work hardening occurring at low strains. The maximum WHR is also very large in this case whereas the ε_u is low due to fracture of the largely martensitic specimen. This behaviour is observed in alloy 6016Cu0 at temperatures up to 40°C, alloy 5623Cu0, 5428Cu0 and 5422Cu13 at 0°C. The H versus ε graphs for these alloys are similar to figure 4.17, where a distinctive peak is present. The parameter H characterises the stability and homogeneity of deformation as a function of strain it is defined by equation 2.9.

Alloys exhibiting good TRIP behaviour

These alloys give the best uniform elongation which may be obtained either from the point of intersection of flow curves and the WHR graphs or where H=1. Their curves also exhibit a positive WHR although the change in WHR from negative to positive occurs at higher strains (usually about 0.15, compared to 0.05 for alloy 6016Cu0 at 0°C). The peak WHR is lower than that of very unstable alloys (a difference of several hundred megapascals between alloy 6016Cu0 at 0°C and alloy 5623Cu0 at room temperature). The copper-alloyed steel 5422Cu13 has a constant and flat WHR up to large strains before it decreases at the point of instability (see figure 4.15). This occurs because copper decreases the strain hardenability of metastable austenitic stainless steels by reducing the amount of martensite which forms during straining. The H versus ε curves for these alloys give less pronounced peaks or a constant H-value up to large strains as illustrated by figure 4.19.

Stable alloys

Stable alloys show a decline in WHR with increasing strains until fracture. This is illustrated in figures 4.5, 4.7, 4.11 and 4.13. This is a result of deformation of an austenitic microstructure which experiences no transformation. Low UTS occurs in this case as shown by the graphs. Metastable alloys also have similar WHR behaviour

at high temperatures because deformation occurs above the Md temperature. Similar behaviour is noted for the H versus ε graphs where there is a continuous decline in H with increasing temperature.

5.2.4 PROOF STRESS (0.2%)

The lack of a distinct yield point in these alloys leaves the 0.2% proof stress as the only means of measuring the yield point. Knowledge of the yield stress is important in determining formability because permanent deformation (which is desired during forming) can only result if the yield stress is exceeded. Therefore a low yield stress indicates improved formability. The yield stress of austenitic stainless steels has been shown[16,17] to depend on the amount of nitrogen alloyed with the steel, grain size, the amount of δ ferrite and deformation temperature. Because of other variables such as chemical composition of the alloys, direct comparison between the GSN, or the nitrogen content and 0.2% proof stress is impossible in this study. A trend can be seen between the nickel equivalent and the 0.2% proof stress for the non copper alloyed test alloys. As the nickel equivalent increases the 0.2% proof stress also increases, probably as a result of solid solution strengthening of the large amounts on nitrogen in the steels with high nickel equivalent. The proof stress of these alloys is lower than the yield point of mild steel and we can therefore expect these alloys to perform better than mild steel in forming operations if all the other variables remain constant.

Boeing Formability Equation

The Boeing formability equation (equation 2.16) combines various parameters from tensile test results to present a stretch formability parameter. Qualitative application of the equation to the tensile test data in table 4.2 shows that a low value of f (which results in good formability) will be achieved if the UTS is moderate, the ε_u is large and if the area under the flow curve is large. It may be assumed that sigmoidal curves have a larger area than hyperbolic curves. Therefore the alloys 5623Cu0, 5428Cu0 and 5422Cu13 will have good stretch formability at room temperature because they have sigmoidal curves with moderate UTS and very high ε_u. Meanwhile alloy 6016Cu0 exhibits a very high UTS, and low ε_u which result in a large value of f. A similar case may result for stable alloys because they have a small area under the stress-strain curves and low ε_u.

5.2.5 STRAIN HARDENING EXPONENT (n-value)

The n-value is another important formability parameter, and it is widely accepted that a high n-value leads to good stretch formability. Jackson[25] hinted that for a 302 stainless steel good formability is obtained if the n-value is above 0.6. Fig 4.20 shows that transformation to martensite greatly increases the n-value and therefore TRIP steels have better stretch formability than stable alloys. Double n behaviour occurs in stable steels, although in a less pronounced manner (see figure 4.21). It is thought that this phenomenon in these steels is caused by the formation of ε-martensite, although a more likely explanation is that it is due to dislocation dynamics[68]. The benefit of a high n-value is that it normally increases the critical strain level for plastic instability and reduces strain concentrations during forming.

5.3 DRAWABILITY

Deep drawability can be determined by using the intrinsic test (where the r value is calculated) or by using a simulative test like the Swift cup test. The Engelhardt test used in this study is a derivative of the Swift cup test. The drawback of a simulative test is that the effects of other factors such as test speed, lubrication and die shape also influence the result as they would in a normal forming operation. These variables were kept constant in this study so that the result is a good comparison of drawability of the alloys. The importance of the drawability test lies in the fact that deep drawing is one of the widest applications of sheet metal. The limiting drawing force (LDF) results in table 4.3 show a good correlation between UTS and the LDF with 5422Cu33 recording the lowest force to fracture and 5623Cu0 recording the highest LDF.

Metastable steels have higher limiting drawing ratios (LDR) which are influenced by the formation of martensite during drawing and this in turn increases the amount of stretching along the cup wall. The voltage response figures which are directly proportional to the amount of drawing induced martensite confirm this, with alloy 6016Cu0 recording the highest voltage (0.397 mV) and the stable alloy 8630Cu0 recording a low 0.011mV. It should be noted that a sheet of AISI 304 was also tested for comparison. The amount of martensite formed by this alloy is moderate because of its increased stability. All the test alloys have a higher LDR than 304 stainless steel indicating that they can produce better results and material savings in forming operations currently using 304 stainless. The result for alloy 5422Cu33 is interesting because this alloy exhibits a reasonable LDR with a low LDF, meaning that low

capacity machines can be used to draw this material. Overall copper lowers the LDF and the LDR of stainless steel. Another advantage of the test alloys over AISI 304 is that they are not susceptible to the earring behaviour experienced by AISI 304 stainless steel. Earring can lead to material wastage when the ears are removed from a drawn article. Earring occurs in materials where $\Delta r \neq 1$, whereas type 301 stainless steel and its derivatives have $\Delta r \approx 1$. Earring therefore is usually not a problem in articles drawn from AISI 301 stainless steel.

Examination of the variation of the drawing induced martensite in the cup walls and cup bottoms is interesting because it can explain the occurrence of fracture in these cups. At small blank diameters, where the drawing forces are low, the drawing induced martensite is more pronounced on the side walls because most of the deformation occurs in this area, while at high blank diameters (high drawing force), the cup bottom has more martensite, as observed by Nohara at al[21]. This results in fracture at the cup bottom. Ward[62] has modelled the equivalent plastic strain distribution (fig 5.4) and the martensite distribution (see fig 4.22) for a metastable austenitic stainless steel where test conditions are similar to those used in this study. Figure 5.4 shows that the highest plastic strain is experienced at the cup bottom, which also has the highest volume fraction martensite.

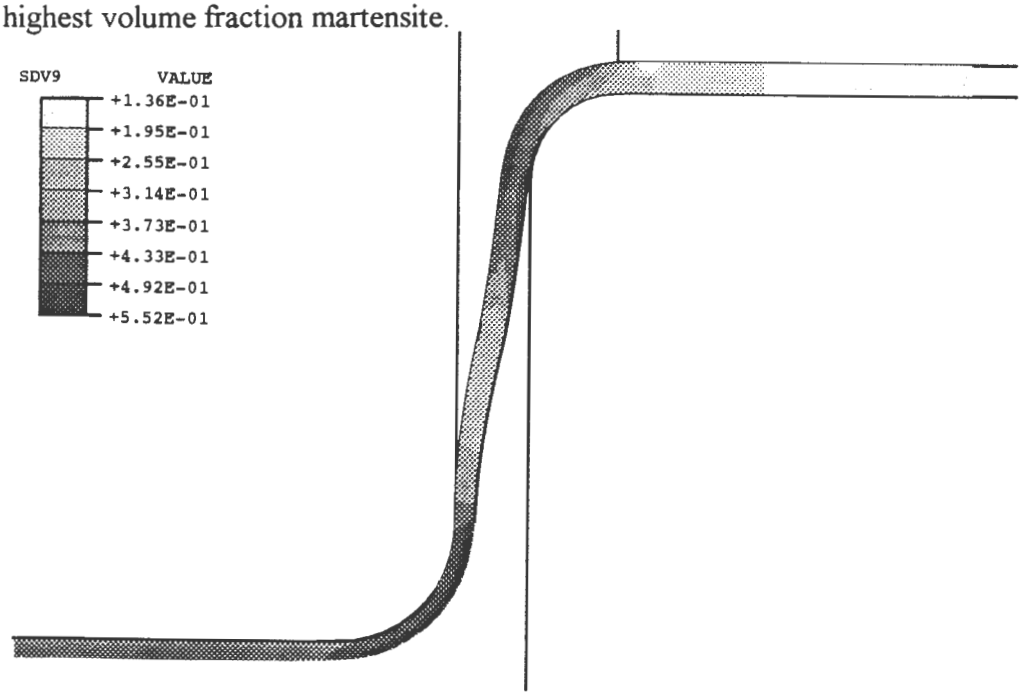

Fig 5.4: Equivalent plastic strain distribution. The insert gives the equivalent plastic strain in relation to the shading on the figure.

5.3.1 DELAYED CRACKING

Although the metastable alloys 5623Cu0 and 5428Cu0 showed promising results in drawability tests, examination of the cups after 24 hours showed the existence of delayed cracking in cups drawn at high blank diameters (resulting in high residual stresses) from these alloys. The seasonal occurrence of delayed cracking has been noted by Hoshino[53] who investigated the effect of chemical composition on season cracking and found that materials with a low stability of austenite had a large amount of strain induced martensite. Investigation of the effect of individual elements found carbon and nitrogen to be the cause of delayed cracking with carbon being more harmful than nitrogen. This is due to the effect of these elements on the toughness of martensite. This conclusion seems to apply in these experimental alloys, since carbon was constant in all alloys but nitrogen was varying. Alloys with over 0.2 percent nitrogen content suffered from delayed cracking except where copper alloying was utilised (alloys 5422Cu33 and 5422Cu13), or where there was high stability of austenite such as in alloy 8630Cu0. Alloy 6016Cu0 showed no cracking, possibly due to its low nitrogen content which leads to the conclusion that α' martensite embrittlement occurred in these alloys. The effect of copper on delayed cracking can be understood by using Nohara and Onos'[21] Md_{30} equation (equation 2.7), which indicates that copper reduces the chances of delayed cracking in austenitic stainless steels because it decreases the Md_{30} temperature of these alloys (see figure 2.13).

The effect of martensite on delayed cracking was also investigated by Ward et al[50] who found that martensite forms in extremely localised areas during drawing, leading to stress concentrations and strain mismatch at the boundaries of the austenitic and martensitic areas. This theory may explain the lack of delayed cracking in alloy 6016Cu0 in that, due to the very high transformation during drawing, the residual stresses disappear because the final microstructure after drawing is mainly martensitic (due to the high magnetic response voltages). Nohara and Ono proposed that delayed cracking will not occur in alloys with less than ten percent volume fraction martensite after drawing. This may be due to the lack of stress concentrations in such alloys.

Divers[52] investigated the problem of delayed cracking in a 301 stainless steel by using the n-values to predict the materials that would suffer from delayed cracking. His conclusion that delayed cracking exists in materials with an n-value above 0.52 is not all encompassing because some alloys, tested in this study and found to have n-values which are greater than 0.52, did not experience this phenomenon. This is demonstrated by the fact that alloy 6016Cu0 has an n-value of 0.753 but it did not

experience any delayed fracture. His conclusion was influenced by the fact that his alloys did not contain large amounts of nitrogen or copper as alloying elements so that their respective detrimental and beneficial effects were not discernible. This is further demonstrated in his regression equation for the calculation of the n-value for delayed cracking. The final polynomial equation only accounted for the effect of carbon and chromium, ignoring the influence of other important elements such as Si, N, and Cu.

Delayed cracking can only be combated by changing the alloy specifications or by annealing the drawn component to relieve the stresses induced by deep drawing.

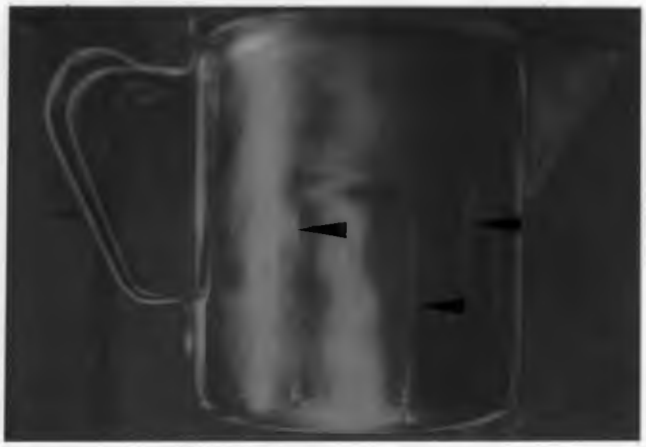

Plate 5.1: Delayed fracture in a deep drawn teapot

5.3.2 EFFECT OF TEMPERATURE ON DRAWABILITY

Warm forming has been advocated for most metastable austenitic stainless steel sheets because most of these steels show an MET at temperatures of about 60°C. Fig 5.1 shows that the experimental alloys tested in this study exhibit METs at temperatures of between 20° and 30°C. Similar results were obtained by Gillissen et al's[67] for an alloy with 6.7% nickel and 0.2% nitrogen. The low MET in these alloys (the test alloys and Gillissen et als' alloys) indicates that warm forming may not be beneficial. The drawability tests for these alloys were performed at room temperature without making any attempts to minimise adiabatic heating. The real drawing temperature could have been higher than 25°C quoted in this study, but the speed and the rate (which was slow) of testing make the effects of adiabatic heating negligible. In a production plant where the forming speeds and rates are high, maintaining low forming temperatures may only be possible after a substantial amount of cooling of the forming tools.

Most forming operations are performed with heated forming tools in what is known as warm press forming. Granzow[51] and Reissner et al[43] ascertained that, if the die is heated and the punch kept at low temperatures, there is an improvement in the LDR of 304 stainless steel. Nohara and Ono also found that warm forming reduces wrinkling of stainless steels because the tensile stresses at the flange are lowered.

5.4 CAVITATION EROSION

The cavitation erosion properties of metastable austenitic stainless steels have been studied by various authors[54,55] because of the interesting effects TRIP has on cavitation erosion resistance. It was discovered that, in general, phase transformations that occur during cavitation erosion lead to improved resistance. In this study the effects of cavitation induced transformations on the erosion resistance of the experimental alloys were investigated. Woodford[55] ascertained that materials with a low SFE have increased erosion resistance. This explains the poor erosion resistance of alloy 8630Cu0 because it has a high nickel alloy content and this nickel raises the SFE. The converse is true for the low nickel alloys (alloys 5623Cu0 and 5428Cu0 are good examples). The reason for low SFE's ability to increase erosion resistance lies in its ability to resist high cycle fatigue. Reduced SFE leads to planar slip and increases the number of cycles needed to nucleate a crack in high cycle fatigue; high cycle fatigue stress and erosion resistance have good correlation. Heathcock[54] concluded that alloys with a high UTS, high WHR and ε_u exhibit good cavitation resistance. These conclusions relate well with the erosion results for the test alloys because all the metastable alloys (5623Cu0, 5428Cu0, 6016Cu0 and 5422Cu13) have the above properties and they also exhibit superior erosion resistance to that of stable steels (8630Cu0 and 5422Cu33).

The properties mentioned by Heathcock[54] are usually exhibited by low SFE materials so that SFE has an important role in the erosion resistance of the alloys. Besides SFE, transformation from austenite to martensite occurs during cavitation erosion and this results in the materials obtaining the properties mentioned by Heathcock as prerequisites for good erosion resistance. The amount of transformation occurring in the alloys was measured by means of XRD. Figure 4.27a shows the XRD trace of a metastable alloy after 14 hours of cavitation and this trace shows distinct martensite peaks, as opposed to figure 4.27b where there are no martensite peaks and the austenite peaks are predominant. The calculated results of volume percent martensite after 14 hours of cavitation are presented in table 4.5. The metastable alloys have

large amounts of transformation (as much as 60% α') and there is a good correlation between the volume percent of martensite and CVL and $\dot{E}$ in table 4.5. The only alloy without an incubation period (period of low wear rate at the beginning of the test) is alloy 8630Cu0, and this probably contributes to its high CVL.

SEM micrographs show that the alloys experienced ductile erosion which normally results in enhanced erosion resistance when compared to brittle erosion. None of the alloys exhibited brittle erosion and this mode of erosion has not been observed in austenitic stainless steels.

CHAPTER 6: SUMMARY AND CONCLUSIONS

6.1 SUMMARY

A study of the formability of six experimental alloys with an AISI 301 base shows that it is possible to substitute nickel with nitrogen and still achieve good formability. However there are certain limitations hindering the immediate application of these materials in forming operations. The alloys were selected from a broad base of alloys which have been found to have promising deformation characteristics. Metastable austenitic stainless steels have good formability which is attributed to the TRIP that exists in these alloys. An added bonus of transformation is that the martensite formed results in good final strength of the formed articles. Substitution of nickel with nitrogen can lead to substantial production cost savings and increase their applications as engineering materials.

Uniaxial tensile tests were performed on the alloys in order to determine whether TRIP existed in the steels and to obtain useful formability parameters from these intrinsic tests. An acceptable austenitic stainless steel for use in metal forming plants should possess the following properties

i. A high uniform elongation and UTS which results in good LDR and stretch formability.
ii. A MET between 20 and 30°C which could lead to exceptional formability at room temperature and eliminate the need for warm forming.
iii. An acceptable surface finish.

Requirement (i) was achieved by the alloys 5623Cu0, 5428Cu0 and to a lesser extent 6016Cu0, these alloys also have better mechanical properties than AISI 301. Although alloy 5422Cu13 had a higher ε_u than AISI 301 stainless steel[69], its UTS was low and therefore the formability in this steel is not exceptional. Achievement of (i) on the test alloys means that huge savings in cost can be realised because less material will be necessary to form an article and the material will be cheaper. It was difficult to assess requirement (ii) in this study because warm forming tests were not carried out. Requirement (iii) was not met by the alloys exhibiting the best drawability because of delayed cracking. Delayed cracking is unacceptable in formed articles therefore application of alloys 5623Cu0 and 5428Cu0 will only be possible if the articles are annealed after drawing (increasing costs).

Cavitation erosion behaviour of these alloys is related to their tensile properties in that alloys which exhibit TRIP are more resistant to erosion. This is linked to the transformation of these alloys during erosion resulting in the enhanced mechanical properties as in tensile testing or deep drawing. SFE also has a part to play because the high nickel alloys (8630Cu0) exhibited poor erosion resistance because nickel raises the SFE, and a high SFE results in poor resistance to cavitation erosion.

Copper in moderate amounts, tends to retard the rate of transformation in the experimental alloys; this results in low WHR or, in the case of the high copper alloy, a continuous decline in the WHR with increasing strain indicating that the alloy is stable.

6.2 CONCLUSIONS

The list of conclusions drawn below provide basic guidelines on the formability of the experimental alloys. However more testing (i.e. r-value, simulative stretch forming test and warm forming) is necessary before the final application of these materials.

1. The alloys are austenitic after solution treatment at 1050°C for 30 minutes. The Schaeffler diagram is a useful aid in predicting the microstructure of the heat treated alloys from their alloy specifications.

2. The level of austenite stability controls the TRIP phenomenon in these alloys. This phenomenon has been observed in alloys with approximately 5.5 weight percent nickel and 0.25 weight percent nitrogen. It is possible to predict the austenite stability using empirical equations such as Md_{30} and Ms.

3. Copper is detrimental to TRIP although this occurs at very high concentrations, whereas nitrogen produces the same effects as copper at low concentrations (about 0.3%).

4. A peak uniform elongation occurs in the metastable alloys. Although the MET for these alloys is at room temperature, this is much lower than 60°C MET observed for AISI 301 and may eliminate the need for warm forming in these alloys.

5. Alloys with room temperature n-values which are more than 0.6, have good formabilty and form large amounts of martensite if strained to fracture at room temperature.
6. The intrinsic test (tensile test) of formability predicts good stretch formability for alloys 5623Cu0 and 5428Cu0 and 5422Cu13 because of their enhanced uniform elongation, UTS, and n-values, whilst retaining reasonably low 0.2% proof stresses.

7. All the experimental alloys exhibit better drawability than AISI 304 and they do not suffer from the earring phenomenon. Slight wrinkling occurs in some of the metastable alloys as a result of increased material strength during drawing because of transformation to martensite.

8. Alloy 5422Cu33 has a reasonable LDR while it fractures at a low LDF. This suggests that this material may be suitable for drawing in low capacity machines,therefore alloying with copper may be useful in making stainless steel for drawing in low capacity machines.

9. Delayed fracture occurs in highly transformable alloys with at least 0.22% nitrogen. Additions of copper not only reduce the susceptibility to this but also lowers the LDR.

10. All the test alloys indicate a higher UTS and 0.2% proof stress than AISI 301. With the exception of 5422Cu33, the ε_u is also improved with respect to AISI 301.

Good cavitation erosion resistance is obtained for alloys which exhibit TRIP, and it may be concluded that the following properties are necessary for this to occur.

1. A high flow stress
2. A high work hardening rate
3. A high strain to fracture
4. A low stacking fault energy
5. Ductile erosion

REFERENCES

1. W ALEXANDER and A STREET. *Metals in the Service of Man. Penguin Books, (1982)*
2. OE SCHMID. *MSc Thesis,* University of Cape Town, (1992)
3. MF ASHBY and DR JONES. *Engineering Materials 1.* p79, Pergamon Press, (1980)
4. FB PICKERING. *Physical Metallurgy and Design of Stainless Steels.* p226-268, Applied Science Publishers, (1978)
5. MB CORTIE. *Journal of the South African Institute of Mining and Metallurgy.* **93**, p165, (1993)
6. OE SCHMID and RD KNUTSEN. *Proceedings of the First International Chromium Steel and Alloys Conference.* Ed HW GLEN. **2**, p151, (1992)
7. D PECKNER and IM BERNSTEIN. *Handbook of Stainless Steels.* p1.7, Mc Graw-Hill, (1977)
8. JP HOFFMAN and AB VICTOR. *FWP Journal.* **November**, p5, (1989)
9. JS STANKO and D WELLBELOVED. *Manganese in Corrosion Resistant Steels.* p10, Samancor, (1991)
10. D PECKNER and IM BERNSTEIN. *Handbook of Stainless Steels.* p12.27, Mc Graw-Hill, (1977)
11. KJ IRVINE, DT LLEWELLYN and FB PICKERING. *Journal of the Iron and Steel Institute.* **October**, p356, (1961)
12. A ROSEN, R JAGO and T KJER. *Journal of Materials Science.* 7, p870, (1972)
13. P MARSHALL. *Austenitic Stainless Steels, Microstructures and Mechanical Properties.* Elsevier Applied Science Publishers, (1984)
14. D PECKNER and IM BERNSTEIN. *Handbook of Stainless Steels.* p4.13, Mc Graw-Hill, (1977)
15. YN TURAN and A KOUSARIS. *Journal of the South African Institute of Mining and Metallurgy.* **93**, p97, (1993)
16. LA NORSTROM. *Metal Science.* p208, (1977)
17. KJ IRVINE, T GLADMAN and FB PICKERING. *Journal of the Iron and Steel Institute.* **July**, p379, (1969)
18. E WERNER. *Materials Science and Engineering.* **A101**, p93, (1988)
19. S Du Toit. *Private Communication.* University of Pretoria, (1993)
20. D PECKNER and IM BERNSTEIN. *Handbook of Stainless Steels.* p4.29, Mc Graw-Hill, (1977)

21. K NOHARA and Y ONO. *Kawasaki Steel Technical Report.* **14**, p131, (1986)
22. KG BRICKNER. *Selection of Stainless Steels.* American Society for Metals, (1968)
23. D PECKNER and IM BERNSTEIN. *Handbook of Stainless Steels.* p4.29, Mc Graw-Hill, (1977)
24. KG BRICKNER and CE SPAEDER Jr. *Metals Engineering Quarterly.* **February**, p1, (1972)
25. R JACKSON. *Sheet Metal Forming and Energy Conservation (9th Biennial Conference of IDDRG).* p264, IDDRG, (1976)
26. T ANGEL, *Journal of the Iron and Steel Institute.* **May**, p402, (1954)
27. FB PICKERING. *Physical Metallurgy and Design of Stainless Steels.* p224, Applied Science Publishers, (1978)
28. XF FANG and W DAHL. *Materials Science and Engineering.* **A141**, p189, (1991)
29. J SCHLIPF. *Materials Science and Engineering.* 77, p76, (1976)
30. UF KOCKS. *Journal of Engineering Materials Technology.* 98, p76, (1976)
31. JRC GUIMARAES and RJ De ANGELIS. *Materials Science and Engineering.* **13**, p109, (1974)
32. PC MAXWELL, A GOLDBERG and JC SHYNE. *Metallurgical Transactions.* **5**, p1305, (1973)
33. VF ZACKAY, ER PARKER, D FARH and R BUSCH. *American Society for Metals Transactions Quarterly.* **60**, p252, (1967)
34. VF ZACKAY, MD BHANDARKAR and ER PARKER. *Advances in Deformation Processing.* ed JJ BURKE and V WEISS. p351, Premium Press
35. GR CHANANI, VF ZACKAY and ER PARKER. *American Society for Metals Transactions Quarterly.* **62**, p965, (1965)
36. C LIVITSANOS and P THOMSON. *Materials Science and Engineering.* **30**, p93, (1977)
37. DC LUDWIGSON and JA BERGER. *Journal of the Iron and Steel Institute.* **January**, p143, (1969)
38. WF BARCLAY. *ASTM Special Technical Publication.* **369**, p26, (1965)
39. E SCHIEL. *Zeitschrift fur Anorganische und Allgemeine Chemie.* **207**, p21, (1932)
40. J BRESSANELLI and A MOSKOWITZ. *Transactions of the American Society for Metals.* **59**, p223, (1966)
41. G HUANG, D MATLOCK and G KRAUSS. *Metallurgical Transactions.* **20A**, p1239, 1989

42. Y FUKASE, K EBATO, N OKUBO and S MURAO. *Transactions of the Iron and Steel Institute of Japan.* **8**, p311, (1968)
43. J REISSNER and H MULDERS. *Proceedings of the International Conference on Stainless Steels.* **vol 2**, Iron and Steel Institute of Japan, p779, (1991)
44. SP KEELER. *Sheet Metal Industries.* **May**, p357, (1971)
45. ASTM. *Standard E646-78.* p734, (1984)
46. AK GOSH, SS HECKER and SP KEELER. *Workability Testing Techniques.* ed. GE DIETER. p135, American Society for Metals, (1984)
47. B TAYLOR. *Metals Handbook.* **vol8**, p547, American Society for Metals
48. SP KEELER, *Sheet Metal Industries.* **July**, p511, 1971
49. D PECKNER and IM BERNSTEIN. *Handbook of Stainless Steel.* p4.34, Mc Graw-Hill, (1977)
50. JDB WARD, CD MERCER, RD KNUTSEN and JB MARTIN. *The Modelling of Transformation Induced Plasticity in Deep Drawing of Stainless Steel.* FEMSA '93, University of Pretoria
51. WG GRANZOW. *Formability of Metallic Materials- 200AD.* ed J.R NEWBY and BA NEIMEIER. **ASTM STP 753**, p137, (1982)
52. CK DIVERS. *Metals Progress.* **August**, p115, (1964)
53. K. HOSHINO. *Transactions of the Iron and Steel Institute of Japan.* **vol20**, p147, (1980)
54. CJ HEATHCOCK. *PhD Thesis.* University of Cape Town, (1980)
55. DA WOODFORD. *Metallurgical Transactions.* **3**, p1137, (1972)
56. CJ HEATHCOCK, BE PROTHEROE and A BALL. *Wear.* **81**, p311, (1982)
57. A BALL, *Wear.* **9**, p201, (1983)
58. DV WILSON, BJ SUNTER and DF MARTIN. *Sheet Metal Industries.* **June**, p465, (1966)
59. MJ DICKSON. *Journal of Applied Crystallography.* **2**, p176, (1969)
60. MJ PAPO. *MSc Thesis.* University of Cape Town, (1993)
61. GF van der VOORT. *Metallography Principles and Practice.* McGraw Hill, (1984)
62. JDB WARD. *MSc Thesis.* University of Cape Town, (1993)
63. BC SYAMALA RAO, P VEERABHADA RAO, NS LAKSHMANA RAO. *Journal of Testing and Evaluation.* 7, p133, (1979)
64. CJ HEATHCOCK, BE PROTHEROE and A BALL. *Proceedings of the Fifth International conference on Erosion by Solid and Liquid Impact.* p63.1, (1979)
65. F LeCROISEY and A PINEAU. *Metallurgical Transactions.* **3**, p387, (1972)
66. D BHANDARKAR, VF ZACKAY and ER PARKER. *Metallurgical Transactions.* **3**, p2619, (1972)

67. C GILLISSEN, J KRAUTSCHICK, T LADWEIN and H MULDERS. *Innnovation in Stainless Steels Conference.* p2.379, (1993)

68. Y BERGSTROM. *Metallurgical Transactions.* **1,** p1029, (1970)

69. MIDDELBURG STEEL AND ALLOYS. *Stainless Steel & 3CR12 Pocket Guide.* p3-4, (1988)

EVALUATION OF THE FORMABILITY PROPERTIES OF NITROGEN ALLOYED METASTABLE AUSTENITIC STAINLESS STEELS

RD Knutsen and M Sibanda

Department of Materials Engineering, University of Cape Town, South Africa

ABSTRACT

Metastable austenitic stainless steels generally provide good forming properties in view of the enhanced ductility achieved by transformation-induced plasticity (TRIP). In addition, the formation of martensite during forming provides good strength in the final product. However, these steels could have much wider application if the alloying cost were to be reduced by minimising the nickel level in the alloy composition. In the present study, nitrogen has been considered as a partial substitute for nickel in a metastable austenitic AISI 301 type alloy. Several experimental alloys, with a range of nickel-to-nitrogen ratios, have been subjected to uniaxial tensile testing and sheet formability tests in order to evaluate the influence of composition variation on the strength and ductility properties. Additions of copper were also made to some of the alloys. Tensile tests, performed at temperatures from 0 to 100°C, allowed the characterisation of the effect of the formation of transformation-induced martensite on ductility. Optimum tensile results were achieved at room temperature and limiting drawing ratio (LDR) tests indicated attractive properties for alloys containing nickel levels as low as 5.5 wt%. The addition of copper was found to have a slight deleterious influence on the ductility of this range of alloys, but is beneficial in the sense that it prevents the occurrence of delayed fracture.

KEYWORDS : Metastable austenite, transformation-induced plasticity, formability.

INTRODUCTION

It is well known that the formation of martensite during the deformation of austenitic stainless steels can influence ductility [1-5]. This is understood to occur as a result of increased work-hardening rate as the newly formed martensite enhances the strength of the deforming austenite-martensite composite structure. When martensite forms at a desirable rate during deformation, the onset of necking is delayed (i.e. the enhancement of uniform elongation) due to the increase in the work-hardening rate, and the steel is said to undergo transformation-induced plasticity (TRIP). However, not all situations giving rise to deformation-induced martensitic transformation lead to TRIP behaviour and the emphasis is on controlling both the extent to which the transformation occurs and the rate at which martensite forms as a function of strain. Optimum martensite formation occurs between the M_s and M_d temperatures and the overall stability of austenite is dependent on both alloy composition and deformation temperature.

Considerable interest in TRIP behaviour is directed towards improving the formability of austenitic steels, particularly in the manufacture of drawn parts for architectural, automotive, industrial, and domestic applications. It has been shown that the TRIP phenomenon is very effective in improving the formability of austenitic steels such as Types 301 and 304 stainless steel [6,7]. In addition, the formation of martensite during the forming operation provides good strength in the final product. However, these steels could have much wider application if the alloying costs were to be reduced by lowering the nickel level in the alloy composition. Although most austenitic stainless steels can be shown to exhibit TRIP behaviour at a particular deformation temperature, the optimum situation arises when a certain alloy composition displays TRIP behaviour under conventional forming conditions. In order to successfully reduce the nickel level in the alloy, the composition must be compensated by the addition of the appropriate amount of alloying element/s to maintain the desired level of austenite stability. Nitrogen has an austenite stabilising potency similar to carbon and a preliminary investigation[8] has shown that enhanced tensile elongation can be achieved at approximately 60°C in an alloy containing 5 wt.% nickel and 0.16 wt.% nitrogen. The present study explores this concept further in that a series of experimental alloys, with a range in nickel-to-nitrogen ratios, are subjected to both uniaxial tensile testing and sheet formability tests in order to compare tensile ductility with deep drawability for these alloys. Furthermore, the influence of copper additions on TRIP behaviour and formability has also been considered.

EXPERIMENTAL PROCEDURE

Six experimental alloys, prepared by Columbus Stainless Steel (Middelburg, South Africa), were selected to provide an alloy composition based on AISI 301 but with a range in nickel-to-nitrogen ratios. Additions of copper were also made to some of the alloys. The compositions of the alloys are presented in Table I, along with the composition of a type 301 alloy for comparative purposes. For easy reference, the alloys are designated according to their nickel, nitrogen and copper levels. For example, the alloy designated 5422Cu33 contains 5.4 wt% Ni, 0.22 wt% nitrogen and 3.3 wt% copper (all figures, unless otherwise stated, are in wt%). Each experimental alloy was hot-rolled from a 5 kg ingot (50mm thick) down to a sheet thickness of 2 - 3 mm. Flat tensile specimens (gauge length 50 mm, gauge width 10 mm, thickness 2 mm) were machined from the sheet stock with the tensile axis parallel to the rolling direction. The sheet material was further rolled down to 1 mm thickness for the biaxial formability tests (limiting drawing ratio).

Prior to testing, all the test specimens were annealed in an argon atmosphere at 1050°C for 30 minutes followed by oil quenching. The tensile tests were performed using a computer-interfaced Zwick tensile tester, which allowed the data to be captured on a computer file. The test set-up incorporated a temperature bath regulated by a Eurotherm controller to within 2°C. Tensile-fracture tests were performed at 0, 25, 40, 60, and 100°C and at least two specimens were tested for each alloy/temperature condition. All the experiments were carried out at an initial strain rate equivalent to 10^{-3} per second. For X-ray diffraction (XRD) phase analysis after deformation, the fractured ends of the tensile specimens were mounted in resin, mechanically polished to a finish using 1μm diamond paste, and finally electropolished in a solution containing chromic and glacial acetic acids. Electropolishing was necessary to remove any deformation-induced martensite that may have formed during the mechanical polishing. The

martensite-austenite volume fraction was calculated from the integrated area under the (200)α, (211)α, (220)γ, and (311)γ diffraction peaks.

TABLE I : Composition of experimental alloys (all figures are in wt.%).

Alloy	C	Cr	Ni	N	Cu	Mn	Si
6016Cu0	0.03	17.4	6.0	0.16	-	1.52	0.3
5623Cu0	0.03	17.0	5.6	0.23	-	1.55	0.3
5428Cu0	0.03	17.7	5.4	0.28	-	1.40	0.4
8630Cu0	0.03	17.1	8.6	0.30	-	1.29	0.4
5422Cu13	0.03	17.6	5.4	0.22	1.3	1.69	0.3
5422Cu33	0.03	17.2	5.4	0.22	3.3	1.54	0.6
AISI 301	0.03	17.7	7.5	0.07	-	1.52	0.4

Deep drawability was assessed by determining the limiting drawing ratio (LDR) according to the method devised by Schmidt[9]. The tests were carried out at a constant hold-down force equivalent to 20kN and the blanks were covered with lubricating polyethylene in order to lower the coefficient of friction. Blank diameters of 50, 55, 65, and 75 mm were used and each test condition was duplicated. Tests were performed on standard AISI 304 for comparison.

RESULTS

Microstructural Analysis

After solution heat treatment, the microstructures of the experimental alloys were examined by light microscopy in order to investigate the presence of δ-ferrite. Ferrite was noted as absent in all instances, and it can therefore be inferred that a single phase austenitic structure existed at the solution temperature (1050°C). The XRD analysis of the phase composition of all the alloys after solution treatment is presented in Table II, and indicates the stability of the austenite during rapid quenching to room temperature. The phase composition was also measured along the tensile gauge length after fracture at each test temperature, and the results are plotted in Fig. 1.

TABLE II : Phase composition of the experimental alloys after solution treatment (1050°C).

Alloy Designation	Retained Austenite (%)
6016Cu0	89 ± 3
5623Cu0	95 ± 3
5428Cu0	96 ± 3
8630Cu0	98 ± 3
5422Cu13	93 ± 3
5422Cu33	99 ± 3

Tensile Properties

The tensile properties for the alloys tested at the various temperatures are summarised in Table III. The maximum uniform strain was measured as the strain level at which the $d\sigma/d\varepsilon$ (work-

hardening rate) value is equivalent to the applied true tensile stress. In view of the fact that maximum uniform strain (ε_u) is an important property when considering formability, the ε_u values are plotted as a function of test temperature in Fig. 2. With the exception of alloys 8630Cu0 and 5422Cu33, elongation generally decreases with temperature increase above 25°C. The highest ε_u occurred at 25°C for alloys 5623Cu0, 5428Cu0, 6016Cu0 and 5422Cu13. Alloy 5422Cu33 demonstrates a decrease in ε_u with increase in temperature above 0°C, whereas alloy 8630Cu0 shows little change in ε_u as a function of temperature.

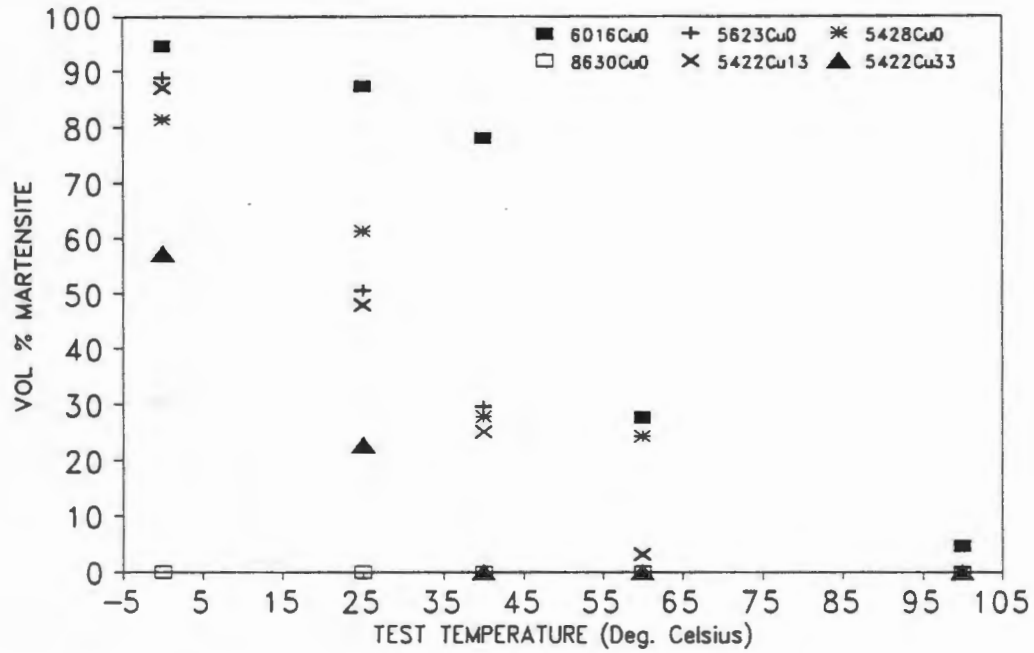

FIG. 1 : Martensite content in fractured specimens as a function of tensile test temperature.

TABLE III : Summary of tensile results (ε_u = uniform strain, UTS = ultimate tensile strength, MPa).

Alloy		0°C	25°C	40°C	60°C	100°C
6016Cu0	ε_u	0.38	0.42	0.38	0.34	-
	UTS	1000	950	1150	850	-
5623Cu0	ε_u	0.45	0.50	0.37	0.34	0.37
	UTS	1700	1080	1000	800	800
5428Cu0	ε_u	0.40	0.50	0.31	0.33	0.32
	UTS	1400	1000	1000	1000	800
8630Cu0	ε_u	0.41	0.40	0.44	0.38	-
	UTS	1300	1250	1200	950	-
5422Cu13	ε_u	0.49	0.52	0.33	0.33	0.34
	UTS	1100	950	900	750	650
5422Cu33	ε_u	0.48	0.36	0.32	0.30	-
	UTS	750	750	800	800	-

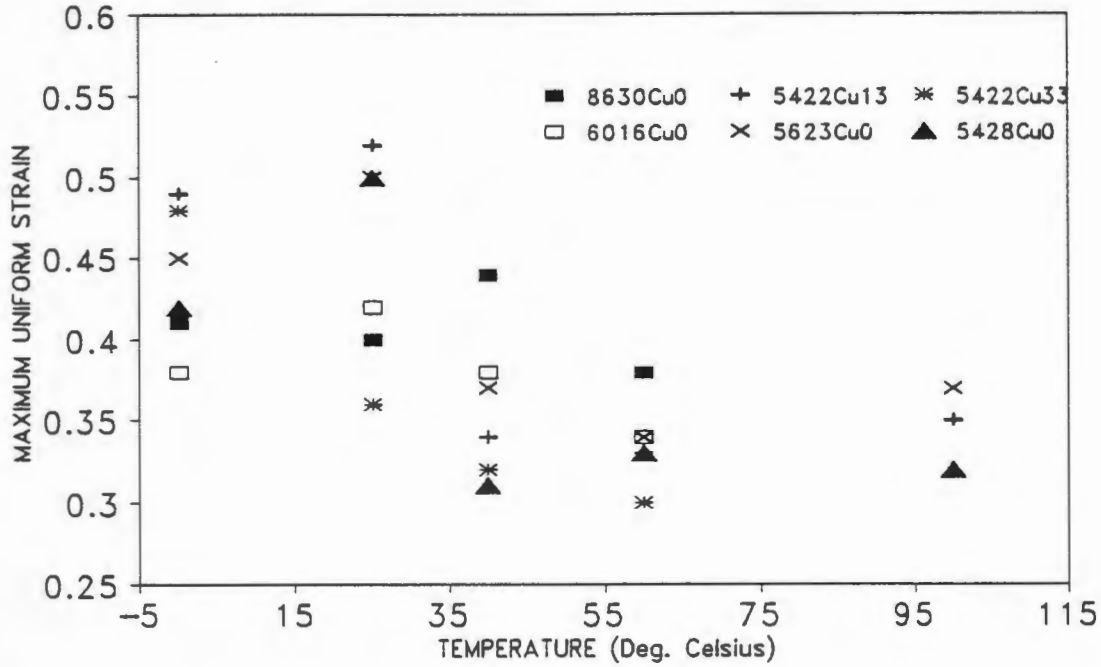

FIG. 2 : Maximum uniform strain as a function of test temperature for the experimental alloys.

In order to understand the variation in maximum uniform elongation as a function of temperature, the work-hardening rate ($d\sigma/d\varepsilon$) was determined as a function of strain and superimposed on the tensile curve information. As indicated previously, ε_u occurs at $d\sigma/d\varepsilon = \sigma$ and therefore ε_u is governed by the shape of the $d\sigma/d\varepsilon$ versus strain (ε) curve. For alloy 5623Cu0, the work-hardening rate yields a local minimum and a local maximum before it finally decreases for tests conducted at 0 and 25°C (Figs. 3 and 4 respectively), whereas the work-hardening rate steadily decreases with increasing strain at 100°C (Fig. 5). A local minimum in $d\sigma/d\varepsilon$ is consistent with the onset of transformation-induced martensite formation[10] and results in an increase in strength. As the material further deforms, an increasing amount of martensite forms and the material continues to strengthen until the rate of martensite formation decreases with concomitant decrease in $d\sigma/d\varepsilon$. The increase in $d\sigma/d\varepsilon$ delays the onset of instability since the condition for $d\sigma/d\varepsilon = \sigma$ occurs at a much higher strain value. In comparing the 0 and 25°C tests for this alloy, $d\sigma/d\varepsilon$ is much higher at 0°C which is understandable in view of the lower stability of austenite at this temperature. For alloy 5422Cu13, a very slight increase in $d\sigma/d\varepsilon$ occurs after the initial minimum (Fig. 6) and $d\sigma/d\varepsilon$ remains fairly constant over a large variation in strain at 25°C. However, at a moderate increase in temperature (40°), $d\sigma/d\varepsilon$ continues to decrease as a function of strain (Fig. 7) and $d\sigma/d\varepsilon = \sigma$ occurs at a low value of strain (approx. 0.33). In the case of alloy 5422Cu33, a similar trend occurs, but the behaviour indicated for 5422Cu13 at 25°C occurs for 5422Cu33 at 0°C. Similarly, the behaviour indicated for 5422Cu13 at 40°C occurs for 5422Cu33 at 25°C. This reflects the greater stability of the austenite phase in alloy 5422Cu33 and demonstrates why a higher uniform strain value is recorded for this alloy at 0°C than at 25°C (Fig. 2).

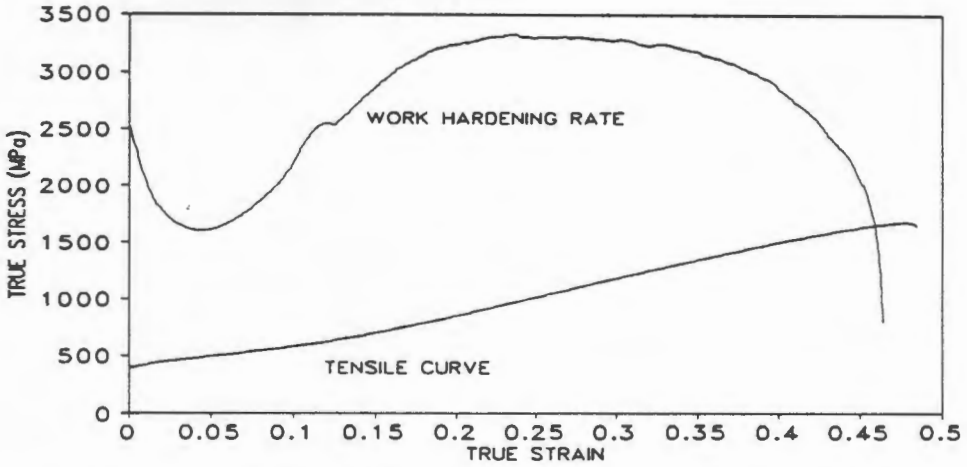

Fig. 3 : Tensile and work-hardening rate curves for alloy 5623Cu0 at 0°C.

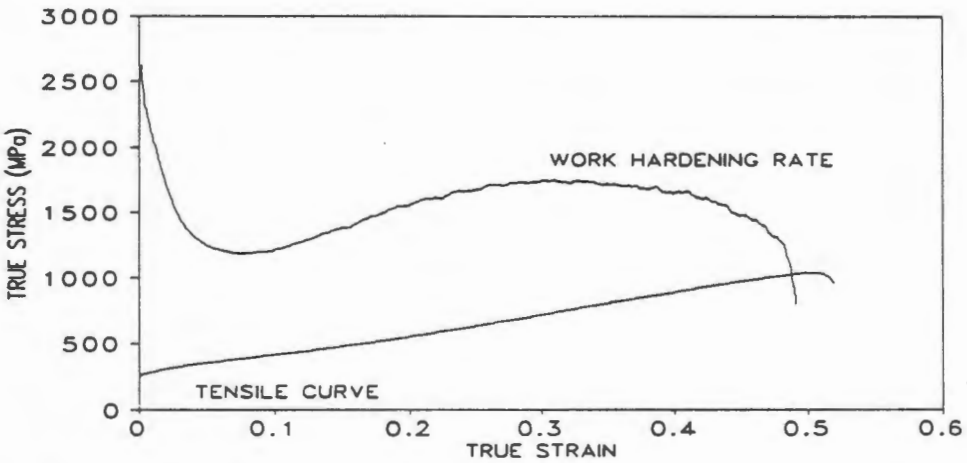

Fig. 4 : Tensile and work-hardening rate curves for alloy 5623Cu0 at room temperature.

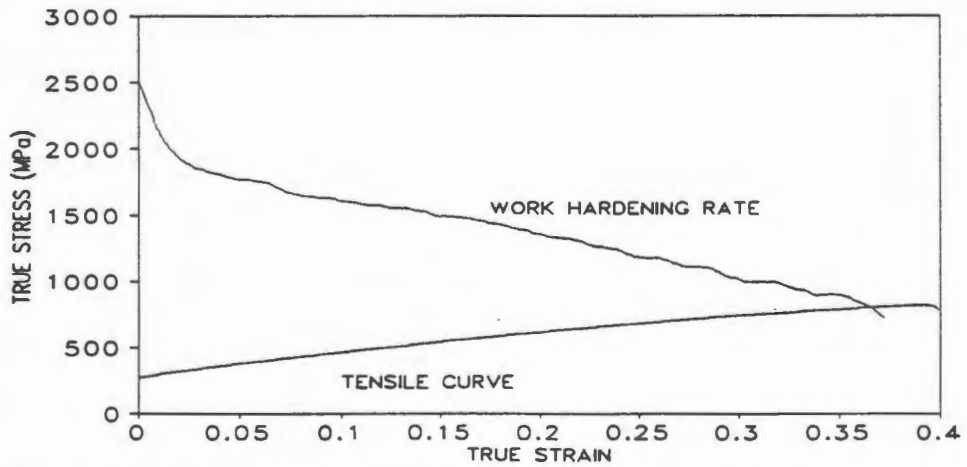

FIG. 5 : Tensile and work-hardening rate curves for alloy 5623Cu0 at 100°C.

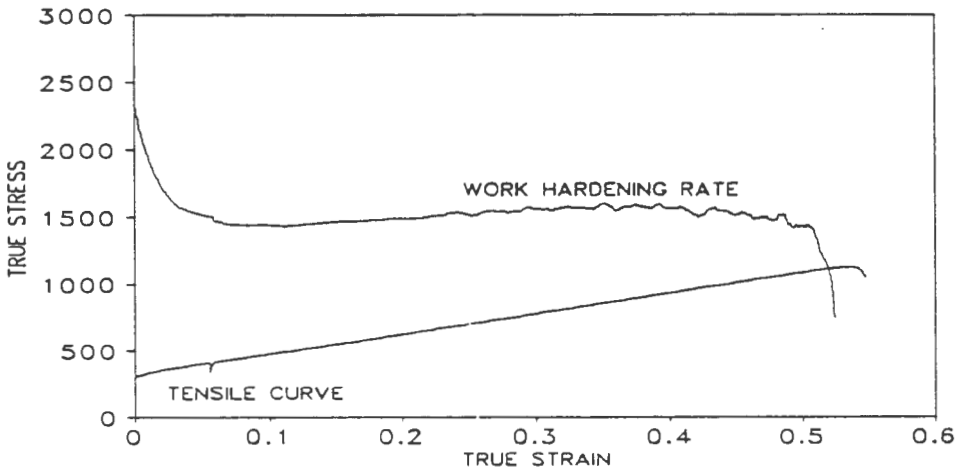

FIG. 6 : Tensile and work-hardening rate curves for alloy 5422Cu13 at room temperature.

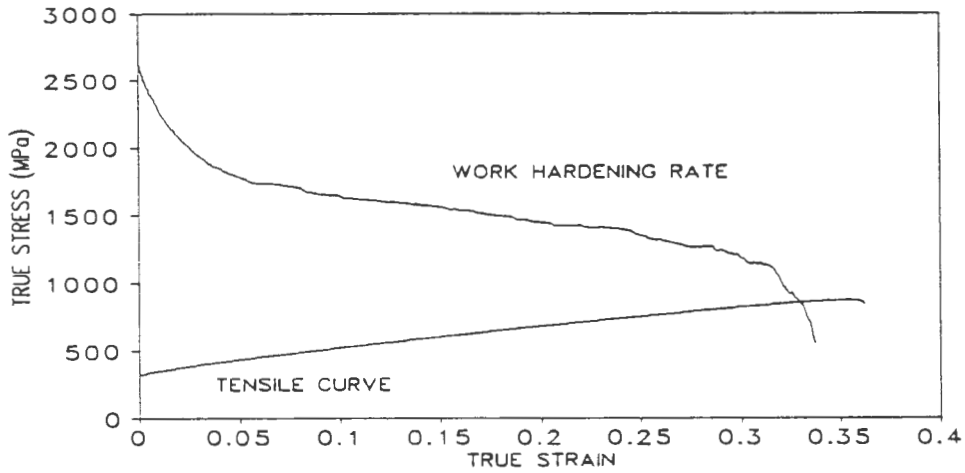

FIG. 7 : Tensile and work-hardening rate curves for alloy 5422Cu13 at 40°C.

Formability tests

The limiting drawing ratios (LDR) of the six experimental alloys as well as a standard 304 type alloy are presented in Table IV. The breaking force (BF) is also included. The drawn cups were examined for minor cracking immediately after drawing and again after a 24 hour period had elapsed. In all cases successfully drawn cups showed no cracking immediately after drawing, but cracking (delayed fracture) was noted for some of the alloys after 24 hours. The extent of this cracking continued to increase with further delay. Table IV summarises the occurrence of delayed cracking and an example of delayed fracture is illustrated in Fig. 8. Similar breaking forces were recorded for all the copper-free experimental alloys and alloy 5422Cu13, and are indicated to be in the region of 90 kN for a 75 mm blank. A much lower breaking force value was recorded for alloy 5422Cu33, once again demonstrating the much lower work-hardening capacity for this alloy.

TABLE IV : Results of the limiting drawing ratio (LDR) tests for the experimental alloys and AISI304.

ALLOY	LDR	BF (kN)	COMMENTS
6016Cu0	2.21	94	No cracking
5623Cu0	2.27	95	Severe delayed cracking
5428Cu0	2.22	93	Severe delayed cracking
8630Cu0	2.14	93	No cracking
5422Cu13	2.15	88	No cracking
5422Cu33	2.19	67	No cracking
Type 304	2.12	77	No cracking

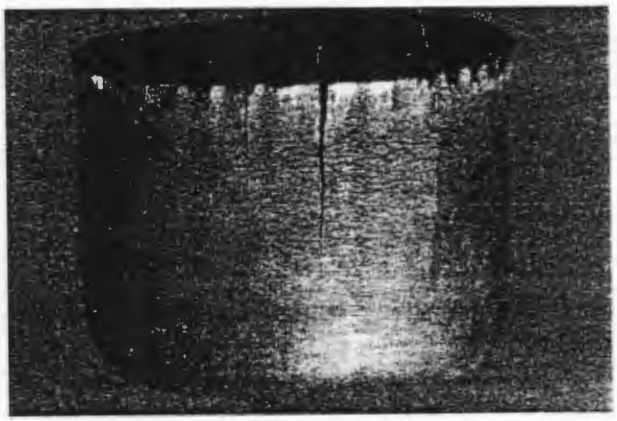

Fig. 8 : Delayed fracture in alloy 5623Cu0 after LDR testing.

DISCUSSION

Microstructural Stability

All the experimental alloys display an austenite stability of at least 90 vol.% retained austenite at room temperature. However, the stability of the alloys varies considerably during deformation as indicated in Fig. 1. The high nickel level in alloy 8630Cu0 results in this alloy being stable over the entire test temperature range. For the remaining alloys, nitrogen and copper are seen to play significant roles in determining the stability of the austenite during deformation. The alloy containing the lowest nitrogen level is least stable, whereas alloys 5623Cu0, 5428Cu0 and 5422Cu13 have similar propensities for the formation of deformation-induced martensite. The addition of 3.3 wt.% copper has resulted in stabilising alloy 5422Cu33 to a much greater extent.

Tensile Behaviour

The tensile behaviour as a function of test temperature for the various alloys is strongly influenced by the formation of martensite during deformation. As is normal for alloys displaying TRIP behaviour, a temperature associated with a peak in uniform elongation can be identified for

some of the experimental alloys. Fig. 2 indicates a peak in uniform elongation at approximately 25°C (room temperature) for alloys 6016Cu0, 5623Cu0, 5428Cu0, and 5422Cu13. Apart from alloy 6016Cu0 which is slightly less stable, these alloys are noted to have similar austenite stability during deformation as mentioned above. It would seem that deformation-induced martensite formation occurs at an optimum rate in these alloys when deformed at room temperature, resulting in good uniform ductility. At higher temperatures the extent of martensite formation is less significant in terms of influencing the work-hardening rate. Optimum uniform elongation is obtained when a maximum occurs in the work-hardening rate curve; however, the maximium must not occur too early on in the deformation process, as would certainly be the case for alloy 6016Cu0 when tested at 0°C. Alloy 5422Cu33 exhibits its highest value for uniform elongation when tested at 0°C which indicates that the alloy is too stable at room temperature. This observation is supported by the trend shown in Fig. 1 for the formation of transformation-induced martensite as a function of test temperature.

Deep Drawability

The experimental alloys all display deep drawability behaviour comparable to Type 304 stainless steel. In fact some of the LDR values (Table IV) are significantly higher than those measured for Type 304, particularly alloys 5623Cu0 and 5428Cu0. The trend exhibited in the LDR values is consistent with the relative tensile ductilities displayed by these alloys when tested at room temperature. This implies that a similar benefit is derived from the formation of deformation-induced martensite during deep drawing compared to tensile deformation. However, the occurrence of delayed fracture in alloys 5623Cu0 and 5428Cu0 is a major concern. Both these alloys contain high nitrogen levels and it would seem that the deformation-induced martensite is too brittle. This observation is in contrast to alloy 6016Cu0 which is less stable but contains a lower nitrogen level, and as a result does not suffer delayed fracture. The addition of 1.3 wt.% Cu is sufficient to stabilise the austenite so as to prevent delayed fracture, albeit with a slight reduction in LDR value. Previous work has shown that delayed fracture occurs when the Md_{30} temperature is too high relative to the deformation temperature[11]. However, delayed fracture could be prevented by annealing immediately after drawing[6], but this could raise serious problems with regard to nitride formation and sensitisation. Work is currently ongoing to investigate this aspect.

CONCLUSIONS

1. The stability of alloys containing much reduced nickel levels can be controlled with additions of up to 0.3 wt.% nitrogen.

2. The level of austenite stability controls uniform tensile strain and TRIP behaviour has been observed at room temperature in alloys containing approximately 5.5 wt.% nickel.

3. Deep drawability, as reflected by LDR values, follows a similar trend to that shown for uniform tensile strain. Alloys containing 5.5 wt.% nickel which exhibit TRIP behaviour at room temperature indicate comparable LDR values to AISI 304 stainless steel.

4. Delayed fracture occurs in metastable alloys containing at least 0.22 wt.% nitrogen. The addition of copper reduces the propensity for delayed fracture, but also slightly lowers the LDR value.

ACKNOWLEDGEMENTS

The authors would like to thank Columbus Stainless Steel, Middelburg, RSA, and the Foundation for Research Development (FRD), Pretoria, RSA, for supporting this work. The assistance of the technical and secretarial staff in the Department of Materials Engineering, UCT, is greatly appreciated.

REFERENCES

1) W.F. BARCLAY, ASTM-Special Tech. Publication 369, (1965), p.26.
2) J.P. BRESSANELLI and A. MOSKOWITZ, ASM Trans. Quart. 59, (1966), p.223.
3) D. FAHR, Metall. Trans. 2, (1971), p.1883.
4) A. ROSEN, R. JAGO and T. KJER, J. Mat. Sci. 7, (1972), p.870.
5) I. TAMURA, Met. Sci. 16, (1982), p.245.
6) C.K. DIVERS, Met. Prog. 86, (1964), p.115.
7) R. JACKSON, Proc. 9th Biennial Congress Int. Deep Drawing Res. Group, Michigan (1976), ASM, Metals Park, Ohio (1977), p.264.
8) O.E. SCHMID and R.D. KNUTSEN, Proc. INFACON 6 (incorporating INCSAC 1), Cape Town (1992), SAIMM, Johannesburg (1992), 2, p.151.
9) G.E. DIETER, Workability Testing Techniques. ASM, Metals Park, Ohio (1984), p.166.
10) X.F. FANG and W.DAHL, Mat. Sci. Eng. A41, (1991), p.189.
11) K. NOHARA and Y. ONO, Kawasaki Steel Tech. Rep. 14, (1986), p.131.